February, 2009

Yoko Kebukawa　　癸生川 陽子

Kinetics of Thermal Decomposition of Organic Matter from Carbonaceous Chondrites and Influence of Minerals

(炭素質コンドライト中有機物の加熱変化の反応速度論と鉱物の効果)

Department of Earth and Space Science,
Graduate School of Science,
Osaka University

Ph.D. Thesis

“I am all that has been,
that is and that shall be,
no mortal has yet raised my veil.”

An inscription at the shrine of Isis

CONTENTS

Abstract

Organic matter in meteorites consists of various forms of organic matter including mainly complex macromolecular materials called insoluble organic matter (IOM), and contains records of their parent body processes. Studying organic matter in meteorites is the key to understand how the solar system has evolved and the processes associated with this. In this thesis research, I first aim to elucidate spatial relationship of organic matter and inorganic phases, then effects of minerals on thermal transformation of organic matter. Finally, I evaluate thermal processing on chondrite parent bodies by kinetic studies of chondritic organic matter using Fourier transform infrared (FTIR) spectroscopy, which is a non-destructive technique for organic components and minerals.

First I checked organic contamination of carbonaceous chondrites for FTIR microspectroscopic analyses. Organic contamination was found on some carbonaceous chondrites containing abundant hydrous minerals by FTIR microspectroscopy on the samples pressed on Al plates. This contamination occurred within one day of storage, when the samples pressed on Al were stored within containers including silicone rubber mats, silicone grease or adhesive tape. Samples stored in glass and polystyrene containers did not show any contamination. Therefore, meteorite samples prepared for micro FTIR measurements should be stored in glass or polystyrene containers without silicone and sticky materials.

Second, I conducted mapping of chondrite by high resolution infrared imaging technique using near-field infrared (NFIR) microspectroscopy for microscopic and spatial characterization of chondritic organic matter. The NFIR spectroscopy has recently been developed to enable infrared spectral mapping beyond the optical diffraction limit of conventional FTIR microspectroscopy. NFIR spectral mapping measurements were conducted on the Bells (CM2) carbonaceous chondrite 300 nm thick sections on Al plates for several μm^2 areas. Heterogeneous distributions of organic functional groups as well as those of inorganic phase such as silicates (Si−O) were observed with less than 1 μm spatial resolution. Some slices of Bells showed ~1 μm aliphatic C−H rich areas which were considered to represent the organic rich areas. One of the organic rich portions in a slice of Bells may contain C−O bonds. Some of organic rich regions might correspond to organic globules which are abundantly distributed in the Bells meteorite. The NFIR imaging method can provide submicron spatial distribution of organic functional groups and their association with minerals.

Third, I conducted heating experiments of IOM and bulk of Murchison (CM2) and

Orgueil (CI1) meteorites to elucidate effects of mineral phases on thermal stability of organic matter under micro FTIR spectroscopy with a heating stage in an inert gas flow. Thermal stability of organic matter was lower in the presence of minerals than IOM for Murchison, while thermal stability was higher in the presence of minerals than IOM for Orgueil. Similarly, heating experiments were conducted using leonardite humic acid (LHA) with and without saponite, antigorite and olivine as analogs of carbonaceous chondrites, under Ar flow and air. The thermal stability of LHA is higher with saponite. On the other hand, antigorite and olivine accelerate the decrease of aliphatic fractions, and decelerates the decrease of aromatic fractions. These effects were dominant in oxidizing atmosphere. These results suggest that thermal stability of organic matter depend on coexisting minerals.

Finally, I conducted heating experiments of bulk and IOM of Murchison to estimate kinetic parameters using infrared bands. Samples are heated at 160-300ºC isothermally in the heating stage under Ar gas flow and air for several hours. Decreases of aliphatic C−H peak heights in Ar flow are well fitted with Ginstling-Brounshtein three dimensional diffusion model, and the rate constants for decreases of aliphatic C−H were determined. Activation energies and frequency factors are estimated from these rate constants at different temperatures using Arrhenius equation. The activation energy and frequency factor for bulk Murchison under Ar flow are 72 ± 6 kJ/mol and 48 s^{-1}, respectively, while these for Murchison IOM under Ar flow are 107 ± 3 kJ/mol and 5.2×10^4 s^{-1}, respectively. Activation energy values of aliphatic C−H decrease are larger for IOM than bulk of Murchison. Hence, the mineral assemblage of Murchison meteorite might have catalytic effect for the organic matter decomposition.

Kinetic heating experiments allow us to constrain the time and temperature range of thermal changes of organic matter in carbonaceous chondrites by using obtained kinetic parameters such as rates and activation energies. For example, aliphatic C−H decrease by half is within ~4 months and to zeto within ~3 years at 100ºC in the presence of Murchison mineral assemblage. Without minerals, aliphatic C−H decrease by half is within ~20 years and aliphatic C−H is lost within ~200 years at 100ºC. Enhanced and additional kinetic studies of thermal processing of organic matter may further help sorting out the thermal history of the parent bodies. In addition, spatial distribution of organic matter with minerals observed by NFIR spectroscopy may help understanding associations and roles of minerals on the parent body processes.

Acknowledgements

I wish to thank Prof. S. Nakashima of Osaka University for giving this subject, valuable advices and encouragements. I am grateful to Dr. M. E. Zolensky and Dr. K. Nakamura-Messenger of Johnson Space Center, NASA, for providing precious meteorite samples, sample preparations and helpful suggestions. I would like to thank Dr. H. Yabuta of Osaka University for her help in acid treatment of meteorites and helpful advices. I would like to thank Dr. T. Hirono, Dr. M. Katsura, Dr. T. Yokoyama, and Dr. K. Saiki of Osaka University for their help and valuable suggestions. Thanks are due to Ms. A. Suzuki, Ms. K. Tokiwai and all the members of Nakashima laboratory for their kindness and help. I thank Dr. Y. Yamanoi for his help in gas flow heating experiments, Mr. M. Ishikawa for his help in NFIR, Dr. T. Otsuka for his help in gas cell FTIR, and Dr. M. Soda for his help in DG-DTA. I am grateful to Mr. K. Aizawa and Mr. T. Inoue of Jasco Co., Ltd. for their technical support on the NFIR spectrometer. I am grateful to constructive comments of Dr. G. Matrajt, Dr. J. S. Watson, Dr. T. Nakamura, Dr. G. J. Flynn and two anonymous reviewers on a part of the manuscript. I also thank Dr. H. Kano of University of Tokyo, Ms. H. Obinata (Tsujikawa) of SII Nano Technology, Prof. K. Kobayashi of Yokohama National University and TANPOPO working group members. I am grateful to Prof. C. J. Spiers of Utrecht University for his helpful advice on this thesis title. Finally, I would like to thank my families for their understanding and encouragements. This research was supported by Research Fellowships of the Japan Society for the Promotion of Science for Young Scientists.

List of Publications and Presentations

Peer Reviewed Papers

1. Kebukawa Y., Nakashima S., Otsuka T., Nakamura-Messenger K., and Zolensky M. E. in press. Rapid contamination during storage of carbonaceous chondrites prepared for micro FTIR measurements. *Meteoritics & Planetary Science*.

2. Kebukawa Y., Nakashima S., Nakamura-Messenger K., and Zolensky M. E. 2009. Submicron distribution of organic matter of carbonaceous chondrite using near-field infrared microspectroscopy. *Chemistry Letters* 38: 22-23.

3. Kebukawa Y. and Nakashima S. 2008. Thermal stabilities of organic matter in carbonaceous chondrites and effects of minerals. *Planetary People* 17: 232-237 (in Japanese).

Other Publications

1. Yamagishi A., Yokobori S., Kawaguchi J., Yinjie Y., Kobayashi K., Yabushita S., Hujisaki K., Yano H., Yamashita M., Okudaira K., Hasegawa N., Kishimoto N., Hashimoto H., Tabata M., Kawai H., Nakajima S., Kebukawa Y., Suzuki A., Mita H., Naraoka H., and Marumo K. 2008. TANPOPO:Astrobiology exposure and micrometeoroid capture. *Space Utilization Research* 24: 218-221.

2. Kobayashi K., Ishikawa Y., Utsumi Y., Okudaira K., Kawai H., Kawasaki Y., Kebukawa Y., Koike J., Suzuki A., Takahashi J., Nakashima S., Naganuma T., Naraoka H., Hashimoto H., Marumo K., Mita H., Yamagishi A., Yamashita M., Imai E., Nakagawa K., Fukushima K., and Yoshimura Y. 2008. Working group report of astrobiology experiments in earth orbit. *Space Utilization Research* 24: 318-321.

3. Kobayashi K., Ishikawa Y., Utsumi Y., Okudaira K., Kawasaki Y., Koike J., Naganuma T., Naraoka H., Hashimoto H., Marumo K., Mita H., Yamagishi A., Yamashita M., Takahashi J., Kebukawa Y., Suzuki A., Sugiura K., Kato M., Kobayashi K., and Yano H. 2007. Astrobiology experiments in earth orbit: Search for organic compounds, microorganisms and ecological systems in space environments. *Space Utilization Research* 23: 410-413.

4. Kebukawa Y. and Nakashima S. 2004. In-situ heating IR microspectroscopy of organics from carbonaceous chondrites – A possible planetary life material science–. *Chikyu Monthly* 26: 507-511 (in Japanese).

Presentations (as the first author, international meetings)

1. Kebukawa Y., Nakashima S., and Zolensky M. Z. Thermal stabilities of organic matter in carbonaceous chondrites using in-situ heating micro FTIR analyses. Poster presentation, Annual Meeting of the Meteoritical Society, Matsue, Japan, July 2008.

2. Kebukawa Y., Nakashima S., Saiki K., and Zolensky M. Z. Experimental simulation of organic matter alteration in carbonaceous chondrites under an in situ micro FTIR spectroscopy. Poster presentation, American Geophysical Union fall meeting, San Francisco, December 2007.

3. Kebukawa Y., Ishikawa M., Nakashima S., Nakamura T., and Zolensky M. E. Infrared microspectroscopic mapping of organic matter in Tagish Lake meteorite for studying organic evolution during aqueous alteration. Oral presentation, Lunar and Planetary Science Conference, Houston, March 2007.

4. Kebukawa Y., Nakashima S., and Zolensky M. E. In-situ micro-FTIR study of thermal changes of organics in carbonaceous chondrites –Behavior of aliphatic hydrocarbons and effects of minerals–. Poster presentation, General Meeting of the International Mineralogical Association, Kobe, Japan, July 2006.

5. Kebukawa Y., Nakashima S., and Zolensky M. E. In-situ heating decrease kinetics of aliphatic hydrocarbons in Tagish Lake meteorite by micro-FTIR. Poster presentation, Lunar and Planetary Science Conference, Houston, March 2005.

6. Kebukawa Y., Nakashima S., Masuda K., and Kuya N. New in-situ micro-characterization methods for organic materials from carbonaceous chondrites. Poster presentation, Goldschmidt Conference, Kurashiki, Japan, September 2003.

Chapter 1

GENERAL INTRODUCTION

1.1. Organic Matter in Carbonaceous Chondrites

In this chapter, I first review organic matter in carbonaceous chondrites and relationship to the early solar system. Then I summarize the scope of this Ph. D thesis, aiming at constraining temperature-time histories of the early solar system thorough organic materials in primitive astro-materials.

Chondrites originated from planetesimals or asteroids that accreted during the formation of the solar system. They are aggregates of many components including chondrules, Fe,Ni-metal grains and/or metal-troilite aggregates, Ca,Al-rich inclusions (CAIs), and amoeboid olivine aggregates (AOAs), all of which can be surrounded by fine-grained rims and occur within a fine-grained matrix (e.g., Krot et al. 2006). Carbonaceous chondrites have survived many of the geological processes on the planets and are among the oldest and most primitive solid materials in the solar system. They retain volatile elements that record the history of their chemical evolution in the universe.

Carbonaceous chondrites contain up to 3 wt% carbon, in the form of a variety of organic compounds which are divided into a soluble fraction and an insoluble one (e.g., Botta and Bada 2002). Organic compounds in carbonaceous chondrites were first observed in 1834 by Berzelius (1834) in the Alais (CI1) carbonaceous chondrite, which fell in France in 1806. Since then, hundreds of investigations have been performed. Organic matter in carbonaceous chondrites may have recorded signatures of its synthesis in the interstellar medium and/or in the solar system. It could also be an important constituent of the prebiotic organic material on the early Earth.

The water and organic solvent soluble fraction consists of a variety of compounds: carboxylic acids, aliphatic and aromatic hydrocarbons, amino acids and other compounds of biological interest (e.g., reviews by Cronin and Chang 1993; Botta and Bada 2002; Sephton, 2002; Pizzarello et al. 2006).

Most of the organic matter in meteorites (70-99%) is complex macromolecular matter that is insoluble in water, acids, or any organic solvent, and is thus defined as insoluble organic matter (IOM). It is isolated through solvent extractions to remove soluble organic compounds and a HF/HCl treatment to remove silicates. The residue obtained is enriched in organic matter, but contains at least 10 wt% of inorganic material (Remusat et al. 2007). The IOM is often described as “kerogen-like” compared to the organic matter of mature terrestrial kerogens (e.g., Hayatsu et al. 1977). IOM chemical structures have been studied extensively by both direct spectroscopic methods and degradative methods, and by electron microscopy (e.g., reviews by Cronin

and Chang 1993; Botta and Bada 2002; Sephton 2002; Pizzarello et al. 2006). The chemical structures of IOM have been investigated by direct spectroscopic and microscopic methods, such as Fourier transform infrared (FTIR) (Hayatsu et al. 1977; Wdowiak et al. 1988; Ehrenfreund et al. 1991, 1992; Murae 1994; Kissin 2003) and Raman spectroscopy (Busemann et al. 2007), solid state ^{13}C nuclear magnetic resonance (NMR) (Cronin et al. 1987; Gardinier et al. 2000; Pizzarello et al. 2001; Cody et al. 2002; Cody and Alexander 2005; Remusat et al. 2005a; Yabuta et al. 2005), Electron Paramagnetic Resonance (EPR) (Binet et al. 2002, 2004a,b; Gourier et al. 2004; Remusat et al. 2008), X-ray Absorption Near Edge Structure (XANES) (Cody et al. 2008), and transmission electron microscopy (TEM) (Garvie and Buseck 2006). And IOM have also been investigated through degradations: chemical degradation (Hayatsu et al. 1977, 1980; Remusat et al. 2005b), various pyrolytic experiments (Komiya et al. 1993; Sephton et al. 1998, 1999, 2000, 2003, 2004, 2005; Remusat et al. 2005a; Oba and Naraoka 2006; Yabuta et al. 2007).

Pizzarello (2007) summarized the structure of IOM as follows. IOM is composed mainly of a macromolecular structure (Fig. 1-1) of condensed aromatic rings joined by aliphatic bridges and containing peripheral alkyl branching, with heteroatoms, N, O, and S, found both in the aromatic and aliphatic portions, for example, in functional groups such as C=O and C=N. The macromolecular portion described above seems to represent only 80% of the total and is itself made up of more than one type of aggregates that differ in isotopic composition (Kerridge et al. 1987), labile response to temperature (Sephton et al. 1998), and aliphatic chain composition (Remusat et al. 2005b). Also distinct nanometer-sized entities (ca. 166 to 830 nm) such as solid or hollow spheres (Fig. 1-1) and tubes can be seen embedded in the IOM by TEM and represent up to 10% of total IOM. These structured inclusions are themselves heterogeneous, with their composition varying from close to pure graphitic carbon (>99%) to containing several percent of oxygen, nitrogen, and sulfur besides carbon (Garvie and Buseck 2004).

Table 1-1 summarizes the classification and chemical properties of meteorites analyzed in this study.

Elemental composition: $C_{100}H_{71}N_3O_{12}S_2$

Macromolecular material: *ca.* 80%

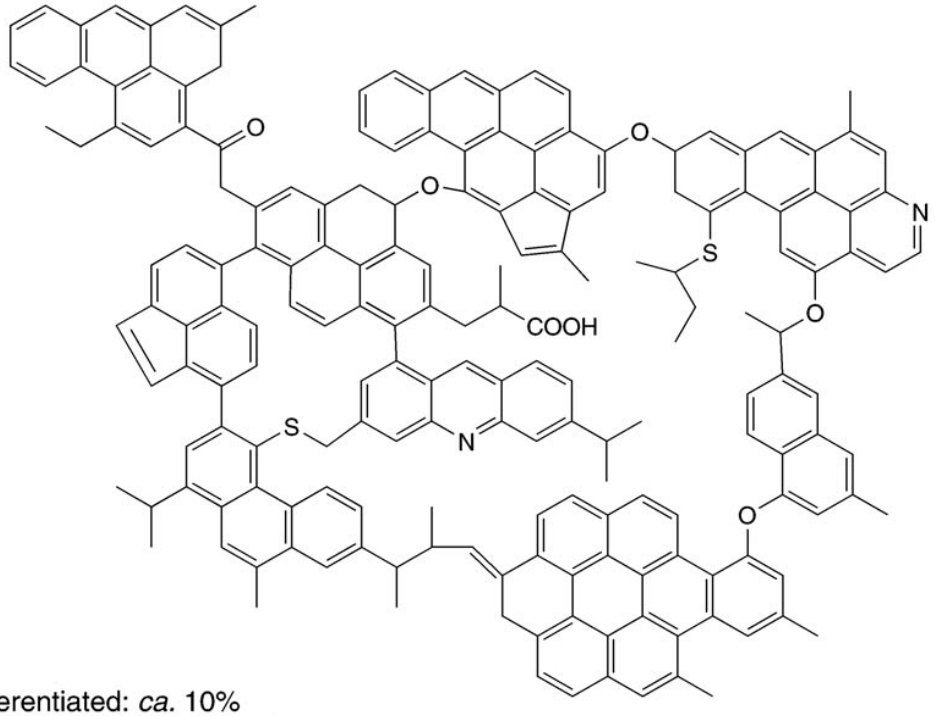

Structurally differentiated: *ca.* 10%
e.g., nanoglobules and nanotubes

Hydrothermally freeable compounds: ca. 10%
e.g., $C_3 - C_{17}$ dicarboxylic acids and methylated pyridines

Exotic carbon from interstellar grains: ppm
e.g., diamond, graphite, and fullerenes; SiC; Si_3N_4

Fig. 1-1. The composition of the insoluble organic material (IOM) of the Murchison meteorite by Pizzarello (2007).

Table 1-1. The meteorites studied in this study. Based on the Catalogue of Meteorites (Natural History Museum, http://www.nhm.ac.uk), Alexander et al. (2007), Bischoff and Schmale (2007), and Greenwood et al. (2007).

Summary	Classification	Fall/find	Shock stage	Date	Location	Mass	Matrix (vol%)	C (wt%)	H/C (at.) ×100	N/C (at.) ×100	O/C (at.) ×100	S/C (at.) ×100	$\delta^{13}C$ (‰)	$\delta^{15}N$ (‰)	δD (‰)	$\delta^{18}O$ (‰)
Orgueil	CI1	Fall		May 14, 1864	Tarn-et-Garonne, France		100	2.00	67.3±1.4	3.49±0.01	18.1±0.2	2.8±1.4	–17.05±0.04	30.7±0.2	972±2	14.5±0.6
Bells	CM2/C2 ungrouped	Fall	S1	September 9, 1961	Texas, United States	375g	81.7	0.96	68.5±0.8	3.37±0.02	20.9±0.3	5.0±1.4	–34.20±0.16	415.3±1.6	3283	14.1±0.2
Murchison	CM2	Fall	S1-2	September 28, 1969	Victoria, Australia	100kg	63.6	0.83	58.8±1.6	3.27±0.03	18.3±0.3	1.8±1.2	–18.91±0.01	–1.0±0.4	777±27	13.2±0.6
Murray	CM2	Fall	S1	September 20, 1950	Kentucky, USA	12.6kg	58.8	0.96	67.7±1.1	3.69±0.01	17.2±1.2	6.0±2.3	–18.05±0.18	7.5±0.1	893	11.5±0.4
Yamato 793321	CM2 (heated)	Find		1979	Queen Maud Land, Antarctica	379.73g		1.31	42.2±0.7	3.00±0.06	15.9±0.3	3.2	–8.39±0.07	35.1±0.7	95±7	9.2±0.1
Tagish Lake	C2 ungrouped	Fall	S1	January 18, 2000	British Columbia, Canada	5-10kg	80	2.00	33.7±1.0	4.28±0.02	16.9±1.4		–14.17±0.13	73.0±1.5	596±4	12.5±0.5
Allende	$CV3_{oxA}$	Fall	S1	February 8, 1969	Chihuahua, Mexico	>2t	38.4	0.18	17.4±1.0	0.48±0.03	12.5±0.5		–17.03±0.19	–51.2±0.6	194±13	5.1±0.4
Moss	CO3.5/3.6	Fall		July 14, 2006	Oslofjord, Norway	~4kg										

1.2. Effects of Parent Body Processes for the Structure of Organic Matter

It is widely accepted that significant amounts of meteoritic organic matter, or its precursor materials, were synthesized in interstellar and nebular environments. Various degrees of aqueous alteration and/or thermal metamorphism have occured after accretion of their parent bodies (e.g., reviews by Huss et al. 2006; Brearley 2006). Hence, the final organic molecular architecture of carbonaceous chondrites was strongly determined by the effects of hydrothermal alteration on their parent bodies. The structural classification of IOM is required for understanding of the early solar system history.

The carbonaceous chondrites are subdivided into several classes, each defined by characteristic mineral and chemical properties, as well as by thermal and aqueous alteration histories (e.g., reviews by Weisberg et al. 2006). The alteration processes that occurred on meteorite parent bodies had the potential to cause chemical reactions and change the chemical and spatial distributions of organic compounds. Such alteration events, caused by thermal activity and liquid water on meteorite parent bodies, had the potential to modify the original distribution of organics. The organic matter in carbonaceous chondrites potentially records a succession of chemical histories that started with reactions in the interstellar medium, followed by reactions that accompanied the formation and evolution of the early solar nebula, and, ultimately, ended with reactions driven by hydrothermal alteration in the meteorite parent bodies. The origin and history of IOM are still being discussed, and no model is so far able to explain its observed structural diversity along with its H and N bulk isotopic compositions (Halbout et al. 1990; Alexander et al. 1998, 2007).

Based on isotopic evidence, it is clear that at least some meteoritic organic components (both free and macromolecular) are interstellar in origin, indicating that meteoritic organic material may provide a record of the chemistry that occurred in the interstellar medium and the solar nebula (Robert and Epstein 1982; Yang and Epstein 1983; Kerridge et al. 1987; Pizzarello et al. 1991; Messenger et al. 1998).

The influence of the asteroidal environment appears to exert on the final constitution of meteoritic organic matter. Low-temperature stepwise combustion exhibited two organic components: a labile portion released between 250 and 350ºC, which is carbon isotopically heavier than –12.4‰, and more stable portion released up to 450ºC, which is carbon isotopically lighter at –18.7‰ (Kerridge et al. 1987). The labile portion can act as a parent for the free aromatic hydrocarbons in meteorites (Sephton et al. 1998). The open structure is relatively susceptible to both thermal degradation and oxidation, whereas more condensed organic material, which would be

relatively resistant to both thermal and oxidative degradation, would not produce degradation products during a relatively mild condition (Sephton et al. 1998). For lower levels of the alteration, the free radical termination by water would have proceeded within the carbonaceous matter itself, leading to greater cross-linking and aromatization (Sephton et al. 1999, 2000).

Several CM and CI chondrites experienced thermal metamorphism after the aqueous alteration (e.g., Zolensky et al. 2005; Tonui et al. in prep). During thermal metamorphism, the (002) interlayer spacing of the graphitic matter decreases to a constant value of 3.35 Å with an increasing degree of ordering of the carbonaceous matter (Rietmeijer and Mackinnon 1985). Murae et al. (1991) found that the chondrite samples analyzed can be classified into five classes which are categorized on the basis of their efficiency of the formation of naphthalene as a pyrolysis product normalized to total carbon content. Shimoyama et al. (1991) evaluated the degree of thermal metamorphism of CM and CI chondrites with a mass spectrometer equipped with a combined differential thermal analyzer and thermogravimetric analyzer (DTA/TG-MS). Komiya et al. (1993) performed laboratory heating experiments with IOM from CM2 chondrites and revealed that less altered and metamorphosed chondrites contain a more thermally labile organic fraction. Kitajima et al. (2002) used pyrolysis-gas chromatography coupled with mass spectrometry (pyr-GC/MS) and found that thermal alteration has been correlated with degrees of graphitization of macromolecular material. Naraoka et al. (2004) proposed an organic parameter of thermal alteration using carbon, hydrogen, and nitrogen concentrations of IOM, and also found that thermal alteration has been correlated with the abundance of soluble organic material. Solid-state ^{13}C NMR spectroscopy of thermally altered CM2 chondrites showed that the aliphatic structures of the IOM could be modified in some way during thermal alteration, by being oxidized, aromatized, graphitized, or lost (Yabuta et al. 2005). MicroRaman studies have shown that the molecular structure of organic matter appear to correlate well with petrologic type (Quirico et al. 2003; Bonal et al. 2006, 2007; Busemann et al. 2007).

1.3. Spatial Relationship between Organic Matter and Minerals

As mentioned above (section 1.2), organic matter modification occurred during parent body aqueous alteration and thermal metamorphism that produced the mineral assemblages. Thus, one might expect a relationship between the chemical and spatial distributions of organics on carbonaceous chondrites and their alteration histories.

However, organic-inorganic relationship of carbonaceous chondrites is poorly understood. Understanding the relationship and spatial depiction of organic and inorganic components is essential for understanding the processes and mechanisms involved in the evolution of organic material in the early solar system.

Several works have already been dedicated to the study of the spatial distribution of the carbonaceous matter in chondrites. Nuclear reaction analysis (NRA) showed that olivine grains in chondritic meteorites generally have carbon content lower than 120 ppm (Varela and Metrich 2000). Faceted graphene sheets with large scale graphitisation were found in the Allende meteorite, especially in Fe-rich matrix of olivine by TEM observations (Brearley 1999; Harris et al. 2000). Pearson et al. (2002) reported that osmium labeled organic matter was associated with clay minerals in CM and CI chondrites, from scanning electron microscope (SEM) observation. Amri et al. (2005) reported that pyroxene, olivine and iron oxide grains were embedded into the mixed carbonaceous material, based on Raman spectroscopy. Garvie and Buseck (2007) investigated carbon-clay assemblages in CI and Tagish Lake meteorites using transmission electron microscopy (TEM) and electron energy-loss spectroscopy (EELS).

1.4. Infrared Spectra of Carbonaceous Chondrites

FTIR spectroscopy is a non-destructive technique for organic components and minerals, and has been successfully applied to chondritic organic matter (Hayatsu et al. 1977; Wdowiak et al. 1988; Ehrenfreund et al. 1991, 1992; Murae 1994; Raynal et al. 2000; Nakamura et al. 2002; Kissin 2003; Matrajt et al. 2004), mainly based on aliphatic stretching features in the region 3000-2800 cm^{-1} (3.4 μm band). The similarity of chemical compositions between IOM and interstellar organic matter has been observed by the typical pattern of the 3.4 μm band observed by infrared spectroscopy both in chondritic IOM and in the interstellar medium.

Fig. 1-2 show micro FTIR spectra of several carbonaceous chondrites (Orgueil, Murchison, Murray, Bells, Y-793321, Tagish Lake, and Allende) pressed on KBr plates (CaF_2 for Orgueil). The 3700-3600 cm^{-1} band is due to structural O−H stretching of phillosilicates. The bands around 3400 due to O−H stretching and 1640 cm^{-1} due to O−H bending are attributed to interlayer molecular water in phyllosilicates and/or water molecules loosely adsorbed to minerals. The bands around 2960 and 2870 cm^{-1} are due to asymmetric and symmetric stretching vibrations of aliphatic CH_3, respectively. The bands around 2930 and 2855 cm^{-1} are due to asymmetric and symmetric stretching

vibrations of aliphatic CH_2, respectively. The shoulder around 1590 cm^{-1} is due to aromatic C=C. The 1450 cm^{-1} band is mainly due to carbonates wish some contribution of aliphatic C−H bending, and 1380 cm^{-1} is due to aliphatic C−H bending.

Thermal stabilities of organic matter of carbonaceous chondrites have also been studied by FTIR spectroscopy. Nakamura et al. (2003) conducted preliminary in-situ FTIR heating experiments of organic matter in the Tagish Lake meteorite and found varying thermal stabilities of different organic functional groups. Flynn et al. (2001) reported that the 3000-2800 cm^{-1} region of the infrared spectrum of Tagish Lake is similar to Orgueil and Murchison but that Tagish Lake contains an organic component that is lost on heating to 100ºC for 1/2 hour. Wdowiak et al. (1988) reported infrared spectra of an acid insoluble residue of Orgueil heated in vacuum up to 500ºC which showed an increase of aromatic features at higher temperatures and a simultaneous decrease for aliphatic features.

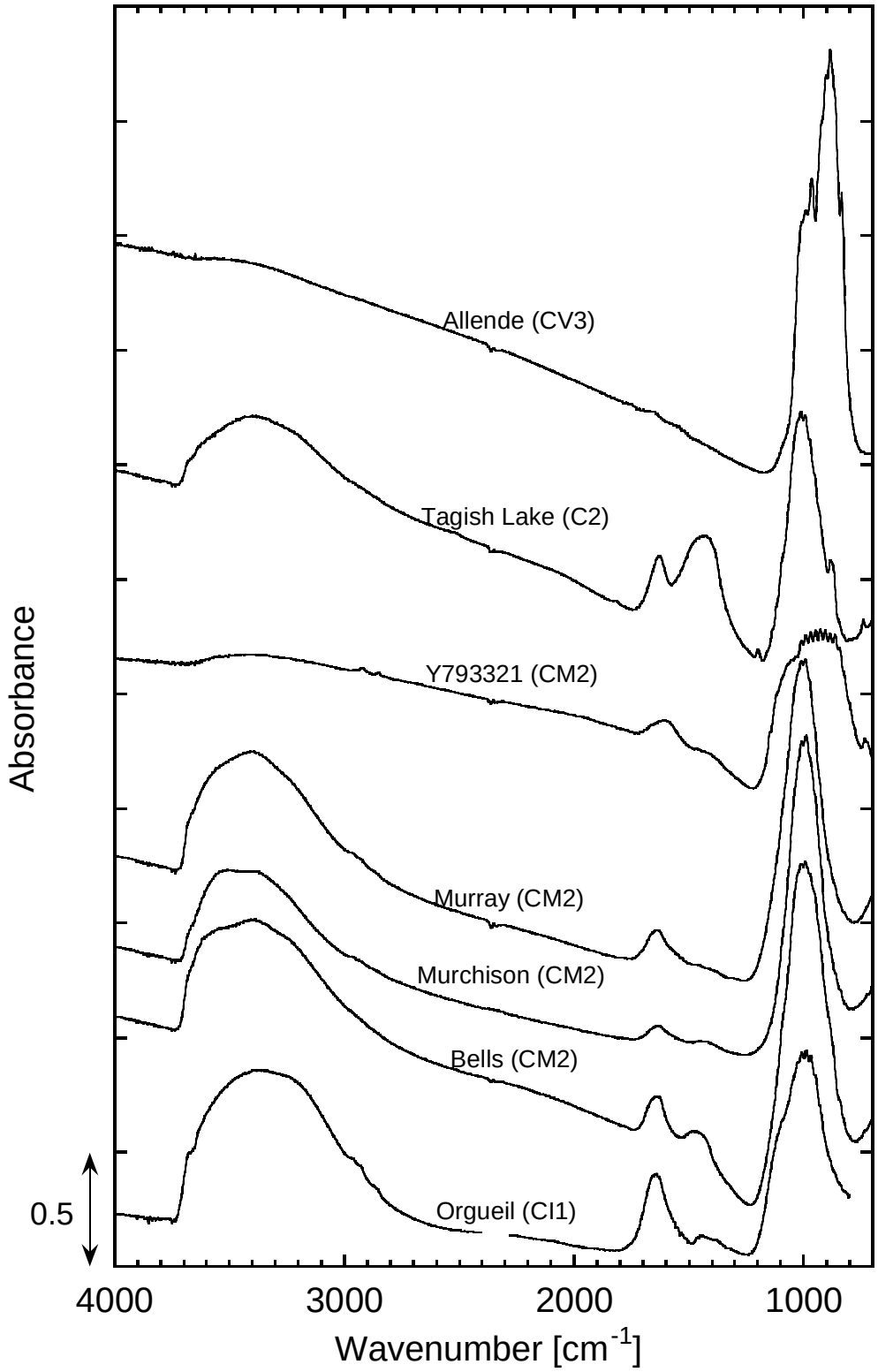

Fig. 1-2. Infrared absorption spectra of crbonaceous chondrites on KBr plates (CaF_2 plate for Orgueil). Orgueil (CI1), Murchison (CM2), Murray (CM2), Bells (CM2), Yamato 793321 (CM2), Tagish Lake (ungrouped C2), and Allende (CV3).

1.5. This Research

Despite the above studies, spatial distribution and microscopic characterization of chondritic organic matter are lacking especially for polar functional groups such as aliphatic C−H and C−O, and effects of minerals for thermal changes of organic matter are not known. Therefore, I aim to elucidate spatial relationship of organic matter and inorganic phases, and effects of minerals on thermal transformation of organic matter, and then I evaluate thermal processing on chondrite parent bodies by kinetic studies of chondritic organic matter using FTIR spectroscopy which is a non-destructive technique for organic components and minerals.

In Chapter 2, I evaluate organic contamination of carbonaceous chondrites by FTIR microspectroscopic analyses. The carbonaceous chondrites are found to have been contaminated during brief (~1 day) storage with a container with silicone rubber mat. I propose the sample preparation and storage methods to avoid contamination. In Chapter 3, I conduct mapping of chondrite by high resolution infrared imaging technique using near-field infrared (NFIR) microspectroscopy for microscopic and spatial characterization of chondritic organic matter. In Chapter 4, I conduct heating experiments of IOM and bulk meteorite, and simulated chondritic materials, in order to elucidate a role of mineral phases for thermal stability of organic matter. In Chapter 5, I conduct heating experiments of carbonaceous chondrites to estimate kinetic parameters using infrared bands. Kinetic data sets would constrain the temperature and time scales for parent body processes of chondritic meteorites. Finally, I discuss the implication for thermal processes of chondrites.

References

Alexander C. M. O'D., Russell S. S., Arden J. W., Ash R. D., Grady M. M., and Pillinger C. T. 1998. The origin of chondritic macromolecular organic matter: A carbon and nitrogen isotope study. *Meteoritics & Planetary Science* 33: 603-622.

Alexander C. M. O'D., Fogel M., Yabuta H., and Cody G. D. 2007. The origin and evolution of chondrites recorded in the elemental and isotopic compositions of their macromolecular organic matter. *Geochimica et Cosmochimica Acta* 71: 4380-4403.

Amri C. E., Maurel M. C., Sagon G., Baron M. H. 2005. The micro-distribution of carbonaceous matter in the Murchison meteorite as investigated by Raman imaging. *Spectrochimica Acta Part A* 61: 2049-2056.

Berzelius J. J. 1834. Ueber Meteorsteine. *Annalen der Physik und Chemie* 33: 113-148.

Binet L., Gourier D., Derenne S., and Robert F. 2002. Heterogeneous distribution of

paramagnetic radicals in insoluble organic matter from the Orgueil and Murchison meteorites. *Geochimica et Cosmochimica Acta* 66: 4177-4186.

Binet L., Gourier D., Derenne S., Pizzarello S., and Becker L. 2004a. Diradicaloids in the insoluble organic matter from the Tagish Lake meteorite: Comparison with the Orgueil and Murchison meteorites. *Meteoritics & Planetary Science* 39: 1649-1654.

Binet L., Gourier D., Derenne S., Robert F., and Ciofini I. 2004b. Occurence of abundant diradicaloid moieties in the insoluble organic matter from the Orgueil and Murchison meteorites: A fingerprint of its extraterrestrial origin? *Geochimica et Cosmochimica Acta* 68: 881-891.

Bischoff A. and Schmale K. 2007. Ca,Al-rich inclusions within the Moss CO3 chondrite - Indications for severe secondary alteration (abstract #1561). 38th Lunar and Planetary Science Conference. CD-ROM.

Bonal L., Quirico E., Bourot-Denise M., Montagnac G. 2006. Determination of the petrologic type of CV3 chondrites by Raman spectroscopy of included organic matter. *Geochimica et Cosmochimica Acta* 70: 1849-1863.

Bonal L., Bourot-Denise M., Quirico E., Montagnac G., and Lewin E. 2007. Organic matter and metamorphic history of CO chondrites. *Geochimica et Cosmochimica Acta* 71: 1605-1623.

Botta O. and Bada J. L. 2002. Extraterrestrial organic compounds in meteorites. *Surveys in Geophysics* 23: 411-467.

Brearley A. J. 1999. Origin of graphitic carbon and pentlandite in matrix olivines in the Allende meteorite. *Science* 285: 1380-1382.

Brearley A. J. 2006. The action of water. In *Meteorites and the early solar system II*, edited by Lauretta D. S., Leshin L. A., and McSween H. Y., Jr. Tucson, Arizona: The University of Arizona Press. pp. 587-624.

Busemann H., Alexander C. M. O'D., and Nittler L. R. 2007. Characterization of insoluble organic matter in primitive meteorites by microRaman spectroscopy. *Meteoritics & Planetary Science* 42: 1387-1416.

Cody G. D., Alexander C. M. O'D., and Tera F. 2002. Solid-state (^{1}H and ^{13}C) nuclear magnetic resonance spectroscopy of insoluble organic residue in the Murchison meteorite: A self-consistent quantitative analysis. *Geochimica et Cosmochimica Acta* 66: 1851-1865.

Cody G. D. and Alexander C. M. O'D. 2005. NMR studies of chemical structural variation of insoluble organic matter from different carbonaceous chondrite groups. *Geochimica et Cosmochimica Acta* 69: 1085-1097.

Cody G. D., Alexander C. M. O'D., Yabuta H., Kilcoyne A. L. D., Araki T., Ade H., Dera P., Fogel M., Militzer B., Mysen B. O. 2008. Organic thermometry for chondritic parent bodies. *Earth and Planetary Science Letters* 272: 446-455.

Cronin J. R., Pizzarello S., and Frye J. S. 1987. ^{13}C NMR spectroscopy of the insoluble carbon of carbonaceous chondrites. *Geochimica et Cosmochimica Acta* 51: 299-303.

Cronin J. R. and Chang S. 1993. Organic matter in meteorites: Molecular and isotopic analyses of the Murchison meteorite. In *The chemistry of life's origins*, edited by Greenberg J. M., Mendoza-Gomez C. X., and Pirronello V. Dordrecht, The Netherlands: Kluwer Academic. pp. 209-258.

Ehrenfreund P., Robert F., d'Hendecourt L., and Behar F. 1991. Comparison of interstellar and meteoritic organic matter at 3.4 microns. *Astronomy and Astrophysics* 252:712-717.

Ehrenfreund P., Robert F., and d'Hendecourt L. 1992. Similarity of the infrared spectrum of an Orgueil organic polymer with interstellar organic compounds in the line of sight towards IRS 7. *Advances in Space Research* 12: 53-56.

Flynn G. J., Keller L. P., Jacobsen C., and Wirick S. 2001. FTIR and carbon-XANES examination of organic carbon in Tagish Lake: Evidence for a moderately volatile organic component (abstract #1593). 32nd Lunar and Planetary Science Conference. CD-ROM.

Gardinier A., Derenne S., Robert F., Behar F., Largeau C., and Maquet J. 2000. Solid state CP/MAS ^{13}C NMR of the insoluble organic matter of the Orgueil and Murchison meteorites: quantitative study. *Earth and Planetary Science Letters* 184: 9-21.

Garvie L. A. J. and Buseck P. R. 2004. Nanosized carbon-rich grains in carbonaceous chondrite meteorites. *Earth and Planetary Science Letters* 224: 431-439.

Garvie L. A. J. and Buseck P. R. 2006. Carbonaceous materials in the acid residue from the Orgueil carbonaceous chondrite meteorite. *Meteoritics & Planetary Science* 41: 633-642.

Garvie L. A. J. and Buseck P. R. 2007. Prebiotic carbon in clays from Orgueil and Ivuna (CI), and Tagish Lake (C2 ungrouped) meteorites. *Meteoritics & Planetary Science* 42: 2111-2117.

Gourier D., Binet L., Scrzypczak A., Derenne S., and Robert F. 2004. Search for EPR markers of the history and origin of the insoluble organic matter in extraterrestrial and terrestrial rocks. *Spectrochimica Acta Part A* 60: 1349-1357.

Greenwood R. C., Pearson V. K., Verchovsky A. B., Johnson D., Franchi I. A., Roaldset E., Raade G., and Bartoschewitz R. 2007. The Moss (CO3) Meteorite: An Integrated Isotopic, Organic and Mineralogical Study (abstract #2267). 38th Lunar and Planetary Science Conference. CD-ROM.

Halbout J., Robert F., and Javoy J. 1990. Hydrogen and oxygen isotope compositions in kerogen from the Orgueil meteorite: Clues to a solar origin. *Geochimica et Cosmochimica Acta* 54: 1453-1462.

Harris P. J. F., Vis R. D., and Heymann D. 2000. Fullerene-like carbon nanostructures in the Allende meteorite. *Earth and Planetary Science Letters* 183: 355-359.

Hayatsu R., Matsuoka S., Anders E., Scott R. G., and Studier M. H. 1977. Origin of organic

matter in the early solar system – VII. The organic polymer in carbonaceous chondrites. *Geochimica et Cosmochimica Acta* 41: 1325-1339.

Hayatsu R., Winans R. E., Scott R. E., McBeth R. L., Moore L. P., and Studier M. H. 1980. Phenolic ethers in the organic polymer of the Murchison meteorite. *Science* 207: 1202-1204.

Huss G. R., Rubin A. E., and Grossman J. N. 2006. Thermal metamorphism in chondrites. In *Meteorites and the early solar system II*, edited by Lauretta D. S., Leshin L. A., and McSween H. Y., Jr. Tucson, Arizona: The University of Arizona Press. pp. 567-586.

Kerridge J. F., Chang S., and Shipp R. 1987. Isotopic characterization of kerogen-like material in the Murchison carbonaceous chondrite. *Geochimica et Cosmochimica Acta* 51: 2527-2540.

Kissin Y. V. 2003. Hydrocarbon components in carbonaceous meteorites. *Geochimica et Cosmochimica Acta* 67: 1723-1735.

Kitajima F., Nakamura T., Takaoka N., and Murae T. 2002. Evaluating the thermal metamorphism of CM chondrites by using the pyrolytic behavior of carbonaceous macromolecular matter. *Geochimica et Cosmochimica Acta* 66: 163-172.

Komiya M., Shimoyama A., and Harada K. 1993. Examination of organic-compounds from insoluble organic-matter isolated from some Antarctic carbonaceous chondrites by heating experiments. *Geochimica et Cosmochimica Acta* 57: 907-914.

Krot A. N., Hutcheon I. D., Brearley A. J., Pravdivtseva O. V., Petaev M. I., and Hohenberg C. M. 2006. Timescales and settings for alteration of chondritic meteorites. In *Meteorites and the early solar system II*, edited by Lauretta D. S., Leshin L. A., and McSween H. Y., Jr. Tucson, Arizona: The University of Arizona Press. pp. 525-553.

Matrajt G., Borg J., Raynal P. I., Djouadi Z., d'Hendecourt L., Flynn G., and Deboffle D. 2004. FTIR and Raman analyses of the Tagish Lake meteorite: Relationship with the aliphatic hydrocarbons observed in the Diffuse Interstellar Medium. *Astronomy and Astrophysics* 416: 983-990.

Messenger S., Amari S., Gao X., Walker R. M., Clemett S. J., Chillier X. D. F., Zare R. N., and Lewis R. S. 1998. Indigenous polycyclic aromatic hydrocarbons in circumstellar graphite grains from primitive meteorites. *Astrophysical Journal* 502: 284-295.

Murae T., Kitajima F., and Masuda A. 1991. Pyrolytic nature of carbonaceous matter in carbonaceous chondrites and secondary metamorphism. *Proceedings of the NIPR Symposium on Antarctic Meteorites* 4: 384-389.

Murae T. 1994. FT-IR spectroscopic studies of major organic matter in carbonaceous chondrites using microscopic technique and comparison with terrestrial kerogen. *Proceedings of the NIPR Symposium on Antarctic Meteorites* 7: 262-274.

Nakamura K., Zolensky M. E., Tomita S., Nakashima S., and Tomeoka K. 2002. Hollow organic globules in the Tagish Lake meteorite as possible products of primitive organic reactions.

International Journal of Astrobiology 1: 179-189.

Nakamura K., Nakashima S., Shiota D., Zolensky M. E., and Keller L. P. 2003. In Situ Heating Behavior by Infrared Microspectroscopy of Organic Components in Tagish Lake Meteorite (abstract #1432). 34th Lunar and Planetary Science Conference. CD-ROM.

Naraoka H., Mita H., Komiya M., Yoneda S., Kojima H., and Shimoyama A. 2004. A chemical sequence of macromolecular organic matter in the CM chondrites. *Meteoritics & Planetary Science* 39: 401-406.

Oba Y. and Naraoka H. 2006. Carbon isotopic composition of acetic acid generated by hydrous pyrolysis of macromolecular organic matter from the Murchison meteorite. *Meteoritics & Planetary Science* 41: 1175-1181.

Pearson V. K., Sephton M. A., Kearsley A. T., Bland P. A., Franchi I. A., and Gilmour I. 2002. Clay mineral-organic matter relationships in the early solar system. *Meteoritics & Planetary Science* 37: 1829-1833.

Pizzarello S., Krishnamurthy R. V., Epstein S., and Cronin J. R. 1991. Isotopic analyses of amino acids from the Murchison meteorite. *Geochimica et Cosmochimica Acta* 55: 905-910.

Pizzarello S., Huang Y., Becker L., Poreda R. J., Nieman R. A., Cooper C., and Williams M. 2001. The organic content of the Tagish Lake meteorite. *Science* 293: 2236-2239.

Pizzarello S., Cooper G. W., and Flynn G. J. 2006. The nature and distribution of the organic material in carbonaceous chondrites and interplanetary dust particles. In *Meteorites and the early solar system II*, edited by Lauretta D. S., Leshin L. A., and McSween H. Y., Jr. Tucson, Arizona: The University of Arizona Press. pp. 625-651.

Pizzarello S. 2007. The chemistry that preceded life's origin: A study guide from meteorites. *Chemistry & Biodiversity* 4: 680-693.

Quirico E., Raynal P. I., and Bourot-Denise M. 2003. Metamorphic grade of organic matter in six unequilibrated ordinary chondrites. *Meteoritics & Planetary Science* 38: 795-811.

Raynal P. I., Quirico E., Borg J., Deboffle D., Dumas P., d'Hendecourt L., Bibring J. P., and Langevin Y. 2000. Synchrotron infrared microscopy of micron-sized extraterrestrial grains. *Planetary and Space Science* 48: 1329-1339.

Remusat L., Derenne S., Robert F., and Knicker H. 2005a. New pyrolytic and spectroscopic data on Orgueil and Murchison insoluble organic matter: A different origin than soluble? *Geochimica et Cosmochimica Acta* 69: 3919-3932.

Remusat L., Derenne S., and Robert F. 2005b. New insight on aliphatic linkages in the macromolecular organic fraction of Orgueil and Murchison meteorites through ruthenium tetroxide oxidation. *Geochimica et Cosmochimica Acta* 69: 4377-4386.

Remusat L., Robert F., and Derenne S. 2007. The insoluble organic matter in carbonaceous chondrites: Chemical structure, isotopic composition and origin. *Comptes Rendus Geoscience*

339: 895-906.

Remusat L., Guillou C. L., Rouzaud J.-N., Binet L., Derenne S., and Robert F. 2008. Molecular study of insoluble organic matter in Kainsaz CO3 carbonaceous chondrite: Comparison with CI and CM IOM. *Meteoritics & Planetary Science* 43: 1099-1111.

Rietmeijer F. J. M. and Mackinnon I. D. R. 1985. Poorly graphitized carbon as a new cosmothermometer for primitive extraterrestrial materials. *Nature* 315: 733-736.

Robert F. and Epstein S. 1982. The concentration and isotopic composition of hydrogen, carbon and nitrogen in carbonaceous meteorites. *Geochimica et Cosmochimica Acta* 46: 81-95.

Sephton M. A., Pillinger C. T., and Gilmour I. 1998. $\delta^{13}C$ of free and macromolecular aromatic structures in the Murchison meteorite. *Geochimica et Cosmochimica Acta* 62:1821-1828.

Sephton M. A., Pillinger C. T., and Gilmour I. 1999. Small-scale hydrous pyrolysis of macromolecular material in meteorites. *Planetary and Space Science* 47:181-187.

Sephton M. A. and Gilmour I. 2000. Pyrolysis-gas chromatography-isotope ratio mass spectrometry of macromolecular material in meteorites. *Planetary and Space Science* 49: 465-471.

Sephton M. A. 2002. Organic compounds in carbonaceous meteorites. *Natural Product Reports* 19: 292-311.

Sephton M. A., Verchovsky A. B., Bland P. A., Gilmour I., Grady M. M., and Wright I. P. 2003. Investigating the variations in carbon and nitrogen isotopes in carbonaceous chondrites. *Geochimica et Cosmochimica Acta* 67: 2093-2108.

Sephton M. A., Love G. D., Watson J. S., Verchovsky A. B., Wright I. P., Snape C. E., and Gilmour I. 2004. Hydropyrolysis of insoluble carbonaceous matter in the Murchison meteorite: New insights into its macromolecular structure. *Geochimica et Cosmochimica Acta* 68: 1385-1393.

Sephton M. A., Love G. D., Meredith W., Snape C. E., Sun C. G., and Watson J. S. 2005. Hydropyrolysis: A new technique for the analysis of macromolecular material in meteorites. *Planetary and Space Science* 53: 1280-1286.

Shimoyama A., Komiya M., and Harada K. 1991. Release of organic compounds from some Antarctic CI and CM chondrites by laboratory heating. *Proceedings of the NIPR Symposium on Antarctic Meteorites* 4: 247-260.

Tonui E., Zolensky M. E., Hiroi T., Nakamura T., Lipschutz M. E., Wang M. -S., and Okudaira K. In preparation. Petrographic, chemical and spectroscopic evidence for thermal metamorphism in carbonaceous chondrites I: CI and CM chondrites. *Geochimica et Cosmochimica Acta*.

Varela M. E. and Metrich N. 2000. Carbon in olivines of chondritic meteorites. *Geochimica et Cosmochimica Acta* 64: 3433-3438.

Wdowiak T. J., Flickinger G. C., and Cronin J. R. 1988. Insoluble organic material of the Orgueil

carbonaceous chondrite and the unidentified infrared bands. *Astrophysical Journal* 328: L75-L79.

Weisberg M. K., McCoy T. J., and Krot A. N. 2006. Systematics and evaluation of meteorite classification. In *Meteorites and the early solar system II*, edited by Lauretta D. S., Leshin L. A., and McSween H. Y., Jr. Tucson, Arizona: The University of Arizona Press. pp. 19-52.

Yabuta H., Naraoka H., Sakanishi K., Kawashima H. 2005. Solid-state ^{13}C NMR characterization of insoluble organic matter from Antarctic CM2 chondrites: Evaluation of the meteoritic alteration level. *Meteoritics & Planetary Science* 40: 779-787.

Yabuta H., Williams L. B., Cody G. D., Alexander C. M. O'D., and Pizzarello S. 2007. The insoluble carbonaceous material of CM chondrites: A possible source of discrete organic compounds under hydrothermal conditions. *Meteoritics & Planetary Science* 42:37-48.

Yang J. and Epstein S. 1983. Interstellar organic-matter in meteorites. *Geochimica et Cosmochimica Acta* 47: 2199-2216.

Zolensky M. E., Abell P. A., and Tonui E. K. 2005. Metamorphosed CM and CI carbonaceous chondrites could be from the breakup of the same earth-crossing asteroid (abstract #2084). 36th Lunar and Planetary Science Conference. CD-ROM.

Chapter 2

RAPID CONTAMINATION DURING STORAGE OF CARBONACEOUS CHONDRITES PREPARED FOR MICRO FTIR MEASUREMENTS

This chapter is in press as:
Kebukawa Y., Nakashima S., Otsuka T., Nakamura-Messenger K., and Zolensky M. E. In press. Rapid contamination during storage of carbonaceous chondrites prepared for micro FTIR measurements. *Meteoritics & Planetary Science*.

Abstract

Organic contamination (~2965 and ~1260 cm^{-1} peaks) was found on Tagish Lake (C2) and Murchison (CM2) carbonaceous chondrites containing abundant hydrous minerals by Fourier transform infrared (FTIR) microspectroscopy on the samples pressed on Al plates. On the other hand, anhydrous chondrite (Moss, CO3) was not contaminated. This contamination occurred within one day of storage, when the samples pressed on Al were stored within containers including silicone rubber mats. Volatile molecules having similar peaks to the contaminants were detected by long-path gas cell FTIR measurements for the silicone rubber mat. Rapid adsorption of the volatile contaminants also occurred when silica gel and hydrous minerals such as serpentine were stored in containers including silicone rubber, silicone grease or adhesive tape. However, they did not show any contamination when stored in glass and polystyrene containers without these compounds. Therefore, precious astronomical samples such as meteorites, interplanetary dust particles (IDPs) and mission returned samples from comets, asteroids and Mars, should be measured by micro FTIR within one day of storage in glass containers without silicone rubber, silicone grease or adhesive tape.

2.1. Introduction

Asteroids and comets could have provided the early Earth with life's precursor molecules, and studies of carbonaceous chondrite meteorites (presumably derived from primitive asteroids) provide a record of organic prebiotic chemistry in the early solar system (Pizzarello et al. 2006). Carbonaceous chondrites are known to contain up to a few wt% of indigenous organic matter which have been successfully analyzed by various methods such as nuclear magnetic resonance (NMR), X-ray absorption near-edge structure (XANES), gas chromatography-mass spectrometry (GCMS), Fourier transform infrared (FTIR) spectroscopy, and Raman spectroscopy (e.g., Botta and Bada 2002; Sephton 2002; Pizzarello et al. 2006).

On the other hand, a number of possible terrestrial contamination sources have already been suggested. The $\delta^{13}C$ values for the n-alkanes from carbonaceous chondrites are identical to those of petroleum-based products and other mixtures of fossil hydrocarbons (Sephton et al. 2001). The compounds pristane and phytane, found in some chondrites, are thought to be biological contaminants partly due to their structural specificity which is unlikely to be produced by abiotic processes (Cronin and

Pizzarello 1990). Plows et al. (2003) suggested that much of the atmospheric PAH pollution emitted from sources such as internal combustion engines contains a large proportion of alkylated PAHs (Kawamura et al. 1994; Gingrich et al. 2001). Cronin and Pizzarello (1990) proposed possible airborne source of terrestrial contamination including petroleum distillates such as vacuum pump oils, lubricating fluids for rock saws for cutting meteorites, and plasticizers. The sesquiterpenoid derivatives detected in the Orgueil meteorite are essentially plant oil-derived terrestrial contaminants (Watson et al. 2003). Phthalate esters and diisopropylnaphthalenes reported in Orgueil are known to be common laboratory contaminants (Watson et al. 2003). Carbonaceous chondrites which have long terrestrial ages, such as Orgueil, can provide valuable evidence of the effects of long term exposure to potential terrestrial contaminants (Watson et al. 2003).

Despite these minor contamination problems, majority of chondritic organic matter can be assumed indigenous due to some evidences such as isotopic composition (e.g., Sephton 2002).

Recently, contamination originated from sample storage bags and containers during curation and preservation has been considered to be an important issue on both terrestrial and extraterrestrial samples. A nylon bag used to store Antarctic meteorite samples yielded ε-amino-n-caproic acid (EACA) by hydrolysis, and EACA found in an Antarctic meteorite (ALH 83100) using liquid chromatography-time of flight-mass spectrometry was assumed to be nylon contamination (Glavin et al. 2006). Polyethylene sampling bags were found to be the main source of contamination for fatty acid amides, butylated hydroxytoluene, branched alkanes with a quaternary carbon atom and alkylcyclopentanes found in some sediment samples using gas chromatography-mass spectrometry (Grosjean and Logan 2007; Brocks et al. 2008).

Fourier transform infrared (FTIR) spectroscopy is a non-destructive technique for organic components and minerals, and has been successfully applied to chondritic organic matter mainly based on aliphatic stretching features in the region 3000-2800 cm^{-1} (Hayatsu et al. 1977; Wdowiak et al. 1988; Ehrenfreund et al. 1991, 1992; Murae 1994; Raynal et al. 2000; Flynn et al. 2001; Keller and Flynn 2001; Nakamura et al. 2002, 2003a; Kissin 2003; Matrajt et al. 2004), hydrated and anhydrous interplanetary dust particles (IDPs) (Sandford and Walker 1985; Swan et al. 1987; Bradley et al. 1992; Clemett et al. 1993; Flynn et al. 1998, 2002, 2003, 2004; Keller et al. 2004; Matrajt et al. 2005), and cometary dust grains captured from Comet 81P/Wild 2 by the Stardust spacecraft (Keller et al. 2006; Sandford et al. 2006; Rotundi et al. 2008).

The organic features such as aliphatic stretching vibrations observed by FTIR of

both bulk chondrites and insoluble organic matter (IOM) occupying the majority of organic matter (over 70 wt%) in carbonaceous chondrites (e.g., Pizzarello et al. 2006) have typically been considered to be of indigenous origin, since terrestrial contaminants are likely to be found in the free fraction (which is relatively susceptible to contamination) but not within the organic macromolecular component (which is less prone to contamination) (Watson et al. 2003). Furthermore, infrared spectra of IOM show an equivalent intensity of the aliphatic C−H stretching absorptions for CH_3 (2960 cm^{-1}) and CH_2 (2920 cm^{-1}), and a lack of aromatic C−H stretching absorption (3040 cm^{-1}), which are similar to the interstellar carbonaceous grains (without terrestrial contamination) (Ehrenfreund et al. 2002). Therefore, the infrared organic features such as aliphatic stretching vibrations of bulk chondrites have been considered to reflect mainly the indigeneous organic matter.

However, in some cases, the C−H bands of infrared reflectance spectra taken from powdered meteorites have been suggested to be due to contamination from volatile hydrocarbons in laboratory air adsorbing on mineral and rock powders (Salisbury and Walter 1989; Salisbury et al. 1991).

Here, I report a new type of rapid contamination (occurring within one day) during storage after sample preparation for micro FTIR (pressed on Al) due to volatile organic compounds from some laboratory materials commonly used for sample preparation and storage. For example, adhesives were used to fix samples particularly when we transfer the sample. Silicone grease was often used with vacuum desiccators. Silicone rubber was used with storage containers and some laboratory equipments. Volatile compounds from these materials can be adsorbed on the samples prepared for micro FTIR measurements. Although these materials are not used during detailed organic analyses on precious samples, these contaminations need to be evaluated for the curation and organic analyses of extraterrestrial and terrestrial samples at least during their initial characterization by micro FTIR and other methods.

2.2. Samples and Experimental Methods

2.2.1. Samples

Carbonaceous chondrites: (a) Tagish Lake meteorite (ungrouped type 2 chondrite) fell in January of 2000 onto a frozen lake in Canada. Its matrix consists mainly of saponite, serpentine, Fe-Ni sulfides, carbonates, olivine and magnetite (Brown et al. 2000; Zolensky et al. 2002; Nakamura et al. 2003b). (b) Murchison (CM2) fell in 1969 in Australia. Its matrix consists mainly of serpentine, tochilinite, Fe-Ni sulfides,

carbonates, olivine and Fe-Ni metal (Zolensky and McSween 1988; Zolensky et al. 1993). (c) Moss (CO3) fell in 2006 in Norway, and consists mainly of olivine, troilite and kamacite (Bischoff and Schmale 2007; Greenwood et al. 2007). Moss has an unusually low matrix-to-chondrule ratio (Greenwood et al. 2007).

Natural and synthetic minerals used were as follows. (d) Antigorite: $(Mg,Fe^{2+})_3Si_2O_5(OH)_4$; from Nakanochaya, Miyatsu, Kyoto, Japan; obtained from Nichika Corp. in fine powder form, (e) Muscovite: $KAl_2(Si_3Al)O_{10}(OH)_2$; from Ishikawa, Fukushima, Japan; Several small muscovite flakes were crushed to a fine powder using an alumina mortar and pestle, (f) Synthetic montmorillonite powder: pure (99%) sodium montmorillonite; $Na_{0.33}(Al,Mg)_2Si_4O_{10}(OH)_2{\cdot}nH_2O$; called Kunipia F®, obtained from Kunimine Industries Co., Ltd.

Chemical regents were as follows. (g) Silica gel: $SiO_2{\cdot}nH_2O$; Wakosil C-300, 40-64 μm (spherical powder); from Wako Pure Chemical Industries, Ltd., (h) Silicon dioxide: SiO_2; from Wako Pure Chemical Industries, Ltd., (i) Potassium bromide: KBr; from JASCO International Co., Ltd.; A cubic crystal of KBr (~5 mm) was crushed to a fine powder using an alumina mortar and pestle. All these samples used in this study were not cleaned or activated.

2.2.2. Sample Preparation Procedures

Micro FTIR spectroscopy is a well-established technique for the identification of organic functional groups. For organic analyses of extraterrestrial samples such as meteorites and IDPs, samples were usually mounted on KBr (Sandford and Walker 1985; Wdowiak et al. 1988; Clemett et al. 1993, 2004; Flynn et al. 1998; Nakamura et al. 2002, 2003a; Matrajt et al. 2004; Quirico and Bonal 2004; Keller et al. 2006; Rotundi et al. 2008) or metal plates (Al: Murae 1994; Nakamura et al. 2003a, Au: Keller et al. 2006; Sandford et al. 2006; Rotundi et al. 2008). In this study, we chose metal (Al) plates for sample mounting, because metal mounted samples can be easily used for other multiple analyses such as scanning electron microscopy (SEM) and visible reflection micro-spectroscopy (Suzuki et al. in press). For the SEM observation, surface charge up of electrons is better prevented by metal substrate than KBr. Infrared spectra obtained from samples on Al (reflection mode) and KBr (transmission mode) shows similar results in the 4000-1100 cm^{-1} range, although spectra collected on Al show complex bands around 1000 cm^{-1} (Si−O) because of strong absorption-reflection on the grain surface. In addition, organic contamination also appeared on samples mounted on KBr and Au during storage in polystyrene trays with silicone rubber mats.

Therefore, the present contamination study can also be applied to any sample mounting procedures.

For the present FTIR spectroscopic measurements, the sample powders were pressed between two Al plates (0.08 mm thick) using an oil pressure pump at about 100 kgw/cm^2 to make the sample flat and fixed on the Al plate. The two Al plates were then separated and the resultant flattened grains on an Al plate were used for infrared transmission-reflection spectroscopy. We used the oil pressure pump because we found that the samples pressed by hand sometimes partially dropped out during storage and handling. Since silica gel samples pressed on Al plates by the oil pressure pump were not contaminated in a glass petri dish and a polystyrene tray (see the results section), oil of the pump was not a source of contamination.

2.2.3. Infrared Microspectroscopy

A ceramic infrared light source, a Mercury-Cadmium-Telluride (MCT) detector and a ×16 Cassegrainian mirror were used for the FTIR spectroscopy (Jasco FT-IR-620 + IRT30).

Transmission-reflection spectra were collected at room temperature in the range 4000-700 cm^{-1}, with a 100 × 100 μm^2 aperture. Infrared incident light was first transmitted through the sample, which was typically a few tens of micrometers thick, then reflected off from the surface of Al plate, and again transmitted through the sample (Okumura and Nakashima 2004). The background spectra were collected on the Al plate.

2.2.4. Storage Procedures

Infrared spectra were collected immediately after sample preparation and then stored in a polystyrene tray with a silicone rubber mat for 14-30 hours in a desiccator. The silicone rubber mat was not heat treated (so not ‘conditioned’). After this storage, infrared spectra of the same sample positions were measured again.

In order to verify the contamination from storage containers, the silica gel samples pressed on Al plates were fixed and stored in the following five different ways: (1) in a polystyrene tray with a silicone rubber mat, (2) in a polystyrene tray without silicone rubber mat, (3) in a glass petri dish, and the dish with its glass cover was wrapped in an Al foil, (4) in a glass petri dish fixed with silicone grease, and the dish with its glass cover was wrapped in an Al foil, (5) in a glass petri dish fixed with adhesive tape, and

the dish with its glass cover was wrapped in an Al foil. All these sample storage containers were stored in a desiccator. After 16-26 hours of storage, infrared spectra of the same sample positions were measured.

2.2.5. Gas Cell FTIR Analyses

A long path gas cell (Infrared Analysis Inc., 10-PA) was used to measure infrared spectra of volatile compounds emitted from the silicone rubber mat. The infrared light pass length was 10 m by 40-fold reflection and the volume was 2.3 L. The gas cell was attached to an FTIR spectrometer (Bomem MB154). Infrared spectra were measured at room temperature with an infrared light source, a MCT detector, and a CsI beam splitter (Ishikawa et al. 2007). The silicone rubber mat (87 × 87 mm^2) was placed into the gas cell. Then infrared spectra of the volatiles from the silicone rubber mat in the atmosphere (air) at room temperature were collected. Infrared spectra were first collected immediately after placing the silicone rubber mat in the gas cell, then every 10 minutes for a total of 26 hours. 128 scans were stacked at 1 cm^{-1} resolution in the 7000-500 cm^{-1} range.

2.2.6. Step Heating Experiments

In order to try to eliminate organic contaminants adsorbed on the natural samples, contaminated Tagish Lake and antigorite on Al plates after the storage in polystyrene trays with silicone rubber mats were set onto a heating stage (Linkam FTIR 600) and placed into the micro FTIR. After measuring the sample spectra at room temperature, the samples were heated at 10 ºC/min from room temperature up to 500ºC using the heating stage under ambient air. During the heating, sample spectra were collected from the same location at every 10ºC step. The temperature was kept constant during the collection of the sample spectra.

2.3. Results

2.3.1. Organic Contamination of Various Materials Stored in Polystyrene Trays with Silicone Rubber Mats

Samples pressed on Al plates stored in polystyrene trays with silicone rubber mats were (a) Tagish Lake, (b) Murchison, (c) Moss, (d) antigorite, (e) muscovite, (f) montmorillonite, (g) silica gel, (h) silicon dioxide and (i) KBr.

(a) Tagish Lake and (b) Murchison samples show weak infrared absorption bands around 2900 and 1260 cm^{-1} just after the sample pressing on Al plates. Intensities of these absorption bands increased after 24-30 hours of storage in the polystyrene tray with the silicone rubber mat (Figs. 2-1a,b and 2-2a,b). On the other hand, no organic features are detected on the (c) Moss meteorite even after 24 hours of storage (Figs. 2-1c and 2-2c). Contamination features observed after ~1 day storage are summarized in Table 1 with each materials and their storage containers.

The infrared absorption spectra before storage of (a) Tagish Lake show a shoulder around 3650 cm^{-1} due to structural hydroxyl (O−H) (Fig. 2-1a). A broad O−H stretching band around 3400 cm^{-1} (Fig. 2-1a) and an H−O−H bending band around 1630 cm^{-1} (Fig. 2-2a) are probably due to water molecules loosely adsorbed to minerals (Murae 1994) and as interlayer molecular water in phyllosilicates (Keller and Flynn 2001). Since serpentine and saponite are reported to be present in the matrix of Tagish Lake (Zolensky et al. 2002; Nakamura et al. 2003b), 3650 and 3400 cm^{-1} bands might correspond to these minerals. The absorption feature at 1450 cm^{-1} (Fig. 2-2a) can be due to carbonates.

The 2963 and 2875 cm^{-1} bands of (a) Tagish Lake are considered to be due to asymmetric and symmetric stretching vibrations of aliphatic CH_3, respectively, while the 2940 cm^{-1} band is due to aliphatic CH_2 vibrations (Figs. 2-1a). The 1262 cm^{-1} band (Figs. 2-2a) can be assigned to Si−CH_3 bending vibrations. These organic features appeared to have increased after storage. The 1450 cm^{-1} band shows a slight increase after storage. This band might therefore include contributions from aliphatic C−H bending vibration modes of contaminants.

The infrared absorption before storage spectra of (b) Murchison show a broad O–H stretching band around 3400 cm^{-1} (Fig. 2-1b) and an H−O−H bending band around 1640 cm^{-1} (Fig. 2-2b) due to water molecules. The 2963 and 2872 cm^{-1} bands due to aliphatic CH_3, the 2940 cm^{-1} band due to aliphatic CH_2 (Figs. 2-1b), and the 1262 cm^{-1} band due to Si−CH_3 (Figs. 2-2b) have increased after storage. The 1530 and 1460 cm^{-1} band appeared after storage (Fig. 2-2b). The 1530 cm^{-1} band is plausibly due to N–H. The 1460 cm^{-1} band is probably due to aliphatic C−H bending.

The infrared absorption spectra before storage of (c) Moss do not show particular bands at 4000-2500 cm^{-1} (Fig. 2-1c) and 1800-1200 cm^{-1} regions (Fig. 2-2c). Noise at 4000-3500 cm^{-1} and 1800-1500 cm^{-1} were due to atmospheric water vapor. No significant spectral changes were observed following storage for 24 hours.

Some organic features appeared in the spectra of (d) antigorite, (e) muscovite, (f) montmorillonite and (g) silica gel, pressed on Al plates and stored in the polystyrene

tray with the silicone rubber after 14-26 hours of storage (Figs. 2-1d,e,f,g and 2-2d,e,f,g; Table 2-1). No organic features appeared in the spectra of (h) silicon dioxide and (i) KBr (Figs. 2-1h,i and 2-2h,i; Table 2-1).

The infrared absorption spectra before storage of (d) antigorite, (e) muscovite and (f) montmorillonite show features around 3600cm^{-1} due to structural O−H (Figs. 2-1d,e,f). The infrared absorption spectra of (d) antigorite, (e) muscovite, (f) montmorillonite and (g) silica gel show a broad O−H stretching band around 3400 cm^{-1} (Figs. 2-1d,e,f,g) and an H−O−H bending band around 1640 cm^{-1} (Figs. 2-2d,e,f,g) due to water molecules. The 1260 cm^{-1} band of muscovite (Fig. 2-2e) can be due to Si−CH_3 which might represent contamination before our present sample preparation, because the muscovite sample was natural and not cleaned.

Infrared spectra of (d) antigorite, (e) muscovite, (f) montmorillonite and (g) silica gel after 14-26 hours of storage show some organic absorption features at ~2965, ~2875 cm^{-1} due to CH_3, ~2940 cm^{-1} due to CH_2 (Figs. 2-1d,e,f,g), and 1470-1370 cm^{-1} due to aliphatic C−H bending (Figs. 2-2d,e,f,g). A band around 1545-1520 cm^{-1} might be due to N−H (Figs. 2-2d,e,f,g). The 1700 cm^{-1} band of (g) silica gel is probably due to C=O (Fig. 2-2g). The ~1260 cm^{-1} band of (d) antigorite, (e) muscovite and (g) silica gel is probably due to Si−CH_3 (Figs. 2-2d,e,g).

The infrared spectrum of (h) silicon dioxide shows bands at 2000-1000 cm^{-1} region due to Si−O stretching absorption within silicates (Fig. 2-2h). A broad O−H stretching band around 3400 cm^{-1} of (h) silicon dioxide was due to adsorbed water molecules (Fig. 2-1h). No significant spectral change was observed on (h) silicon dioxide and (i) KBr after storage for 25 hours.

In summary, the infrared spectra of samples pressed on Al plates stored in polystyrene trays with silicone rubber mats for (a) Tagish Lake, (b) Murchison, (d) antigorite, (e) muscovite, (f) montmorillonite and (g) silica gel showed organic features after storage, while those for (c) Moss, (h) silicon dioxide and (i) KBr did not (Figs. 2-1 and 2-2; Table 2-1).

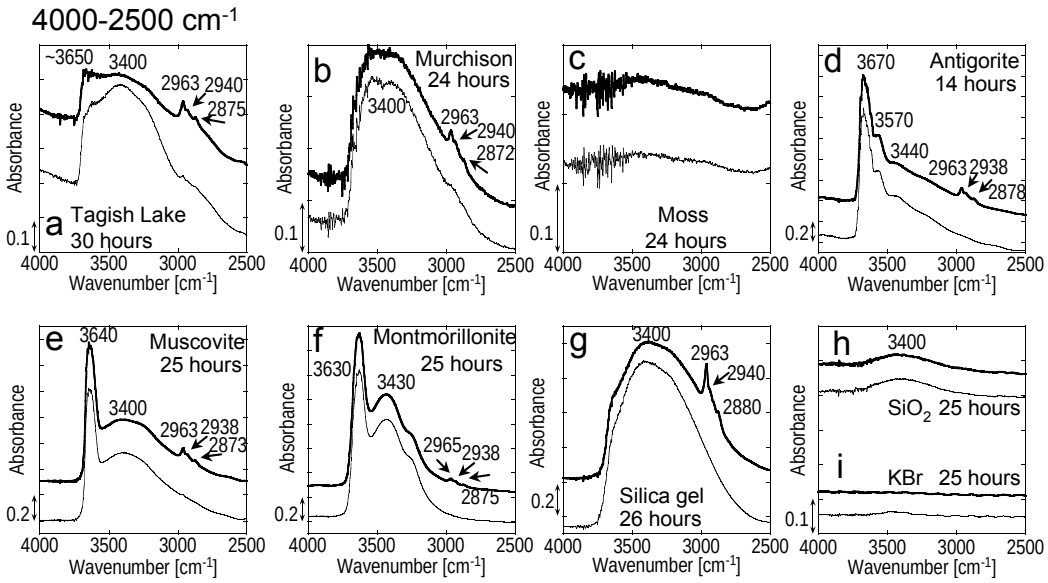

Fig. 2-1. Infrared transmission-reflection spectra of 4000-2500 cm^{-1} regions of the samples pressed on Al plates before (thin curves) and after (thick curves) storage in the polystyrene tray with the silicone rubber mat for 14-30 hours. (a) Tagish Lake meteorite, (b) Murchison meteorite, (c) Moss meteorite, (d) antigorite, (e) muscovite, (f) montmorillonite, (g) silica gel, and (h) silicon dioxide and (i) KBr.

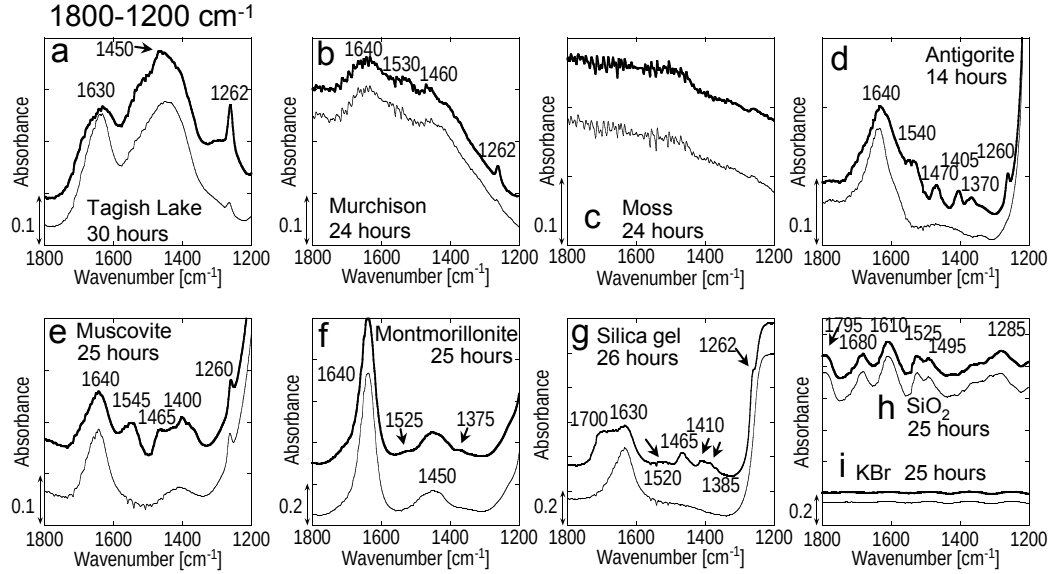

Fig. 2-2. Infrared transmission-reflection spectra of 1800-1200 cm^{-1} regions of the samples pressed on Al plates before (thin curves) and after (thick curves) storage in the polystyrene tray with the silicone rubber mat for 14-30 hours. (a) Tagish Lake meteorite, (b) Murchison meteorite, (c) Moss meteorite, (d) antigorite, (e) muscovite, (f) montmorillonite, (g) silica gel, and (h) silicon dioxide and (i) KBr.

Table 2-1. Summary of contamination of the tested materials and the storage containers.

Storage containers	Materials	Aliphatic C−H	C=O	N−H ?	$Si-CH_3$	
		2970-2870, 1470-1370	1700	1545-1520	1265-1260	[cm^{-1}]
Polystyrene tray + silicone rubber mat	Tagish Lake	+	−	−	+	
	Murchison	+	−	+	+	
	Moss	−	−	−	−	
	Antigorite	+	−	+	+	
	Muscovite	+	−	+	+	
	Montmorillonite	+	−	+	−	
	Silica gel	+	+	+	+	
	Silicon dioxide	−	−	−	−	
	KBr	−	−	−	−	
Polystyrene tray	Silica gel	−	−	−	−	
Glass petri dish	Silica gel	−	−	−	−	
Glass petri dish + silicone grease	Silica gel	+	−	−	+	
Glass petri dish + adhesive tape	Silica gel	+	−	−	−	

+:detected, −: not detected

2.3.2. Changes with Time of the Organic Features of Silica Gel Samples

For studying time scales of the above organic contamination, infrared spectral changes with time were measured at room temperature during 52 hours on two locations of the silica gel sample pressed on the Al plate stored in the polystyrene tray with the silicone rubber mat. The aliphatic C−H stretching peak at 2965 cm^{-1} with 3000-2890 cm^{-1} baseline for one silica gel sample position steadily increased during 52 hours of storage, and that for the other position increased up to 28 hours then became constant (Fig. 2-3). These results indicate organic adsorption on the silica gel within a few days.

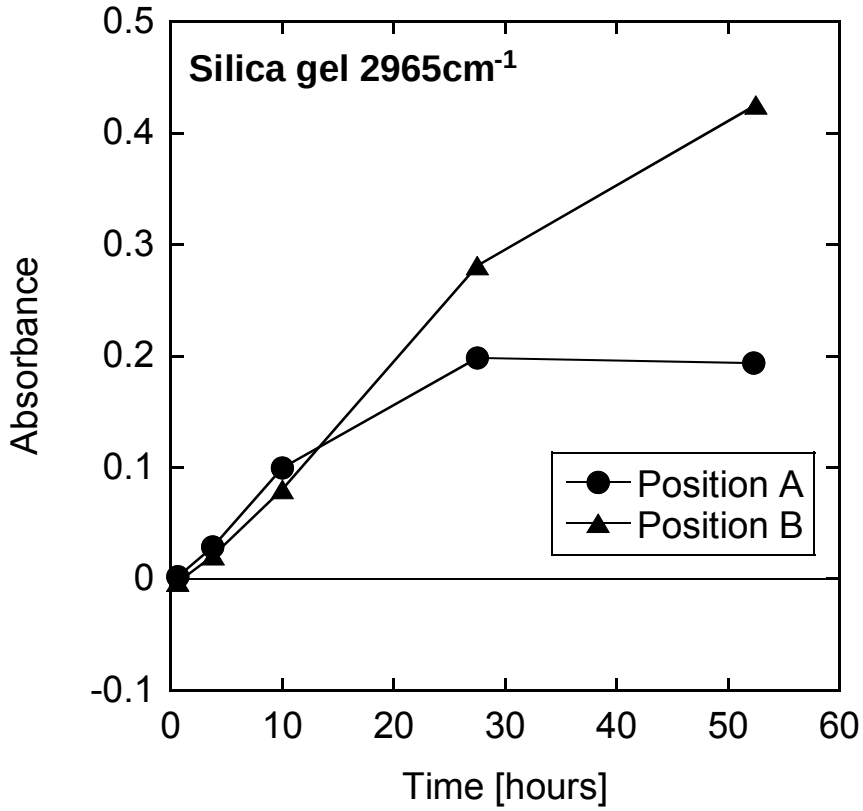

Fig. 2-3. Changes with time of aliphatic C−H peak heights at 2965 cm^{-1} of silica gel stored in the polystyrene tray with a silicone rubber mat at room temperature. The two different symbols represent different parts of the silica gel samples.

2.3.3. The Gas Cell FTIR Measurements

In order to investigate origins of organic contamination on the above samples, volatile organic compounds were measured with long path gas cell FTIR method. Infrared spectra were first collected immediately after placing the silicone rubber mat in

the gas cell, then every 10 minutes for 26 hours. Fig. 2-4 shows a spectrum for volatiles from the silicone rubber mat in the atmospheric air of the gas cell after 3 hours. The 3250 cm^{-1} band can be due to O−H or N−H, the 2970 and 2905 cm^{-1} bands are due to CH_3, the 1265 cm^{-1} band is due to Si−CH_3, the 1080 cm^{-1} band is due to Si−O, and the 900, 850 and 810 cm^{-1} bands are due to Si−C. Absorption intensities of these organic features rapidly increased within approximately one hour then increased slowly (Figs. 2-5 and 2-6). Volatile compounds including CH_3, Si−CH_3, Si−O and Si−C bonds are emitted rapidly from the silicone rubber mat. These are then considered to be adsorbed on the contaminated materials such as the silica gel within a few days.

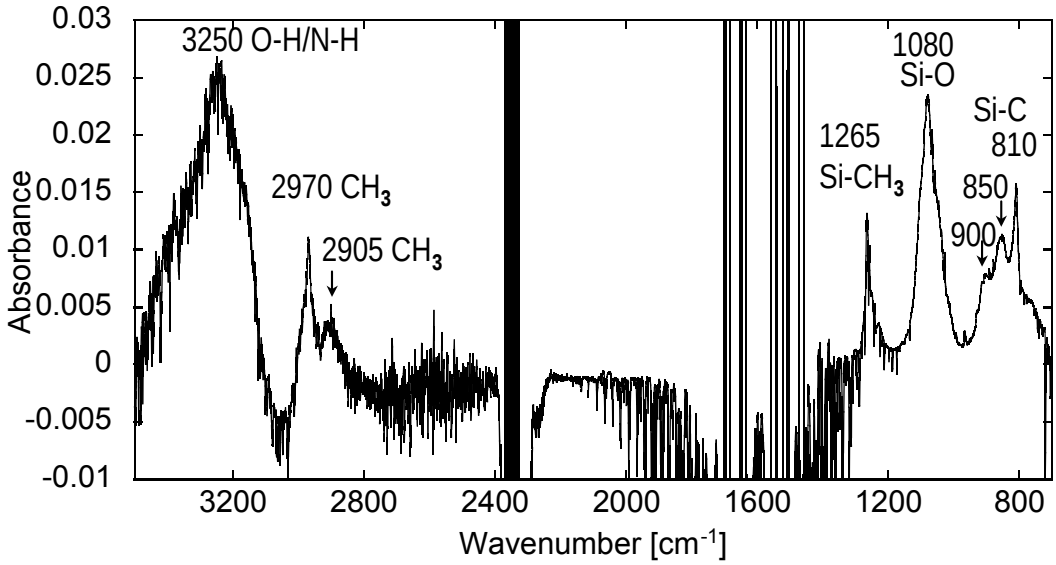

Fig. 2-4. The infrared spectrum of volatiles from the silicone rubber mat in the air of the gas cell after 3 hours: 3250 cm^{-1} band is due to O−H or N−H, 2970 and 2905 cm^{-1} bands are due to CH_3, 1265 cm^{-1} band to Si−CH_3, 1080 cm^{-1} band to Si−O, and 900, 850 and 810 cm^{-1} bands to Si−C.

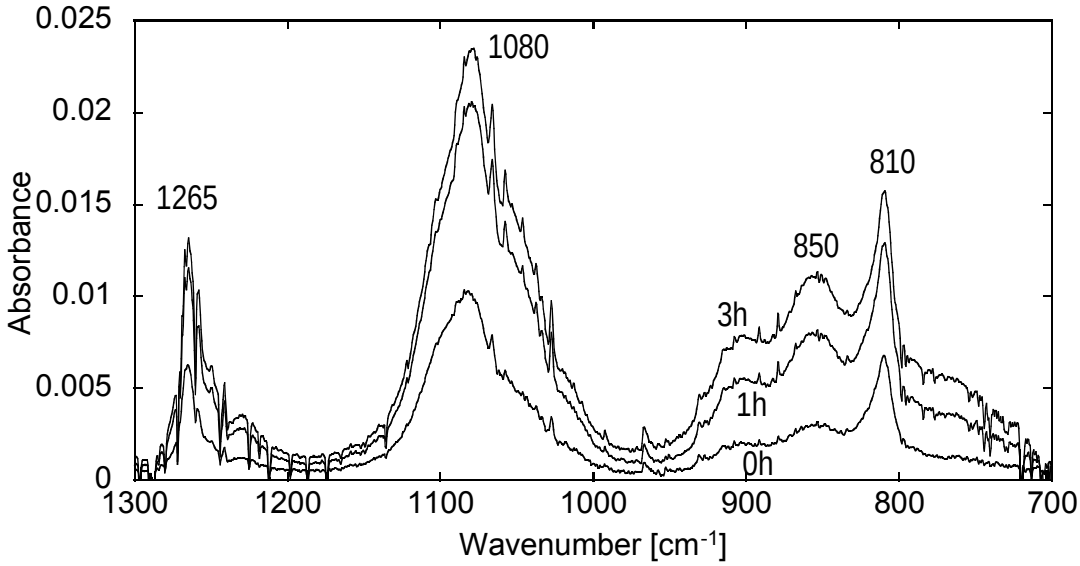

Fig. 2-5. The infrared spectra of 1300-700 cm^{-1} regions of volatiles from the silicone rubber mat in the air of the gas cell, immediately after the placement of the silicone rubber mat in the gas cell (0 hour), after 1 hour and 3 hours.

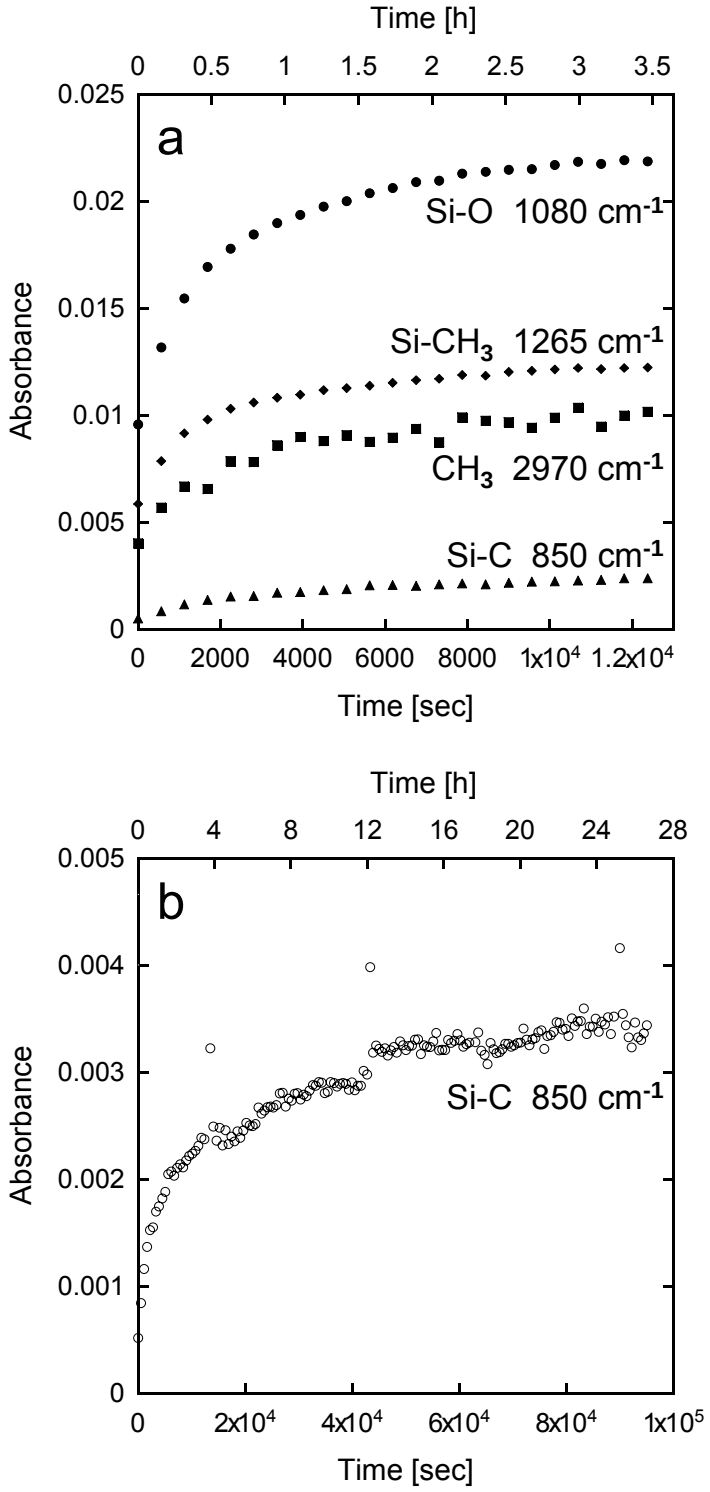

Fig. 2-6. Changes with time in infrared absorption peak heights of volatiles from the silicone rubber in the long path gas cell. (a) 2970 cm^{-1} peak due to CH_3, 1265 cm^{-1} peak due to Si−CH_3, 1080 cm^{-1}peak due to Si−O, and 850 cm^{-1} peak due to Si−C for 3.5 hours. (b) 850 cm^{-1} peak due to Si−C for 26 hours.

2.3.4. Contamination Experiments with Silica Gel

In order to search for storage conditions avoiding organic contamination on precious samples, infrared spectra were measured after 16-26 hours of storage in various conditions on the silica gel which showed significant contamination by the storage (1) in the polystyrene tray with the silicone rubber mat (Figs. 2-1g and 2-2g; Table 2-1).

No organic features appeared on the spectra of (2) silica gel pressed on Al plates stored without the silicone rubber mat in the polystyrene tray for 24 hours (Figs. 2-7a and 2-8a; Table 2-1). The polystyrene tray itself is not the contamination source.

The polystyrene stray (95 × 95 mm^2) with the silicone rubber mat (87 × 87 mm^2) was first selected for the storage container because of easiness of placing samples pressed on Al plates (about 5 × 5 mm^2) in hollow grids (6 × 8 grids, each 10 × 10 mm^2 in size) of the silicone rubber mat. However, the polystyrene tray without the silicone rubber mat grid is too large to store only one sample. Therefore, the glass petri dish of about 50 mm in diameter was used here to store these small samples. This container made of glass was considered to be the most appropriate organic-free container. In fact, IR spectra for (3) the silica gel pressed on Al plates stored in the glass petri dish for 26 hours did not show any organic features (Figs. 2-7b and 2-8b; Table 2-1).

If we should transport these small samples in the glass petri dishes, we need to fix the samples on Al plates. Silicone grease and adhesive tapes are often used to fix this kind of samples. Silicone grease is also used for sealing vacuum chambers of sample storage and some instruments. The spectra of (4) the silica gel sample pressed on the Al plate, which was fixed with silicone grease in a glass petri dish and stored for 16 hours show some organic absorption features at 2967 cm^{-1} peak due to stretching absorptions of CH_3 (Fig. 2-7c), 1410 cm^{-1} due to C−H bending, and 1265 cm^{-1} due to Si−CH_3 (Fig. 2-8c). The spectra of (5) the silica gel sample pressed on the Al plate, which was fixed with adhesive tape in a glass petri dish and stored for 25 hours show some organic absorption features at 2957 and 2870 cm^{-1} due to CH_3 (Fig. 2-7d) and 1480, 1470, 1455, 1395 and 1367 cm^{-1} bands due to aliphatic C−H bending (Fig. 2-8d). Therefore, the silicone grease and the adhesive tape appeared to contain volatile organic contaminants and should not be used for storing and transporting the samples pressed on Al plates.

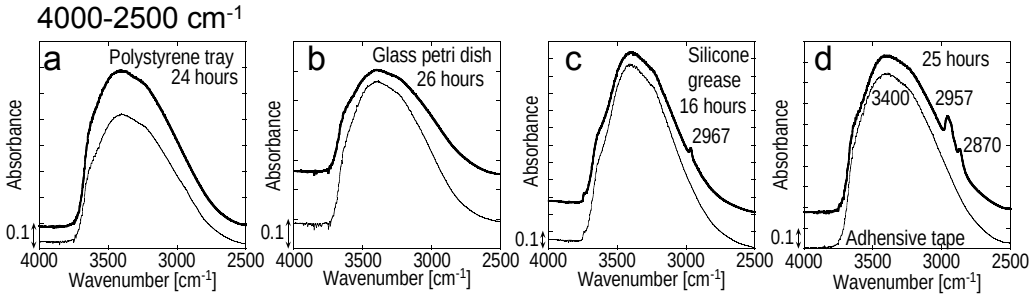

Fig. 2-7. Infrared transmission-reflection spectra of 4000-2500 cm^{-1} regions of silica gel pressed on Al plates before (thin curves) and after (thick curves) the following storage conditions for 16-26 hours: (a) in a polystyrene tray without silicone rubber, (b) in a glass petri dish and the dish with its glass cover was wrapped in an Al foil, (c) in a glass petri dish fixed with silicone grease, and the dish with its glass cover was wrapped in an Al foil, and (d) in a glass petri dish fixed with adhesive tape, and the dish with its glass cover was wrapped in an Al foil.

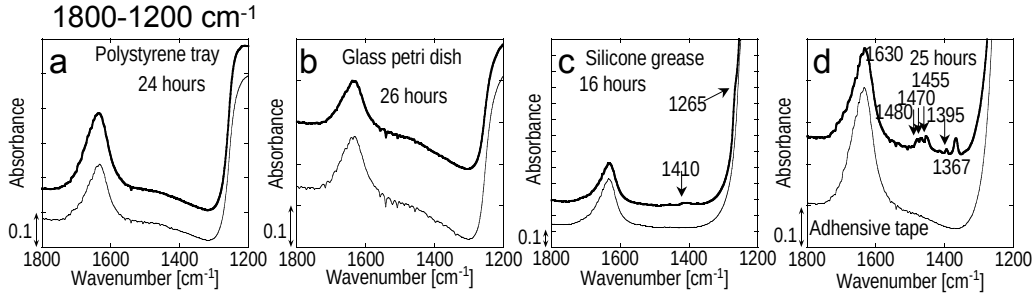

Fig. 2-8. Infrared transmission-reflection spectra of 1800-1200 cm^{-1} regions of silica gel pressed on Al plates before (thin curves) and after (thick curves) the following storage conditions for 16-26 hours: (a) in a polystyrene tray without silicone rubber, (b) in a glass petri dish and the dish with its glass cover was wrapped in an Al foil, (c) in a glass petri dish fixed with silicone grease, and the dish with its glass cover was wrapped in an Al foil, and (d) in a glass petri dish fixed with adhesive tape, and the dish with its glass cover was wrapped in an Al foil.

2.4. Discussion

2.4.1. Contamination from Silicone Materials and Adhesive Tape

Organic contaminants appeared on some samples pressed on Al plates stored in

polystyrene trays with silicone rubber mats or glass petri dishes with silicone grease or adhesive tapes. These samples were never directly in contact with anything except for laboratory air and the sample mounting Al plates during one day storage.

Although polystyrene is known to contain volatile organic compounds such as styrene, alkyl benzene and benzyl alcohol (Kusch and Knupp 2004), the silica gel sample stored in the polystyrene tray as well as the glass petri dish did not show any organic contamination after storage in one day (Figs. 2-7a,b and 2-8a,b; Table 2-1). Therefore, organic volatile molecules from the silicone rubber mats, silicone grease and adhesive tapes must have been adsorbed on the samples.

Silicone rubber is mainly composed of polydimethylsiloxane with minor carboxylic acids and phthalates (Deshpande and Rezac 2001). Degradation products decomposed and vaporized from silicone rubber are reported to be primarily cyclic methylsiloxane oligomers (Deshpande and Rezac 2001). 2970 (CH_3) , 2905 (CH_3), 1265(Si−CH_3), 1080 (Si−O), 900 (Si−C), 850 (Si−C) and 810 cm^{-1} (Si−C) absorption peaks observed by the gas cell FTIR for volatile compounds from the silicone rubber mat (Fig. 2-4) can therefore be due mainly to methylsiloxane oligomers. The 2970 and 1265 cm^{-1} absorption peaks (due to CH_3 and Si−CH_3 groups, respectively) of the volatile compounds from the silicone rubber mat (Fig. 2-4) are similar to the contamination organics on the samples (~2965 and ~1260 cm^{-1}, respectively) (Figs. 2-1 and 2-2; Table 2-1).

Contamination also appeared on the silica gel samples stored in glass petri dishes fixed with silicone grease and adhesive tape (Figs. 2-7c,d and 2-8c,d; Table 2-1). The spectra of (4) the silica gel sample stored with silicone grease showed some organic absorption features at 2967 and 1410 cm^{-1} peak due to C−H, and 1265 cm^{-1} due to Si−CH_3 (Figs. 2-7c and 2-8c; Table 2-1). These features were almost similar to the contamination features from silicone rubber and considered to be due to methylsiloxane volatiles. On the other hand, the spectra of (5) the silica gel sample stored with adhesive tape showed aliphatic C−H absorption features (Fig. 2-7d and 2-8d; Table 2-1). Adhesives are known to contain a variety of different volatile organic compounds such as alcohol, ester, glycol, aliphatic hydrocarbons and aromatic hydrocarbons (e.g., Järnström et al. 2008). Therefore, these aliphatic C−H features on the sample stored with adhesive tape were mainly due to aliphatic hydrocarbons.

2.4.2. Contamination Behavior on Different Materials

Organic contamination was recognized for (a) Tagish Lake, (b) Murchison, (d)

antigorite ($(Mg,Fe^{2+})_3Si_2O_5(OH)_4$), (e) muscovite ($KAl_2(Si_3Al)O_{10}(OH)_2$), (f) montmorillonite ($Na_{0.33}(Al,Mg)_2Si_4O_{10}(OH)_2 \cdot nH_2O$) and (g) silica gel ($SiO_2 \cdot nH_2O$) pressed on Al plates stored for about one day in polystyrene trays with silicone rubber mats (Figs. 2-1 and 2-2; Table 2-1). On the other hand, (c) Moss, (h) silicon dioxide (SiO_2) and (i) KBr did not show any contamination (Figs. 2-1 and 2-2; Table 2-1).

Tagish Lake chondrite is known to contain clay minerals (saponite) (Zolensky et al. 2002; Nakamura et al. 2003b), which can be indicated by an infrared peak around 3650 cm^{-1} due to OH species (Matrajt et al. 2004) (Fig. 2-1a). Murchison includes serpentine and tochilinite (possibly a shoulder around 3600 cm^{-1}; Fig. 2-1b) (Zolensky and McSween 1988; Zolensky et al. 1993). On the other hand, Moss does not contain these hydrous minerals (Bischoff and Schmale 2007; Greenwood et al. 2007) and do not show particular bands at 4000-2500 cm^{-1} regions (Fig. 2-1c). Antigorite, muscovite and montmorillonite show strong infrared peaks at 3670, 3640 and 3630 cm^{-1}, respectively, due to structural OH.

The specific surface area of the silica gel used here is 475 m^2/g, while that of silicon dioxide is ~0.1 m^2/g. Silica gels with high surface area are known to contain abundant surface silanol groups (Si−OH), where water and other molecules can be adsorbed (Zhuravlev 1987; Parida et al. 2006). In fact, infrared spectra of the silica gel indicate a broad band around 3400 cm^{-1} (due to molecular water) with a shoulder at around 3650 cm^{-1} (Si−OH) (Figs. 2-1g and 2-7), while those for the silicon dioxide only show a weak 3400 cm^{-1} band (Fig. 2-1h). KBr is a representative hygroscopic material but show only a small amount of adsorbed water molecules based on infrared spectra (Fig. 2-1i). Note that the 'hygroscopic' nature of KBr can be attributed to its high solubility to water and is different from that of silica gel adsorbing water molecules by its abundant surface silanol groups.

Since only hydrous materials showed organic adsorption, materials with abundant surface OH groups or high surface area are susceptible to organic contamination. This organic contamination on hydrous minerals can be supported by our micro FTIR mapping results on Tagish Lake which showed that organic contamination rich areas were included in the mineral OH rich areas (Kebukawa et al. 2007).

We should be aware of possible rapid organic contamination in normal laboratory environments with silicone compounds and adhesive tapes on carbonaceous chondrites with less degrees of thermal metamorphism having higher porosity and permeability such as Murchison, Tagish Lake and Orgueil.

2.4.3. Heating Behavior of Contaminated Tagish Lake Meteorite and Antigorite

In order to try to eliminate organic contaminants adsorbed on the natural samples, infrared spectral changes were observed in-situ upon heating of Tagish Lake and antigorite contaminated by the storage in the polystyrene tray with the silicone rubber mat.

For the Tagish Lake, the following peak heights were determined with corresponding baselines; 2963 cm^{-1} peak (CH_3) with 3000-2950 cm^{-1} baseline and 1265 cm^{-1} peak (Si−CH) with 1280-1255 cm^{-1} baseline. Changes in these organic peak heights during step heating from room temperature up to 500ºC at 10 ºC/min are presented in Figs. 2-9a,b (thick curves). The CH_3 peak at 2963 cm^{-1} decreased rapidly from 100 to 300ºC, and finally disappeared at 310-320ºC. The 1265 cm^{-1} peak (Si−CH_3) decreased gradually from 25ºC up to approximately 200ºC.

For the antigorite sample, the following peak heights were determined with corresponding baselines; 2963 cm^{-1} peak (CH_3) with 3000-2950 cm^{-1} baseline and 1262 cm^{-1} peak (Si−CH_3) with 1275-1255 cm^{-1} baseline. The CH_3 peak at 2963 cm^{-1} decreased from 50ºC to approximately 300ºC, and finally disappeared at 330-340ºC. The 1262 cm^{-1} peak (Si−CH_3) decreased gradually from 40ºC up to approximately 300ºC (Fig. 2-9c,d; thin curves).

The decrease of 2963 cm^{-1} (CH_3) and ~1265 cm^{-1} (Si−CH_3) peak heights of Tagish Lake and antigorite from room temperature to around 200-300ºC (Fig. 2-9) can be understood mainly by desorption of methylsiloxane-like contaminants. The CH_3 band at 2963 cm^{-1} of Tagish Lake (Fig. 2-9a) had a similar disappearance temperature to antigorite (Fig. 2-9c), and were more thermally stable than that of antigorite from room temperature to around 100ºC. On the other hand, the Si−CH_3 band at ~1265 cm^{-1} disappeared at approximately 200ºC for Tagish Lake (Fig. 2-9b) and 300ºC for antigorite (Fig. 2-9d). Since Tagish Lake contains clay minerals such as saponite in addition to serpentine minerals (Zolensky et al. 2002), these differences can be due to desorption of methylsiloxane-like contaminants from different hydrous minerals. The presence of other contaminants and/or indigenous organic compounds in the Tagish Lake meteorite (Pizzarello et al. 2001) might also affect the thermal behavior of these organics.

Nakamura et al. (2003a) reported that aliphatic C−H peaks at 2952, 2925 and 2854 cm^{-1} in Tagish Lake organics began to decrease upon heating to 160ºC, and disappeared at 320ºC. Although the contaminated CH_3 appeared to be less stable than the above Tagish Lake aliphatic C−H peaks, their disappearance temperatures are almost the same.

Therefore, it is difficult to selectively eliminate contaminated organics before the degradation of indigenous organics by this kind of heating.

The departure of these contaminants on the Tagih Lake and antigorite samples up to 300ºC is in agreement with the suggestion of Sephton et al. (2003) that the first release peak at 300ºC of stepped combustion products of IOM is probably due to isotopically light terrestrial contamination.

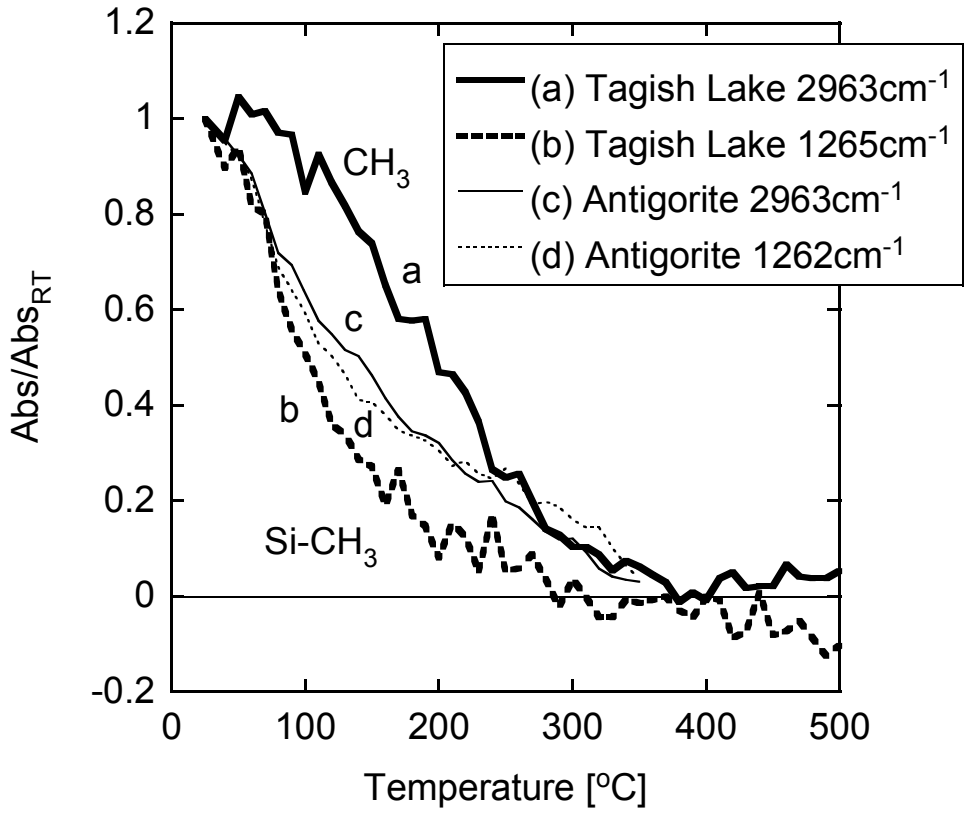

Fig. 2-9. Changes in organic peak heights upon heating of the Tagish Lake meteorite (thick curves) and antigorite (thin curves) samples contaminated by silicone rubber. (a) CH_3 peak at 2963 cm^{-1} and (b) $Si-CH_3$ peak at 1265 cm^{-1} of Tagish Lake (c) CH_3 peak at 2963 cm^{-1} and (d) $Si-CH_3$ peak at 1262 cm^{-1} of antigorite.

2.4.4. How to Avoid Contamination of Samples Prepared for Micro FTIR Analyses

Volatile materials were detected immediately (within a few tens of minutes) after the placement of the silicone rubber mat in the gas cell (Fig. 2-5 and 2-6), indicating

rapid release of significant amounts of volatiles from the silicone rubber. They were subsequently rapidly adsorbed on samples within a few hours (Fig. 2-3). The contamination appeared only after sample preparation for micro FTIR analyses (samples pressed on Al plates). Newly formed surfaces by pressing samples on Al plates might quickly adsorb volatile contaminants. In the case of storage with the silicone rubber mat, the sample-containing polystyrene tray can be rapidly filled with volatile materials such as methylsiloxane, and they can be rapidly adsorbed on the samples.

This is a new type of rapid contamination during storage of samples pressed on Al plates for micro FTIR analyses. Some literatures evaluated organic contamination of terrestrial rock and meteorite samples using mass spectrometry during storage in plastic bags made of polyethylene (contaminants: fatty acid amides, branched alkanes with quaternary carbon centers, alkylcyclopentanes and so on) (Grosjean and Logan 2007; Brocks et al. 2008) and nylon (contaminants: ε-amino-*n*-caproic acid) (Glavin et al., 2006). Since mass spectrometry has much higher sensitivity for the detection of trace organic contaminants than infrared spectroscopy, these reported trace contaminations were not likely to be detected by FTIR. Salisbury and Walter (1989) and Salisbury et al. (1991) previously reported that the C−H bands of infrared reflectance spectra taken from powdered meteorites and terrestrial rock samples may be contamination due to volatile hydrocarbons adsorbed from laboratory atmospheric environments. However, they do not indicate conditions of sample storage. In this study, organic volatile contaminants appeared within a short storage time (one day) for only some limited conditions: newly formed surfaces of hydrous or high surface area materials stored with silicone or adhesive compounds.

Since sample preparation such as pressing on a plate (Al, Au, KBr etc.) is required for obtaining high quality infrared spectra of precious microscopic samples without infrared scattering on rough sample surfaces, newly formed surfaces are inevitable. If certain sample amounts are available, the sample preparation procedure for micro FTIR should be done just before the measurement. However, if sample amounts are very limited and several sample handling procedures are required before infrared analyses, which is often encountered in the sample return missions, the risk for the organic contamination found in this study might arise.

Therefore, we recommend here the following procedures for the safer micro FTIR analyses of precious extraterrestrial and terrestrial samples.

(1) Micro FTIR measurements should be conducted within a short period of time (within a few hours) after the sample preparation (pressing of sample grains on Al, Au or KBr plates).

(2) If the sample storage for a short time period (one day) is needed, glass containers should be used and silicone materials (silicone rubber and grease) and adhesives should be avoided.
(3) If the sample storage for a longer time period than one day is needed, the above glass containers without silicone materials and adhesives can be stored in a clean chamber keeping a positive pressure than the atmospheric environment.
(4) When the sample needs to be fixed for transportation, the sample can be placed between two dimple glass slides (or a dimple slide and a plane slide), and both sides of glass slides can be fixed by clips.
(5) A blank test should be conducted by micro FTIR on silica gel or clay mineral powders under the same sample preparation and storage procedures, in order to check the organic contamination.

2.5. Conclusions

I examined organic contamination by micro FTIR measurements of carbonaceous chondrite samples, and obtained the following conclusions.

1. The carbonaceous chondrites containing hydrous minerals (Tagish Lake and Murchison) pressed on Al plates and measured by micro FTIR were found to be contaminated during storage after only one day, as revealed by an increase of ~2965 cm^{-1} (CH_3) and ~1260 cm^{-1} ($Si{-}CH_3$) peaks. The Moss meteorite which contains no hydrous minerals, did not show an increase of these peaks, indicating no organic contamination. This difference is probably related to the differing mineralogy and physical properties (including porosity and permeability) of these chondrites.
2. Silica gel ($SiO_2{\cdot}nH_2O$) and hydrous minerals such as antigorite ($(Mg,Fe^{2+})_3Si_2O_5(OH)_4$), muscovite ($KAl_2(Si_3Al)O_{10}(OH)_2$), montmorillonite ($Na_{0.33}(Al,Mg)_2Si_4O_{10}(OH)_2{\cdot}nH_2O$) showed organic contamination by the same infrared measurements, while anhydrous materials such as SiO_2 and KBr showed no contamination. These results indicate importance of surface OH groups and/or surface area for the organic contamination.
3. Long path gas cell FTIR measurements for silicone rubber revealed the presence of volatile molecules having 2970 and 2905 cm^{-1} (CH_3), 1265 cm^{-1} ($Si{-}CH_3$), 1080 cm^{-1} ($Si{-}O$) and 900, 850 and 800 cm^{-1} ($Si{-}C$) peaks. These are considered to be methylsiloxane oligomers released from the silicone rubber.

4. This contamination occurred when the samples were stored within containers which included silicone rubber, silicone grease or adhesive tape. However, if stored in glass containers, the samples do not show any signs of contamination. Therefore, it is recommended for curation purposes that storage containers should be preferentially made of glass free of organic compounds.
5. In-situ heating infrared measurements on the contaminated antigorite and Tagish Lake showed difference in trend of desorption of volatile contaminants, which might be due to different hydrous mineral assemblages. The heating cannot eliminate preferentially the organic contaminants before the indigenous organic matter.
6. For micro FTIR analyses, once samples are pressed on metal (Al, Au, etc.) or KBr plates, the sample analyses should be done as soon as possible before contamination. If storage is needed, glass containers are appropriate for a short storage, and silicone materials and adhesives should be avoided.

These results indicate that careful preparation and storage are essential if one is to make FTIR organic measurements for precious astromaterial samples such as meteorites, IDPs and samples returned from comets, asteroids and Mars, as well as terrestrial rock samples. Every possible contamination source should be evaluated before anything is done to these samples. Very short exposure times are all that are needed to compromise valuable, and often irreplaceable samples.

References

Bischoff A. and Schmale K. 2007. Ca,Al-rich inclusions within the Moss CO3 chondrite − Indications for severe secondary alteration (abstract #1561). 38th Lunar and Planetary Science Conference. CD-ROM.

Botta O. and Bada J. L. 2002. Extraterrestrial organic compounds in meteorites. *Surveys in Geophysics* 23: 411-467.

Bradley J. P., Humecki H. J., and Germani M. S. 1992. Combined infrared and analytical electron-microscope studies of interplanetary dust particles. *Astrophysical Journal* 394: 643-651.

Brocks J. J., Grosjean E., and Logan G. A. 2008. Assessing biomarker syngeneity using branched alkanes with quaternary carbon (BAQCs) and other plastic contaminants. *Geochimica et Cosmochimica Acta* 72: 871-888.

Brown P. G., Hildebrand A. R., Zolensky M. E., Grady M., Clayton R. N., Mayeda T. K., Tagliaferri E., Spalding R., MacRae N. D., Hoffman E. L., Mittlefehldt D. W., Wacker J. F., Bird J. A.,

Campbell M. D., Carpenter R., Gingerich H., Glatiotis M., Greiner E., Mazur M. J., McCausland P. J. A., Plotkin H., and Mazur T. R. 2000. The fall, recovery, orbit, and composition of the Tagish Lake meteorite: A new type of carbonaceous chondrite. *Science* 290: 320-325.

Clemett S. J., Maechling C.R., Zare R. N., Swan P. D., and Walker R. M. 1993. Identification of complex aromatic-molecules in individual interplanetary dust particles. *Science* 262: 721-725.

Clemett S. J., Keller L. P., Nakamura K., and McKay D. S. 2004. The nature and origin of aromatic organic matter in the Tagish Lake meteorite (abstract #2026). 35th Lunar and Planetary Science Conference. CD-ROM.

Cronin J. R. and Pizzarello S. 1990. Aliphatic-Hydrocarbons of the Murchison meteorite. *Geochimica et Cosmochimica Acta* 54: 2859-2868.

Deshpande G. and Rezac M. E. 2001. The effect of phenyl content on the degradation of poly (dimethyl diphenyl) siloxane copolymers. *Polymer Degradation and Stability* 74: 363-370.

Ehrenfreund P., Robert F., d'Hendecourt L., and Behar F. 1991. Comparison of interstellar and meteoritic organic matter at 3.4 microns. *Astronomy and Astrophysics* 252: 712-717.

Ehrenfreund P., Robert F., and d'Hendecourt L. 1992. Similarity of the infrared spectrum of an Orgueil organic polymer with interstellar organic compounds in the line of sight towards IRS 7. *Advances in Space Research* 12: 53-56.

Ehrenfreund P., Irvine W., Becker L., Blank J., Brucato J. R., Colangeli L., Derenne S., Despois D., Dutrey A., Fraaije H., Lazcano A., Owen1 T., Robert F., and International Space Science Institute ISSI-Team. 2002. Astrophysical and astrochemical insights into the origin of life. *Reports on Progress in Physics* 65: 1427-1487.

Flynn G. J., Keller L. P., and Miller M. A. 1998. FTIR Detection of Organic Carbon in Interplanetary Dust Particles (abstract #1157). 29th Lunar and Planetary Science Conference.

Flynn G. J., Keller L. P., Jacobsen C., and Wirick S. 2001. FTIR and carbon-XANES examination of organic carbon in Tagish Lake: Evidence for a moderately volatile organic component (abstract #1593). 32nd Lunar and Planetary Science Conference. CD-ROM.

Flynn G. J., Keller L. P., Joswiak D., and Brownlee D. E. 2002. Infrared analysis of organic carbon in anhydrous and hydrated interplanetary dust particles: FTIR identification of carbonyl (C=O) in IDPs (abstract #1320). 33rd Lunar and Planetary Science Conference. CD-ROM.

Flynn G. J., Keller L. P., Feser M., Wirick S., and Jacobsen C. 2003. The origin of organic matter in the solar system: Evidence from the interplanetary dust particles. *Geochimica et Cosmochimica Acta* 67: 4791-4806.

Flynn G. J., Keller L. P., Jacobsen C., and Wirick S. 2004. An assessment of the amount and types of organic matter contributed to the Earth by interplanetary dust. *Advances in Space Research* 33: 57-66.

Gingrich S. E., Diamond M. L., Stern G. A., and McCarry B. E. 2001. Atmospherically derived organic surface films along an urban-rural gradient. *Environmental Science & Technology* 35: 4031-4037.

Glavin D. P., Dworkin J. P., Aubrey A., Botta O., Doty J. H., Martins Z., and Bada J. L. 2006. Amino acid analyses of Antarctic CM2 meteorites using liquid chromatography-time of flightmass spectrometry. *Meteoritics & Planetary Science* 41: 889-902.

Greenwood R. C., Pearson V. K., Verchovsky A. B., Johnson D., Franchi I. A., Roaldset E., Raade G., and Bartoschewitz R. 2007. The Moss (CO3) Meteorite: An Integrated Isotopic, Organic and Mineralogical Study (abstract #2267). 38th Lunar and Planetary Science Conference. CD-ROM.

Grosjean E. and Logan G. A. 2007. Incorporation of organic contaminants into geochemical samples and an assessment of potential sources: Examples from Geoscience Australia marine survey S282. *Organic Geochemistry* 38: 853-869.

Hayatsu R., Matsuoka S., Anders E., Scott R. G., and Studier M. H. 1977. Origin of organic matter in the early solar system – VII. The organic polymer in carbonaceous chondrites. *Geochimica et Cosmochimica Acta* 41: 1325-1339.

Ishikawa K., Tani A., Otsuka T., and Nakashima S. 2007. Transformation of gamma-ray-formed methyl radicals in methane hydrate at 10 Mpa. *Japanese Journal of Applied Physics* 46: 455-460.

Järnström H., Saarela K., Kalliokoski P., Pasanen A. L. 2008. Comparison of VOC and ammonia emissions from individual PVC materials, adhesives and from complete structures. *Environment International* 34: 420-427.

Kawamura K., Suzuki I., Fujii Y., and Watanabe O. 1994. Ice core record of polycyclic aromatic-hydrocarbons over the past 400 years. *Naturwissenschaften* 81: 502-505.

Kebukawa Y., Ishikawa M., Nakashima S., Nakamura T., and Zolensky M. E. 2007. Infrared microspectroscopic mapping of organic matter in Tagish Lake meteorite for studying organic evolution during aqueous alteration (abstract #1450). 38th Lunar and Planetary Science Conference. CD-ROM.

Keller L. P. and Flynn G. J. 2001. Matrix Mineralogy of the Tagish Lake Carbonaceous Chondrite: TEM and FTIR Studies (abstract #1639). 32nd Lunar and Planetary Science Conference. CD-ROM.

Keller L. P., Messenger S., Flynn G. J., Clemett S., Wirick S., and Jacobsen C. 2004. The nature of molecular cloud material in interplanetary dust. *Geochimica et Cosmochimica Acta* 68: 2577-2589.

Keller L. P., Bajt S., Baratta G. A., Borg J., Bradley J. P., Brownlee D. E., Busemann H., Brucato J. R., Burchell M., Colangeli L., d'Hendecourt L., Djouadi Z., Ferrini G., Flynn G., Franchi I. A.,

Fries M., Grady M. M., Graham G. A., Grossemy F., Kearsley A., Matrajt G., Nakamura-Messenger K., Mennella V., Nittler L., Palumbo M. E., Stadermann F. J., Tsou P., Rotundi A., Sandford S. A., Snead C., Steele A., Wooden D., Zolensky M. 2006. Infrared spectroscopy of Comet 81P/Wild 2 samples returned by Stardust. *Science* 314: 1728-1731.

Kissin Y. V. 2003. Hydrocarbon components in carbonaceous meteorites. *Geochimica et Cosmochimica Acta* 67: 1723-1735.

Kusch P. and Knupp G. 2004. Analysis of residual styrene monomer and other volatile organic compounds in expanded polystyrene by headspace solid-phase microextraction followed by gas chromatography and gas chromatography/mass spectrometry. *Journal of Separation Science* 25: 539-542.

Matrajt G., Borg J., Raynal P. I., Djouadi Z., d'Hendecourt L., Flynn G., and Deboffle D. 2004. FTIR and Raman analyses of the Tagish Lake meteorite: Relationship with the aliphatic hydrocarbons observed in the Diffuse Interstellar Medium. *Astronomy and Astrophysics* 416: 983-990.

Matrajt G., Caro G. M. M., Dartois E., d'Hendecourt L., Deboffle D., and Borg J. 2005. FTIR analysis of the organics in IDPs: Comparison with the IR spectra of the diffuse interstellar medium. *Astronomy and Astrophysics* 433: 979-995.

Murae T. 1994. FT-IR spectroscopic studies of major organic matter in carbonaceous chondrites using microscopic technique and comparison with terrestrial kerogen. *Proceedings of the NIPR Symposium on Antarctic Meteorites* 7: 262-274.

Nakamura K., Zolensky M. E., Tomita S., Nakashima S., and Tomeoka K. 2002. Hollow organic globules in the Tagish Lake meteorite as possible products of primitive organic reactions. *International Journal of Astrobiology* 1: 179-189.

Nakamura K., Nakashima S., Shiota D., Zolensky M. E., and Keller L. P. 2003a. In Situ Heating Behavior by Infrared Microspectroscopy of Organic Components in Tagish Lake Meteorite (abstract #1432). 34th Lunar and Planetary Science Conference. CD-ROM.

Nakamura T., Noguchi T., Zolensky M. E., and Tanaka M. 2003b. Mineralogy and noble-gas signatures of the carbonate-rich lithology of the Tagish Lake carbonaceous chondrite: evidence for an accretionary breccia. *Earth and Planetary Science Letters* 207: 83-101.

Okumura S. and Nakashima S. 2004. Water diffusivity in rhyolitic glasses as determined by in situ IR spectroscopy. *Physics and Chemistry of Minerals* 31: 183-189.

Parida S. K., Dash S., Patel S., and Mishra B. K. 2006. Adsorption of organic molecules on silica surface. *Advances in Colloid and Interface Science* 121: 77-110.

Pizzarello S., Huang Y., Becker L., Poreda R. J., Nieman R. A., Cooper C., and Williams M. 2001. The organic content of the Tagish Lake meteorite. *Science* 293: 2236-2239.

Pizzarello S., Cooper G. W., and Flynn G. J. 2006. The nature and distribution of the organic

material in carbonaceous chondrites and interplanetary dust particles. In *Meteorites and the early solar system II*, edited by Lauretta D. S., Leshin L. A., and McSween H. Y., Jr. Tucson, Arizona: The University of Arizona Press. pp. 625-651.

Plows F. L., Elsila J. E., Zare R. N., and Buseck P. R. 2003. Evidence that polycyclic aromatic hydrocarbons in two carbonaceous chondrites predate parent-body formation. *Geochimica et Cosmochimica Acta* 67: 1429-1436.

Quirico E. and Bonal L. 2004. An infrared study of the matrices of CI1 and CM2 chondrites (abstract #1803). 35th Lunar and Planetary Science Conference. CD-ROM.

Raynal P. I., Quirico E., Borg J., Deboffle D., Dumas P., d'Hendecourt L., Bibring J. P., and Langevin Y. 2000. Synchrotron infrared microscopy of micron-sized extraterrestrial grains. *Planetary and Space Science* 48: 1329-1339.

Rotundi A., Baratta G. A., Borg J., Brucato J. R., Busemann H., Colangeli L., D'Hendecourt L., Djouadi Z., Ferrini G., Franchi I. A., Fries M., Grossemy F., Keller L. P., Mennella V., Nakamura K., Nittler L. R., Palumbo M. E., Sandford S. A., Steele A., and Wopenka B. 2008. Combined micro-Raman, micro-infrared, and field emission scanning electron microscope analyses of comet 81P/Wild 2 particles collected by Stardust. *Meteoritics & Planetary Science* 43: 367-397.

Salisbury J. W. and Walter L. S. 1989. Thermal infrared (2.5-13.5 μm) spectroscopic remote-sensing of igneous rock types on particulate planetary surfaces. *Journal of Geophysical Research* 94: 9192-9202.

Salisbury J. W., d'Aria D. M., and Jarosewich E. 1991. Midinfrared (2.5-13.5 μm) reflectance spectra of powdered stony meteorites. *Icarus* 92: 280-297.

Sandford S. A. and Walker R. M. 1985. Laboratory infrared transmission spectra of individual interplanetary dust particles from 2.5 to 25 microns. *Astrophysical Journal* 291: 838-851.

Sandford S. A., Aléon J., Alexander C. M. O'D., Araki T., Bajt S., Baratta G. A., Borg J., Bradley J. P., Brownlee D. E., Brucato J. R., Burchell M. J., Busemann H., Butterworth A., Clemett S. J., Cody G., Colangeli L., Cooper G., d'Hendecourt L., Djouadi Z., Dworkin J. P., Ferrini G., Fleckenstein H., Flynn G. J., Franchi I. A., Fries M., Gilles M. K., Glavin D. P., Gounelle M., Grossemy F., Jacobsen C., Keller L. P., Kilcoyne A. L. D., Leitner J., Matrajt G., Meibom A., Mennella V., Mostefaoui S., Nittler L. R., Palumbo M. E., Papanastassiou D. A., Robert, F., Rotundi A., Snead C. J., Spencer M. K., Stadermann F. J., Steele A., Stephan T., Tsou P., Tyliszczak T., Westphal A. J., Wirick S., Wopenka B., Yabuta H., Zare R. N., and Zolensky M. E. 2006. Organics captured from Comet 81P/Wild 2 by the Stardust spacecraft. *Science* 314: 1720-1724.

Sephton M. A. 2002. Organic compounds in carbonaceous meteorites. *Natural Product Reports* 19: 292-311.

Sephton M. A., Pillinger C. T., and Gilmour I. 2001. Normal alkanes in meteorite : molecular $\delta^{13}C$ values indicate an origin by terrestrial contamination. *Precambrian Research* 106: 47-58.

Sephton M. A., Verchovsky A. B., Bland P. A., Gilmour I., Grady M. M., and Wright I. P. 2003. Investigating the variations in carbon and nitrogen isotopes in carbonaceous chondrites. *Geochimica et Cosmochimica Acta* 67: 2093-2108.

Suzuki A., Yamanoi Y., Nakamura T., and Nakashima S. In press. Micro-spectroscopic characterization of organic and hydrous components in weathered Antarctic micrometeorites. *Earth, Planets and Space*.

Swan P., Walker R. M., Wopenka B., and Freeman J. J. 1987. 3.4 μm Absorption in Interplanetary Dust Particles: Evidence for Indigenous Hydrocarbons and a Further Link to Comet Halley. *Meteoritics* 22: 510-511.

Watson J. S., Pearson V. K., Gilmour I., and Sephton M. A. 2003. Contamination by sesquiterpenoid derivatives in the Orgueil carbonaceous chondrite. *Organic Geochemistry* 34: 37-47.

Wdowiak T. J., Flickinger G. C., and Cronin J. R. 1988. Insoluble organic material of the Orgueil carbonaceous chondrite and the unidentified infrared bands. *Astrophysical Journal* 328: L75-L79.

Zhuravlev L. T. 1987. Concentration of hydroxyl-groups on the surface of amorphous silicas. *Langmuir* 3: 316-318.

Zolensky M. and McSween H.Y., Jr. 1988. Aqueous alteration. In *Meteorites and Early Solar System*, edited by Kerridge J. R. and Matthews M. S. Tucson, Arizona: The University of Arizona Press. pp. 114-143.

Zolensky M. Barrett R., and Browning L. 1993. Mineralogy and composition of matrix and chondrules rims in carbonaceous chondrites. *Geochimica et Cosmochimica Acta* 57: 3123-3148.

Zolensky M. E., Nakamura K., Gounelle M., Mikouchi T., Kasama T., Tachikawa O., and Tonui E. 2002. Mineralogy of Tagish Lake: An ungrouped type 2 carbonaceous chondrite. *Meteoritics & Planetary Science* 37: 737-761.

Chapter 3

NEAR-FIELD INFRARED MICROSPECTROSCOPY FOR MICROSCOPIC ORGANIC MATTER IN CARBONACEOUS CHONDRITE

Some parts (mainly 3.3.1) are published as:
Kebukawa Y., Nakashima S., Nakamura-Messenger K., and Zolensky M. E. 2009. Submicron distribution of organic matter of carbonaceous chondrite using near-field infrared microspectroscopy. *Chemistry Letters* 38: 22-23.

Abstract

Using near-field infrared (NFIR) spectroscopy, I measured distributions of organic functional groups as well as inorganic features in Bells (CM2) carbonaceous chondrite. NFIR spectroscopy has recently been developed to enable infrared spectral mapping beyond the optical diffraction limit of conventional Fourier transform infrared (FTIR) microspectroscopy. NFIR spectral mapping of the Bells 300 nm thick sections on Al plates for several μm^2 areas showed ~1 μm aliphatic C−H rich areas which were considered to represent the organic rich areas. Heterogeneous distributions of organic functional groups as well as those of inorganic phase such as silicates (Si−O) were observed with less than 1 μm spatial resolution. One of the aliphatic C−H rich portions (~1 μm) in other slices of Bells may contain C−O bonds. Some of organic rich regions might correspond to organic globules which are abundantly distributed in the Bells meteorite. The NFIR imaging method can provide submicron spatial distribution of organic functional groups and their association with minerals.

3.1. Introduction

Carbonaceous chondrite meteorites contain up to a few wt% organic carbon (Botta and Bada 2002). These meteorites are known to be the most primitive meteorites and contain records of the early solar system. The larger fraction of the organic carbon (70-99%) is a complex and insoluble macromolecular material (Pizzarello et al. 2006). Organic matter in carbonaceous chondrites is reported to be strongly associated with clay minerals, which may have had important trapping and possibly catalytic roles in the evolution of organics in the early solar system (Pearson et al. 2002). Pearson et al. (2002) reported that osmium labeled organic matter was associated with clay minerals in CM and CI chondrites, from scanning electron microscope (SEM) observation. Amri et al. (2005) reported that pyroxene, olivine and iron oxide grains were embedded into the mixed carbonaceous material, based on Raman spectroscopy. Garvie and Buseck (2007) investigated carbon-clay assemblages in CI and Tagish Lake meteorites using transmission electron microscopy (TEM) and electron energy-loss spectroscopy (EELS). Despite these studies, the detailed nature of microscopic organics is still not known, because methods for organic characterization at the submicron scale are lacking.

On the other hand, macromolecular carbonaceous material can also be found as distinct nanometer-sized entities such as aromatic flakes, solid or hollow spheres, and tubes in several CI, CM and Tagish Lake meteorites (Nagy et al. 1962; Rossignol-Strick

and Barghoorn 1971; Alpern and Benkheir 1973; Pflug 1984; Nakamura et al. 2002; Garvie and Busek 2004). They are analyzed by TEM-EELS. Their carbon is aromatic in nature, containing several percent of O, N, and S; e.g., the elemental composition of a Tagish Lake carbonaceous globule was observed to be $C_{100}S_{2.7}N_{5.0}O_{10}$ (bonded H is not detected by EELS and excluded from the above calculations) (Garvie and Busek 2004). Functional groups such as C=O and C=N are also observed in some nanostructures (Garvie and Busek 2004). Organic globules in Bells meteorite (an unusual CM2 chondrite) are more abundant than in Tagish Lake, and recently found to be ^{15}N-rich by nano-scale secondary ion mass spectrometry (NanoSIMS) analysis (Messenger et al. 2008).

Fourier transform infrared (FTIR) microspectroscopy is useful for characterizing both organic and mineral structures. However, its spatial resolution is limited to ~10 μm at maximum (Nakashima et al. 1989). Near-field infrared (NFIR) microspectroscopy has recently been developed to permit infrared spectral mapping beyond the optical diffraction limit with a spatial resolution of several hundred nanometers (Kuya et al. 2004). This method is, therefore, expected to measure nondestructively the distribution of organic polar functional groups including H-bearing ones together with those for hydrous minerals.

Here we apply this new high-resolution NFIR microspectroscopy to the analysis of organic matter in the Bells meteorite, in order to elucidate spatial distribution and microscopic characterization of organic matter.

3.2. Samples and Experimental Methods

3.2.1. Near-Field Infrared (NFIR) Microspectroscopy

In order to obtain higher spatial resolution infrared spectral mapping of carbonaceous chondrites, I used a NFIR microspectroscopy. NFIR microspectroscopy has recently been developed to permit infrared spectral mapping beyond the optical diffraction limit with a spatial resolution of several hundred nanometers (Kuya et al. 2004).

The description of the system is as follows (Kuya et al. 2004). A FTIR microspectrometer was combined with a near-field (NF) optics by using Cassegrainian mirrors (Jasco NFIR-300N; Figs. 3-1 and 3-2). The ceramic infrared light source from the FTIR is focused by a Cassegrainian mirror onto a probe tip (having 1 μm curvature) placed within several tens of nm of a sample surface. The probe tip scatters NF signals localized around the probe-sample region, and another Cassegrainian mirror collects the

scattered light which is passed via a Ge coated KBr beam splitter and the FT interferometer onto a mercury-cadmium-telluride (MCT) detector. The aperture-less near-field probe was made of a quartz optical fiber coated with gold. The curvature of probe tip was in the order of 1 μm, which determines primarily the spatial resolution of the system. This probe tip is oscillated at its resonant frequency around 10-20 kHz. Sample is mounted on a piezoelectric XYZ stage. When this tip is approaching to the sample surface within a few tens of nm, the oscillation amplitude is decreased as a result of shear force interaction with the sample (Betzig and Trautman 1992). A laser is applied to the probe tip and amplitude of reflected laser light is detected by a Si photo detector; the amplitude of modulation of this detected light provides a measure of the amplitude of the probe's oscillation. This is then used as the control signal for a feedback system (Fig. 3-2), which maintains a constant separation between the probe tip and the sample surface. By recording the height (Z) position of the sample needed to maintain a constant probe-sample separation, as the sample is raster scanned in the XY plane, a topographic map of the sample surface may be built up.

NF signals scattered by the probe trip are detected by the MCT detector and sent to the FTIR to convert them into IR spectra. Typically 100 scans were accumulated with a wavenumber resolution of 8 cm^{-1}, in the wavenumber range of 4000-900 cm^{-1}. The NFIR system enables measurements of both topography and IR mapping of the sample surface in areas of up to 20 × 20 μm.

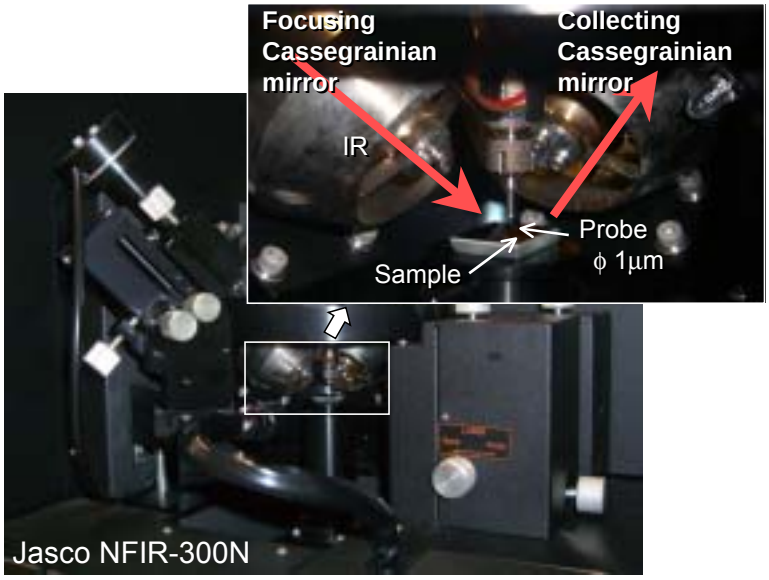

Fig. 3-1. Photographic images of the optics of the near-field infrared (NFIR) microspectrometer (Jasco NFIR-300N).

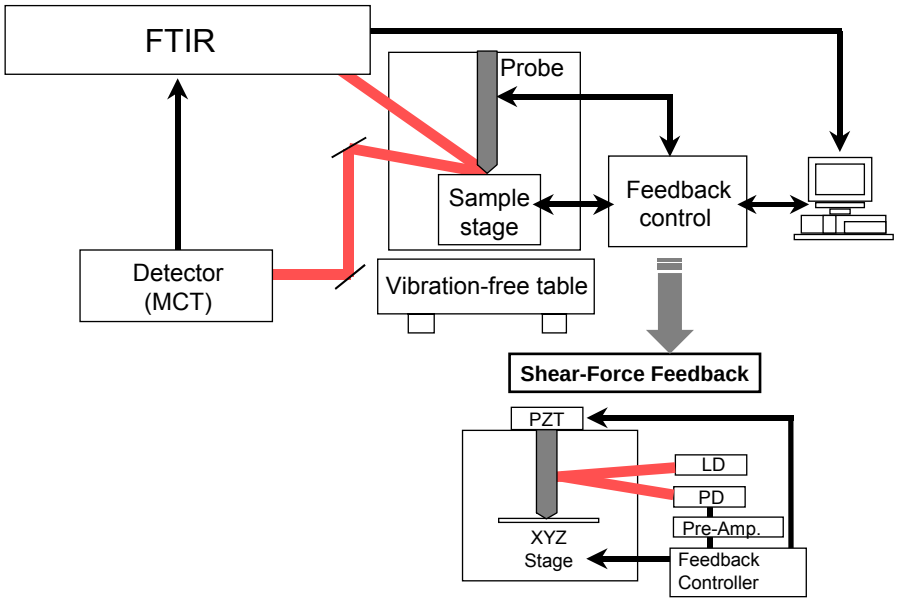

Fig. 3-2. Schematic system configuration of the near-field infrared (NFIR) microspectrometer (Jasco NFIR-300N).

3.2.2. Samples

Several ultramicrotome thin sections of Bells meteorite were used to obtain ~1 μm resolution IR mapping using the NFIR spectroscopy.

Bells meteorite which is obtained from the research collection of Dr. M. E. Zolensky at NASA Johnson Space Center is a CM2 carbonaceous chondrite with unusual petrologic characteristics (Zolensky et al. 1993; Brearley 1995; Browning et al. 1996). Bells meteorite fell on September 9, 1961 in Texas, United States. According to Monnig (1963), seven fragments with a total weight of about 280 g were collected over distance of about 7.5 km. The first fragment hit the roof of a house and was picked up the following morning in a perfect state. The remaining specimens were found after a hurricane and rainfall in a more or less altered state. Two of these were substantially intact but the other four had shattered on impact or crumbled through weathering. The Bells samples used here are believed to be intact ones (Dr. M. E. Zolensky, personal communication, 2008).

Bells is known to content high abundant saponite and magnetite which are rare in typical CM chondrite (Zolensky et al. 1993; Brearley 1995). The formation of saponite in Bells probably resulted from the dissolution of relatively silica-rich phases, such as pyroxene and olivine, which were derived from chondrules (Brearley 1995).

The C, H, and N systematic of Bells are also unusual for CM chondrites with both highly variable distributions of ^{13}C, D, and ^{15}N and extremely large enrichments in these isotopes (Kerridge 1985). Bells is one of the most primitive chondrites by their isotopic compositions (Alexander et al. 2007). In the Bells meteorite, organic globules less than 1 μm in diameter are quite abundant in the serpentine-saponite matrix according to TEM observation (Messenger 2008). These globules in Bells are often filled, and hollow ones such as those found in Tagish Lake are less common (Messenger 2008).

Matrix fragments (~20 μm) of the Bells meteorite were embedded in elemental S for ultramicrotomy. The samples were sliced into 300 nm-thick sections and deposited onto Al plates. As a consequence, typically a dozen of sections are mounted on each Al plate, and each Al plate is named Sample#1, 2, 3 and each section on the Al plate is named such as Sample#1-1. Elemental S was sublimated in vacuo before analysis. Sample preparation using ultramicrotome was performed by Dr. K. Nakamura-Messenger at NASA Johnson Space Center. This sample preparation procedure enables microscopic organic materials to be studied in-situ while preserving their structures.

3.3. Results

3.3.1. NFIR Mapping of Bells Meteorite (Sample#1)

In order to find organic rich slices out of a dozen of ultramicrotome slices on an Al plate (Sample#1), transmission-reflection spectra of the samples were collected using a conventional micro FTIR (JASCO FT-IR-620 + IRT30), in the range 4000-700 cm^{-1}, with a 40 × 40 μm^2 aperture, 1000 scans at the resolution of 4 cm^{-1}. The background spectra were collected on the Al plate. Fig. 3-3a shows a conventional FTIR spectrum of one of the most organic rich slice of the Bells meteorite (Sample#1-7).

In order to analyze organic matter distribution and mineral associations at the submicron scale spatial resolution, NFIR spectral mapping of the organic rich slices of Bells (Sample#1-7) ware conducted at 0.21 μm steps for 4.0 × 2.1 μm^2 area. The background spectra were collected on an Al mirror. Figs. 3-3b and Fig. 3-3c show NFIR spectra of an organic-rich and an organic-poor positions, respectively, of the same slice collected during mapping analyses. Most of the weak infrared absorption bands in the conventional transmission-reflection spectra can be observed in the NFIR spectra.

The band at 3620 cm^{-1} is considered to be due to structural O−H of hydrous minerals, while the band around 3300 cm^{-1} is probably due to O−H stretching vibrations

of molecular water. Bells is known to contain abundant phyllosilicates, particularly serpentines, and tochilinite (a sulfide-hydroxide mineral) (Zolensky et al. 1993). The band around 2880 cm^{-1} is due to aliphatic C−H vibrations. The band at 1025 cm^{-1} is due to Si−O stretching vibrations of phyllosilicates. The 2960 and 1260 cm^{-1} bands are due to CH_3 and Si−CH_3, respectively (peak assignments are based on Socrates 2001). These two bands are considered to be due to contaminants from silicone grease fixing the Al plate holding the sample onto the sample stage. The conventional FTIR spectrum (Fig. 3-3a) taken before using silicone grease had much lower intensity of 2960 cm^{-1} band compared to NFIR spectra (Figs. 3-3b and 3-3c) and did not show 1260 cm^{-1} band. The fine features around 3900-3600 cm^{-1} are considered to be noises of water vapor in the atmosphere.

Fig. 3-4 shows NFIR spectral mapping of the Bells meteorite on the Al plate. The band depths (downward peak heights in reflectance with linear baselines) were determined for 2880 cm^{-1} due to aliphatic C−H, 3300 cm^{-1} due to molecular H_2O, 3620 cm^{-1} due to structural O−H, and 1260 cm^{-1} due to contaminated Si−CH_3. The contaminants (1260 cm^{-1}: Si−CH_3) are commonly distributed in the area with some high spots (Fig. 3-4d). Structural O−H (3620 cm^{-1}), probably due to phyllosilicates, is also ubiquitously distributed with a highly concentrated portion at the center (Fig. 3-4c). The molecular H_2O (3300 cm^{-1}) is lacking at two areas on the right and left sides (Fig. 3-4b). Aliphatic C−H at 2880 cm^{-1} appeared to be distributed in the above water-free areas (Fig. 3-4a). This distribution is clearly different from that of contaminants (1260 cm^{-1}: Si−CH_3). Therefore, aliphatic C−H at 2880 cm^{-1} is considered to be indigenous to the meteorite.

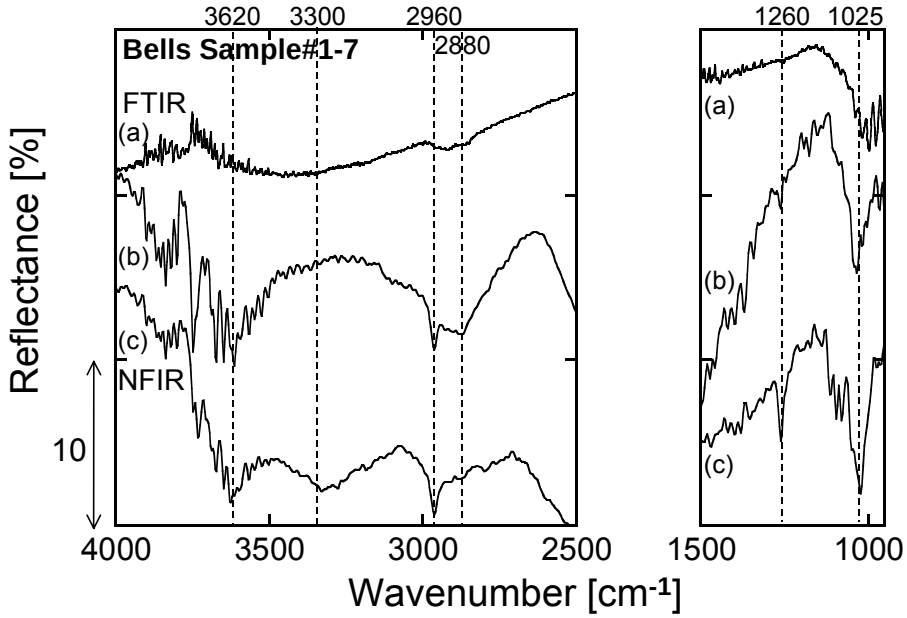

Fig. 3-3. (a) Conventional FTIR spectrum of a slice (about 300-nm thick) of Bells meteorite (Sample#1-7). (b,c) Representative NFIR spectra of Bells Sample#1-7 for an organic-rich point (mark B in Fig. 3-4), and a water-rich point (mark C in Fig. 3-4), respectively.

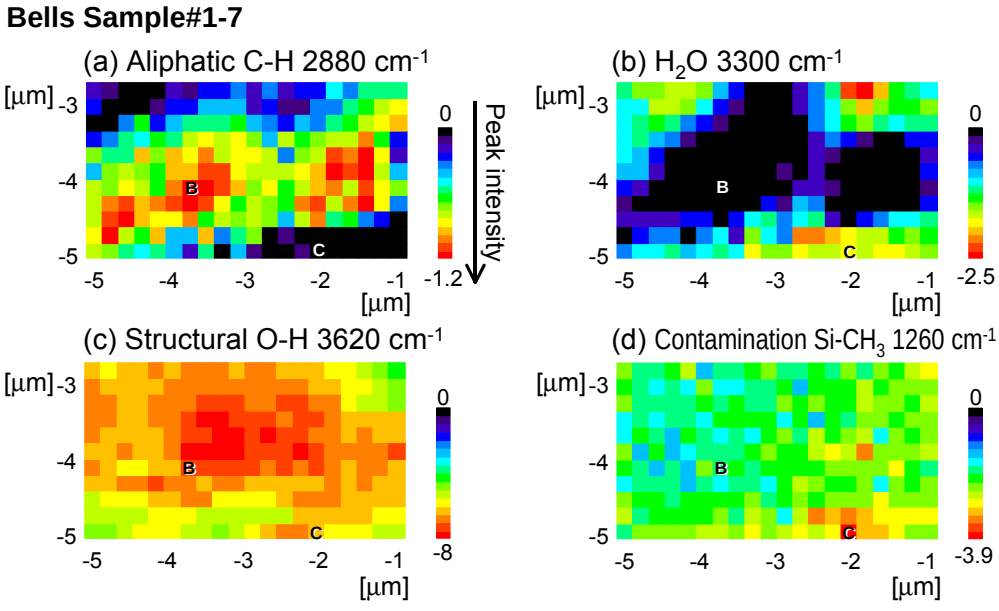

Fig. 3-4. NFIR spectral mapping of the band depths of Bells Sample#1-7. (a) 2880 cm^{-1} due to aliphatic C−H, (b) 3300 cm^{-1} due to molecular O−H, (c) 3620 cm^{-1} due to structural O−H, and (d) 1260 cm^{-1} due to contaminated Si−CH_3.

3.3.2. NFIR Mapping of Bells Meteorite (Sample#2)

In order to avoid silicone grease contamination, another suite of Bells ultramicrotome slices was prepared on an Al plate (~5 × 5 mm). This time, the Al plate was fixed on the NFIR sample holder using KBr for NFIR spectral mapping. A KBr plate (~1 μm thick) placed on the sample holder was wetted by Milli-Q water. Then the sample holding Al plate was placed on the KBr plate, and dried around 50ºC in an oven. The NFIR sample holder and the Al plate were fixed by solidification of dissolving KBr on surface of the KBr plate, without using contamination source materials such as silicone grease and adhesives (see Chapter 2).

Fig. 3-5a shows a conventional FTIR spectrum of a slice of Bells Sample#2-7 with a 20 × 20 μm^2 aperture, 1000 scans at the resolution of 4 cm^{-1}. Fig. 3-5b shows a NFIR spectrum of the same slice of the Bells meteorite. Organic and inorganic features were observed in the NFIR spectrum while these features did not appear in the conventional FTIR spectrum. The band around 3300 cm^{-1} is considered to be due to O−H stretching vibrations of interlayer and/or adsorbed water. The band at 2930 and 2870 cm^{-1} is due to aliphatic C−H vibrations. The band around 1600 cm^{-1} is probably due to aromatic C=C, 1450 cm^{-1} is due to carbonates with some contribution of aliphatic C-H bending, 1250 cm^{-1} is due to C−O. The 1040 cm^{-1} band is due to Si−O stretching vibrations.

Fig. 3-6a and Fig. 3-6b show NFIR spectra of an organic-rich and an organic-poor points, respectively, of Bells Sample#2-8. Fig. 3-7 shows NFIR spectral mapping of Bells Sample#2-8 with 0.3 μm steps for 6.0 × 4.2 μm^2 area. The band depths (downward peak heights in reflectance with linear baselines) were determined for 2930 cm^{-1} due to aliphatic C−H, 1285 cm^{-1} probably due to C−O, and 1010 cm^{-1} due to Si−O. Aliphatic C−H at 2930 cm^{-1} appeared to be distributed in the lower half of the determining area (Fig. 3-7a). Si−O (1010 cm^{-1}) due to silicates is distributed at right and left side (Fig. 3-4c). C−O (1285 cm^{-1}) is distributed at the center of aliphatic C−H rich area (Fig. 3-4b).

In order to confirm the reproducibility, mapping of the same point of Bells Sample#2-8 were conducted (Fig. 3-8). The general trend of distributions of absorption bands are consistent with the previous results shown in Fig. 3-7.

Fig. 3-9a and Fig. 3-9b show NFIR spectra of an organic-rich and an organic-poor points, respectively, of the other slice of Bells Sample#2-6. Fig. 3-10 shows NFIR spectral mapping of Bells Sample#2-6 with 0.3 μm steps for 6.0 × 4.2 μm^2 area. The band depths were determined for 2930 cm^{-1} due to aliphatic C−H, 1370 cm^{-1} probably due to COOH, 3400 cm^{-1} due to molecular water, and 1040 cm^{-1} due to Si−O. Aliphatic

C−H at 2930 cm^{-1} appeared to be distributed in the left side (Fig. 3-10a). Si−O (1040 cm^{-1}) due to silicates is distributed at right and left sides with a highly concentrated portion at the upper right (Fig. 3-4c). COOH (1370 cm^{-1}) is ubiquitously distributed in the area with some high spots (Fig. 3-4b). Molecular water (3400 cm^{-1}) is commonly distributed in the area with highly concentrated portions at the right and lower left (Fig. 3-4d).

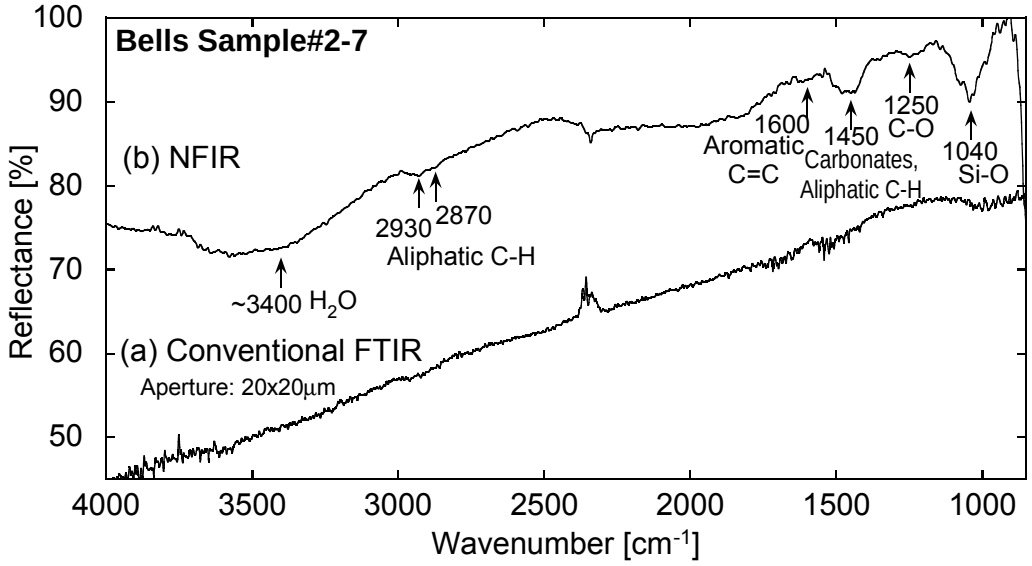

Fig. 3-5. (a) Conventional FTIR spectrum of Bells Sample#2-7. (b) NFIR spectra of Bells Sample#2-7.

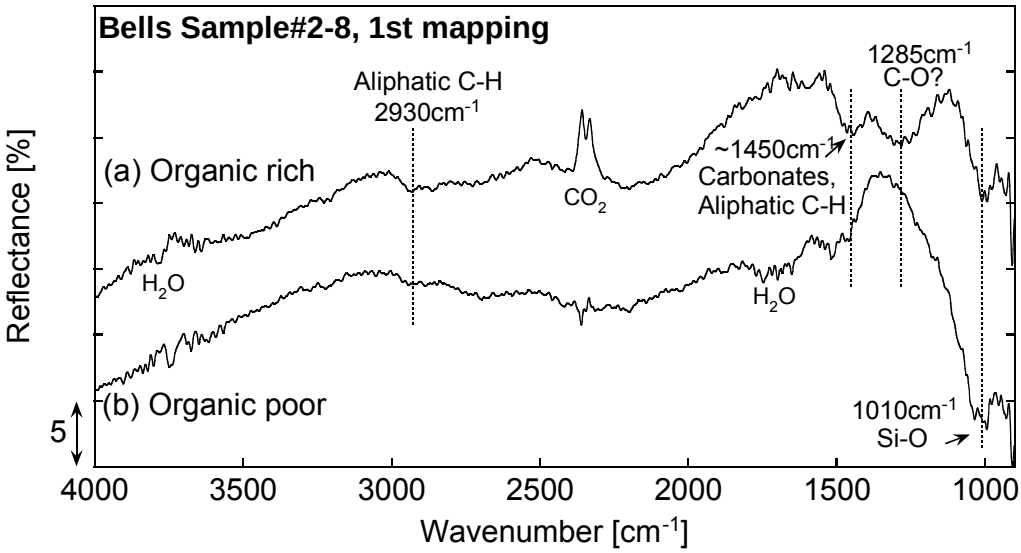

Fig. 3-6. Representative NFIR spectra of Bells Sample#2-8, 1st mapping for (a) an organic-rich point (mark A in Fig. 3-7), and (b) a organic-poor point (mark B in Fig. 3-7).

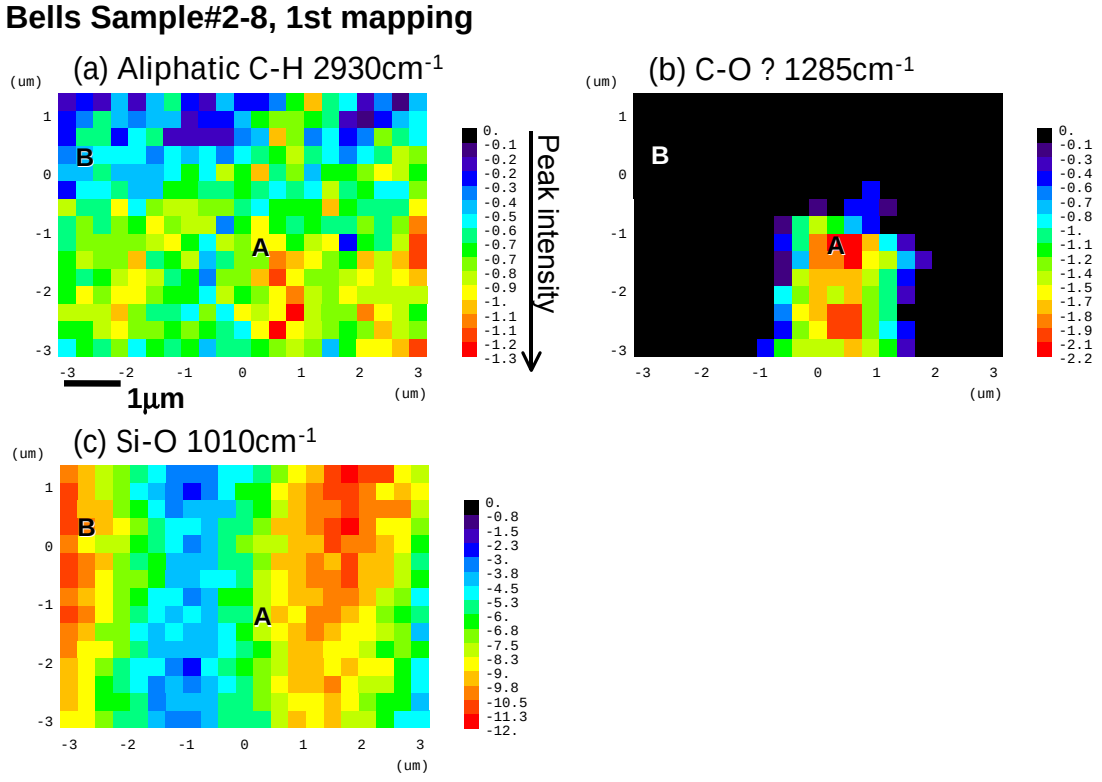

Fig. 3-7. NFIR spectral mapping of the band depths of Bells Sample#2-8, 1st mapping. (a) 2930 cm^{-1} due to aliphatic C−H, (b) 1285 cm^{-1} probably due to organic C−O, (c) 1010 cm^{-1} due to Si−O.

Bells Sample#2-8, 2nd mapping

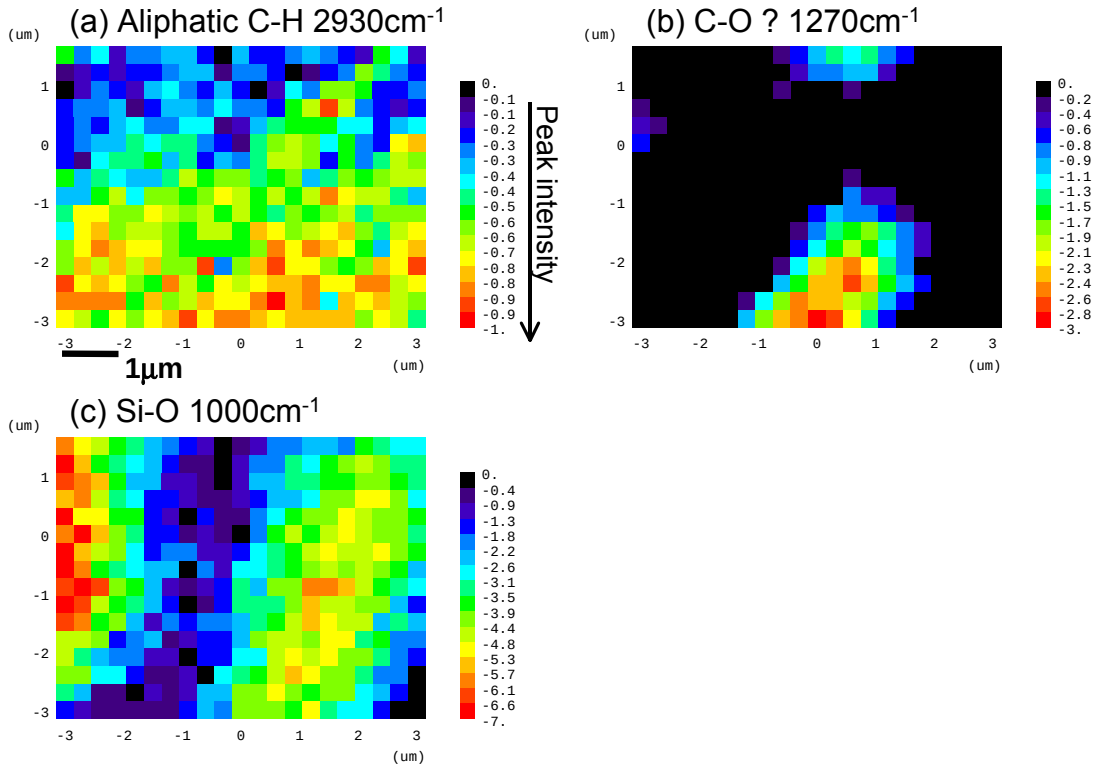

Fig. 3-8. NFIR spectral mapping of the band depths of Bells Sample#2-8, 2nd mapping. (a) 2930 cm^{-1} due to aliphatic C−H, (b) 1270 cm^{-1} probably due to organic C−O, (c) 1000 cm^{-1} due to Si−O.

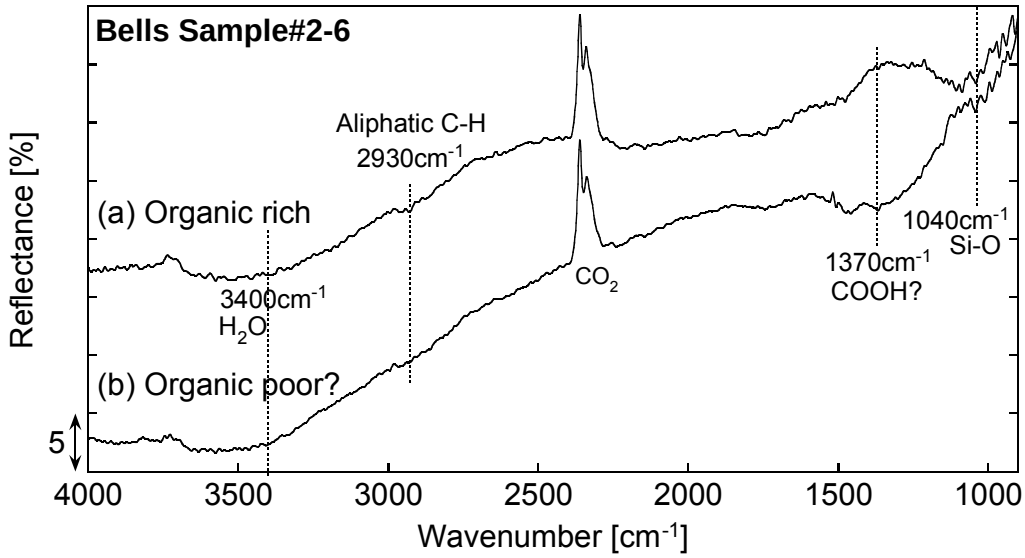

Fig. 3-9. Representative NFIR spectra of Bells Sample#2-6 for (a) an organic-rich point (mark A in Fig. 3-10), and (b) a organic-poor point (mark B in Fig. 3-10).

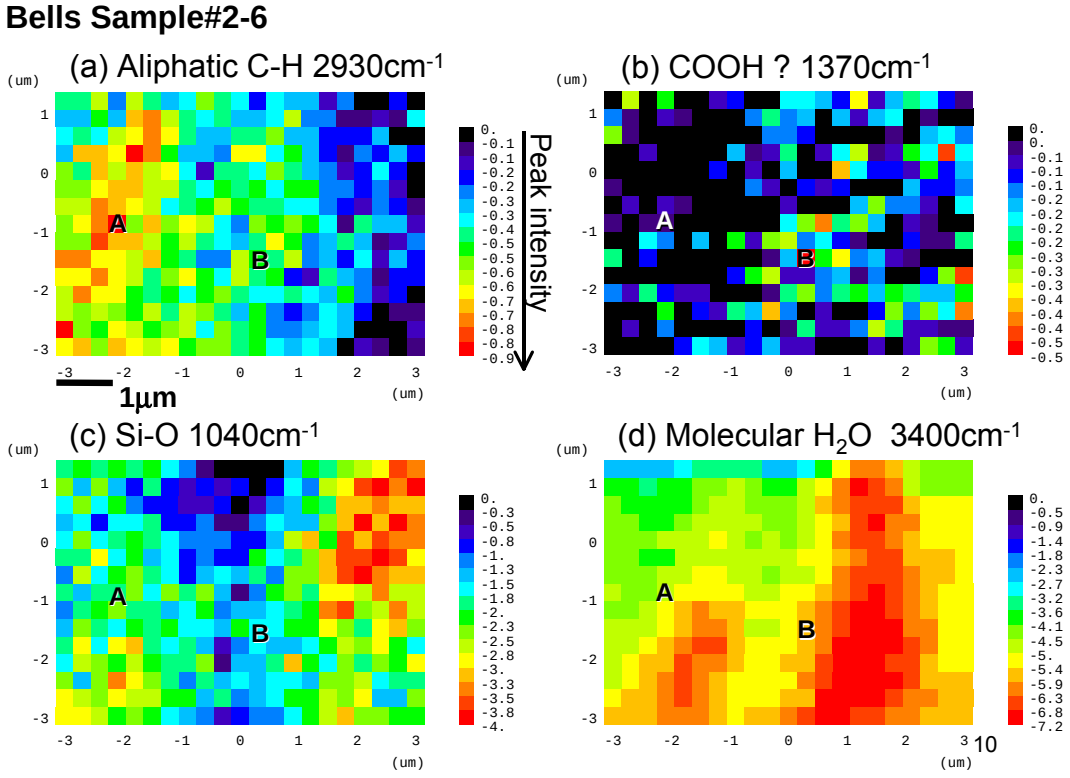

Fig. 3-10. NFIR spectral mapping of the band depths of Bells Sample#2-6. (a) 2930 cm^{-1} due to aliphatic C−H, (b) 1370 cm^{-1} probably due to COOH, (c) 1040 cm^{-1} due to Si−O, (d) 3400 cm^{-1} due to Molecular H_2O.

3.3.3. NFIR Mapping of Bells Meteorite (Sample#3)

In order to ascertain mapping position in the sample, topographic image over the sample was taken before NFIR mapping by using a revised NFIR instrument at JASCO Co., Ltd. This measurement was operated by Mr. Aizawa at JASCO Co., Ltd. Fig. 3-11a shows optical microscopic image of Bells Sample#3-11 taken before NFIR mapping analyses. Fig. 3-11b shows topographic image of Bells Sample#3-11. Squared area in Figs. 3-11a,b is analyzed by NFIR.

Fig. 3-12 shows NFIR spectral mapping of a slice of Bells Sample#3-11 with 0.3 μm steps for 7.5 × 7.5 μm^2. During NFIR mapping analysis, topographic image was collected simultaneously (Fig. 3-11c). Fig. 3-12a and Fig. 3-12b show NFIR spectra of organic rich point and organic poor point, respectively, collected during mapping analyses. The band depths (downward peak heights in reflectance with linear baselines) were determined for 2960 cm^{-1} due to aliphatic CH_3, 2930cm^{-1} due to aliphatic CH_2, 1480 cm^{-1} due to carbonate, and 1040 cm^{-1} due to Si−O. Aliphatic C−H at 2960 and 2930 cm^{-1} appeared to be distributed in the center and the lower right of the mapped area (Figs. 3-13a,b). Si−O (1040 cm^{-1}) due to silicates is distributed at the center but not exactly overlapping the aliphatic C−H rich area (Fig. 3-13d). Carbonate (1480 cm^{-1}) is distributed at the right center and lower right area (Fig. 3-13c).

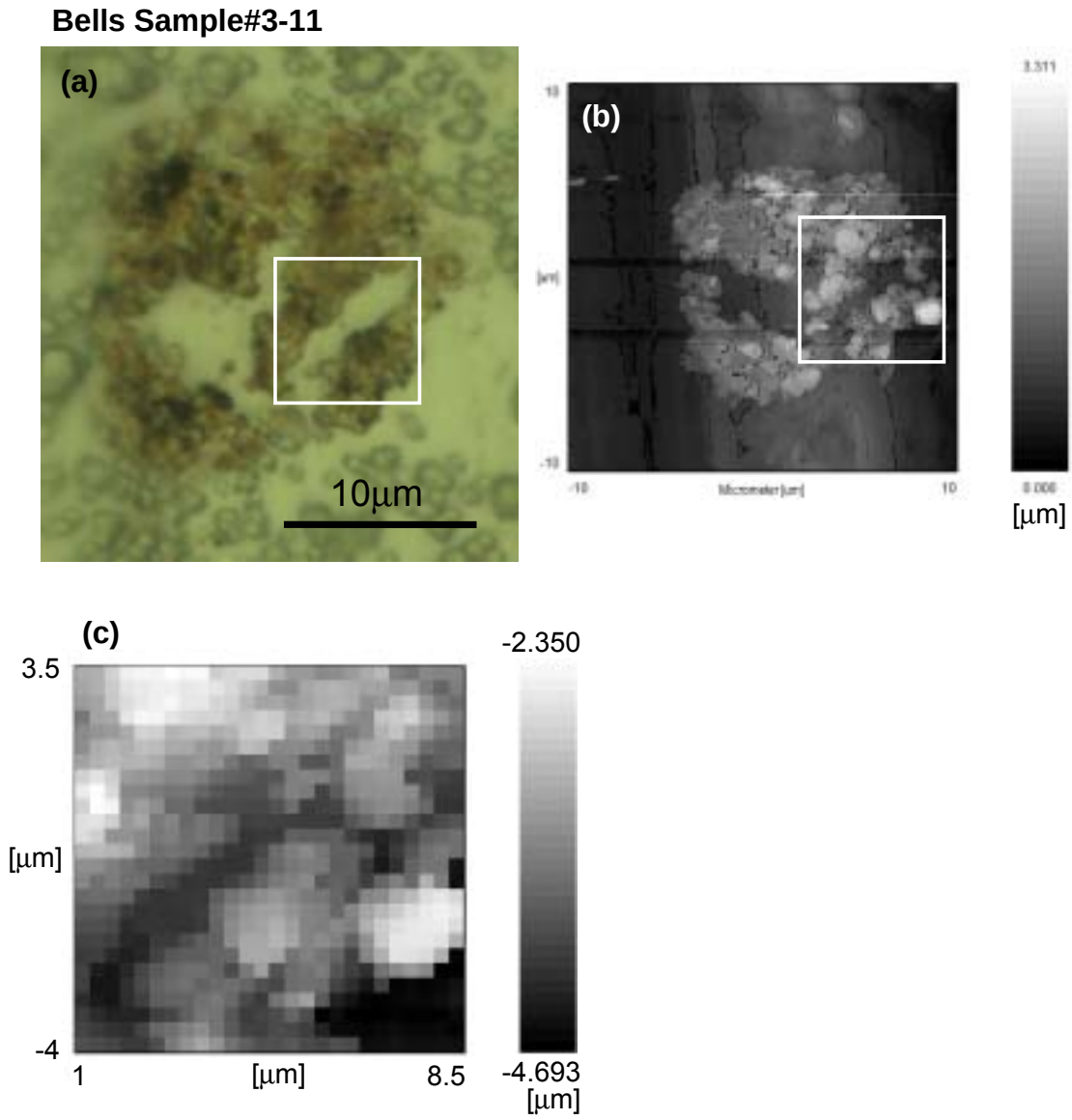

Fig. 3-11. (a) Optical microscopic image of Bells Sample#3-11. Sample is shown in brownish color. Surrounding transparent grains are sulfur which is sublimated before analysis. (b) Topographic image of Bells Sample#3-11. (c) Topographic image of NFIR mapping area (squared area in **a** and **b**).

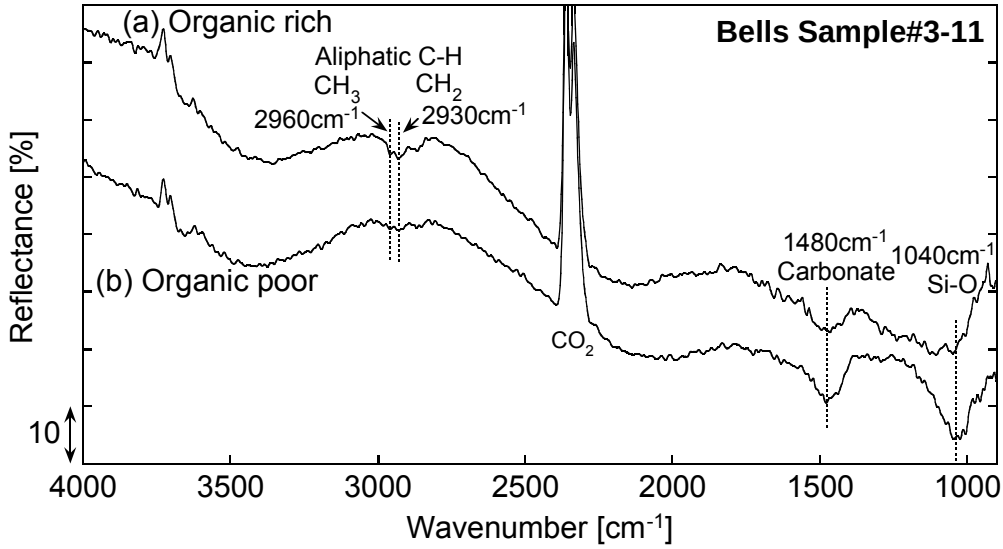

Fig. 3-12. Representative NFIR spectra of Bells Sample#3-11 for (a) an organic-rich point (mark A in Fig. 3-13), and (b) a organic-poor point (mark B in Fig. 3-13).

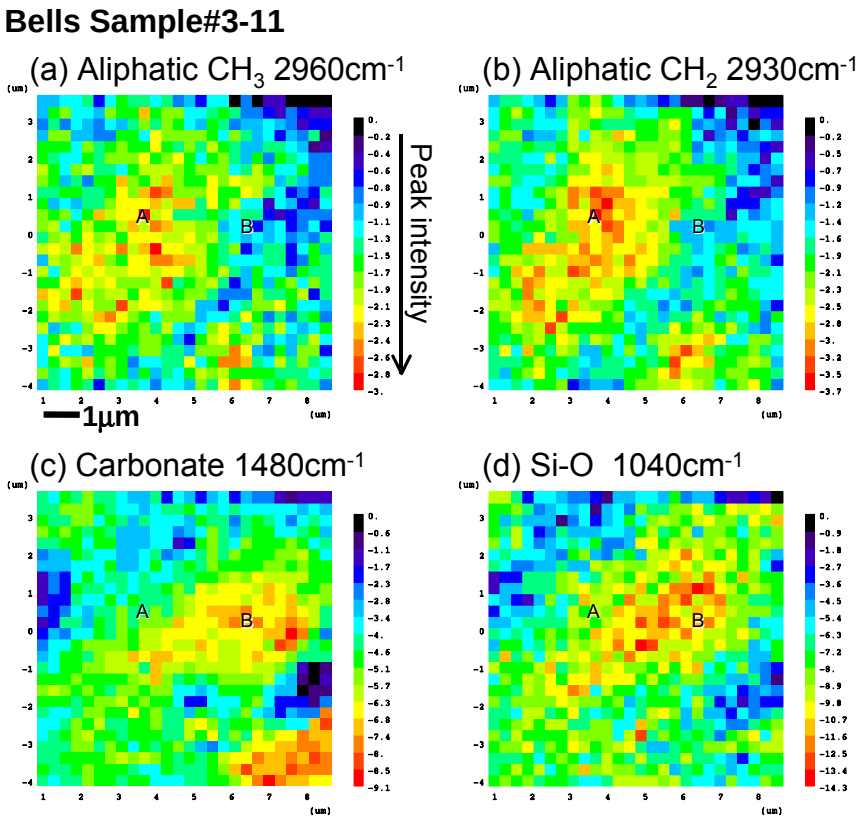

Fig. 3-13. NFIR spectral mapping of the band depths of Bells Sample#3-11. (a) 2960 cm^{-1} due to aliphatic CH_3, (b) 2930 cm^{-1} due to aliphatic CH_2, (c) 1480 cm^{-1} due to carbonate, (d) 1040 cm^{-1} due to Si−O.

3.4. Discussion

3.4.1. Association of Organic Matter and Minerals

Bunch and Chang (1980) reported that carbonaceous matter in altered CM matrices is largely associated with poorly characterized phases (PCP) which are later found to be coherent tochilinite-serpentine intergrowth (Mackinnon and Zolensky 1984). Pearson et al. (2002) suggested that organic matter is strongly associated with phyllosilicates among CM chondrites. The association of organic matter with phyllosilicates observed by the present NFIR agrees with these previous works.

Phyllosilicates are known to have capabilities of adsorption and catalytic transformation of organic matter. Smectite is known to sustain organic matter in the interlayer surface and protect against its oxidation (Kennedy et al. 2002). Sedimentary organic carbon content has a positive correlation with specific surface area and so sedimentary organic matter is considered to be mostly adsorbed on minerals (Mayer 1994a,b). Salmon et al. (2000) reported that sedimentary organic matter appears to be physically protected by clays due to sorptive protection mechanism, and suggested the adsorption of labile organic compounds onto minerals, thus preventing their diagenetic degradation and promoting their subsequent condensation into kerogen.

Organic matter is likely to accrete with anhydrous minerals to chondrite parent body. Then aqueous alteration would yield hydrous minerals such as phyllosilicates. The chondritic organic matter could have been protected by phyllosilicates during parent body aqueous alteration and subsequent thermal metamorphism. The submicron scale characterization of organic matter and its association with hydrous minerals would elucidate the evolution history of extraterrestrial organic matter. Further improvement of the present NFIR method would provide more information on the nature of microscopic organic matter by the organic functional groups other than aliphatic C−H such as aromatic C=C.

3.4.2. Relation to Organic Globules

The other organic functional groups such as C=C and C=N could not be detected owing to strong absorption of water vapor fluctuation in the atmosphere in the 1800-1500 cm^{-1} region. Therefore, the aliphatic C−H rich areas in Fig. 3-4a were considered to represent the organic-rich areas. The organic-rich portions seemed to be around 1 micrometer in size (Fig. 3-4a). However, their boundary might be blurred by the contribution of transmitted-reflected light other than NFIR signals at the surface. Therefore, the organic-rich areas might be smaller than 1 μm or several hundreds of nm

in size (yellow to red regions in Fig. 3-4a). These portions might, therefore, correspond to submicron organic globules found in CI, CM, and Tagish Lake meteorites (Nakamura et al. 2002; Garvie and Buseck 2004). These organic globules are thought to be amorphous carbon, and some of them contain functional groups such as C=O and C=N based on TEM-EELS (Garvie and Buseck 2004). In the Bells meteorite, such organic globules less than 1 μm in diameter are quite abundant in the serpentine-saponite matrix according to the TEM observation by Dr. K. Nakamura-Messenger at NASA Johnson Space Center. Fig. 3-14 shows a typical bright field TEM image of organic globules ubiquitously distributed in the Bells meteorite. These globules in Bells are often filled, and hollow ones such as those found in Tagish Lake are less common (Messenger et al. 2008). Since we cannot use the same slice for the TEM observation and NFIR measurement, it remains unknown whether the structures shown in Fig. 3-4a are organic globules or not.

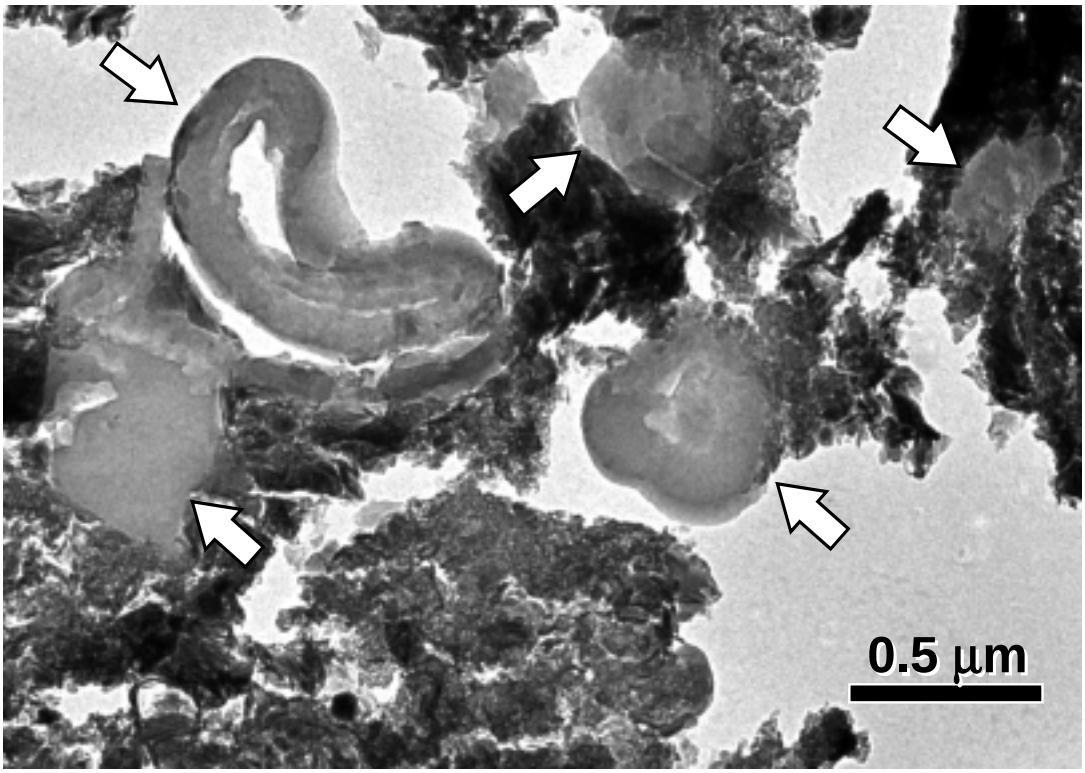

Fig. 3-14. A typical bright field TEM image of five organic globules from Bells (CM2) meteorite embedded in saponite matrix. Scale bar is 0.5 μm. Microtomed slice different from that analyzed by NFIR. The TEM observation was performed by Dr. K. Nakamura-Messenger.

3.4.3. Distribution of Organic Functional Groups

Assuming that the NFIR mapping of Sample#2-8 on 1285 cm^{-1} (Fig. 3-7b) shows distribution of organic C−O, the C−O rich area accounts for only 1-2 μm of organic rich area which can be represented by aliphatic C−H rich area (Fig. 3-7a). Hence, C−O containing moieties might be heterogeneously distributed in Bells meteorites in 1 μm scale. Both C−O and aliphatic C−H do not show any association with Si−O (Fig. 3-7). Organic phases might not form organic-silicate complexes.

1370 cm^{-1} of Sample#2-6 might be due to COOH. Although, 1370 cm^{-1} is usually assigned to aliphatic C−H bending, NFIR maps of 1370 cm^{-1} and 2930 cm^{-1} due to aliphatic C−H stretching do not show similar trends (Figs. 3-10a,b). COOH might be heterogeneously distributed in a few μm scale.

1040 cm^{-1} due to Si−O (silicates) and 3400 cm^{-1} due to molecular H_2O show similar distributions (Figs. 3-10c,d). Hence the silicate is likely to be phyllosilicates. The NFIR mapping results suggest that phyllosilicates are more closely associated with COOH than aliphatic C−H.

In the NFIR mapping of Bells Sample#3-11, organic matter (aliphatic C−H) is distributed near but different from carbonates and silicates (Si−O) (Fig. 3-13). Organic phases are independent from silicate phases. Therefore, these organic rich portions might correspond to organic globules around 1 μm in size, found in CI, CM, and Tagish Lake meteorites (Nakamura et al. 2002; Garvie and Buseck 2004). Since the organic rich positions can be identified in the optical image (Fig. 3-11a), another analytical methods such as scanning electron microscope with energy dispersive X-ray spectrometry (SEM/EDS) and NanoSIMS should be conducted for further characterization of these organic rich areas.

3.5. Conclusions

In order to obtain high spatial resolution infrared spectral mapping of organic matter in carbonaceous chondrites, mapping of Bells (CM2) carbonaceous chondrite is conducted using a near-field infrared (NFIR) spectroscopy which has been developed to enable infrared spectral mapping beyond the optical diffraction limit of conventional FTIR microspectroscopy. A series of experiments provided the following results.

1. NFIR measurement on Al plate method enables us to obtain organic and inorganic features of chondrite samples which are too small and thin to obtain spectra by conventional FTIR. Hence, NFIR is expected to be a powerful tool for small astronomical samples such as interplanetary dust particles (IDPs) and

mission returned samples.

2. Heterogeneous distributions of organic functional groups such as aliphatic C−H as well as those of inorganic phases such as silicates (Si−O) were observed with less than 1 μm spatial resolution in several μm^2 areas.
3. One of the aliphatic C−H rich portions (~1 μm) in other slices of Bells may contain C−O bonds.
4. Some of organic rich regions might correspond to organic globules which are abundantly distributed in the Bells meteorite.

The NFIR imaging method can provide submicron spatial distribution of organic functional groups and their association with minerals. Further improvement of the present NFIR method would provide more information on the nature of microscopic organic matter.

References

Alexander C. M. O'D., Fogel M., Yabuta H., and Cody G. D. 2007. The origin and evolution of chondrites recorded in the elemental and isotopic compositions of their macromolecular organic matter. *Geochimica et Cosmochimica Acta* 71: 4380-4403.

Alpern B. and Benkheir Y. 1973. Distribution of organic-matter in Orgueil meteorite using fluorescence microscopy. *Earth and Planetary Science Letters* 19: 422-428.

Amri C. E., Maurel M. C., Sagon G., Baron M. H. 2005. The micro-distribution of carbonaceous matter in the Murchison meteorite as investigated by Raman imaging. *Spectrochimica Acta Part A* 61: 2049-2056.

Betzig E. and Trautman J. K. 1992. Near-field optics − microscopy, spectroscopy, and surface modification beyond the diffraction limit. *Science* 257: 189-195.

Botta O. and Bada J. L. 2002. Extraterrestrial organic compounds in meteorites. *Surveys in Geophysics* 23: 411-467.

Brearley A. J. 1995. Aqueous alteration and brecciation in Bells, an unusual, saponite-bearing, CM chondrite. *Geochimica et Cosmochimica Acta* 59: 2291-2317.

Browning L. B., McSween H. Y., and Zolensky M. E. 1996. Correlated alteration effects in CM carbonaceous chondrites. *Geochimica et Cosmochimica Acta* 60: 2621-2633.

Bunch T. E. and Chang S. 1980. Carbonaceous chondrites. 2. Carbonaceous chondrite phyllosilicates and light-element geochemistry as indicators of parent body processes and surface conditions. *Geochimica et Cosmochimica Acta* 44: 1543-1577.

Garvie L. A. J. and Buseck P. R. 2004. Nanosized carbon-rich grains in carbonaceous chondrite meteorites. *Earth and Planetary Science Letters* 224: 431-439.

Garvie L. A. J. and Buseck P. R. 2007. Prebiotic carbon in clays from Orgueil and Ivuna (CI), and Tagish Lake (C2 ungrouped) meteorites. *Meteoritics & Planetary Science* 42: 2111-2117.

Kennedy M. J., Pevear D. R., and Hill R. J. 2002. Mineral surface control of organic carbon in black shale. *Science* 295: 657-660.

Kerridge J. F. 1985. Carbon, hydrogen and nitrogen in carbonaceous chondrites: Abundances and isotopic compositions in bulk samples. *Geochimica et Cosmochimica Acta* 49: 1707-1714.

Kuya N., Nakashima S., Okumura S., Nakauchi M., Kimura S., and Narita Y. 2004. Near-field infrared microspectroscopy on the distribution of water and organics insubmicron area. In *Physicochemistry of Water in Geological Systems*, edited by Nakashima S., Spiers C. J., Mercury L., Fenter P. A. and Hochella M. F., Jr. Tokyo, Japan: Universal Academy Press. pp. 179-187.

Mackinnon I. D. R. and Zolensky M. E. 1984. Proposed structures for poorly characterized phases in C2M carbonaceous chondrite meteorites. *Nature* 309: 240-242.

Mayer L. M. 1994a. Relationships between mineral surfaces and organic-carbon concentrations in soils and sediments. *Chemical Geology* 114: 347-363.

Mayer L. M. 1994b. Surface-area control of organic-carbon accumulation in continental-shelf sediments. *Geochimica et Cosmochimica Acta* 58: 1271-1284.

Messenger S., Nakamura-Messenger K., and Keller L. P. 2008. 15N-rich organic globules in a cluster IDP and the Bells CM2 chondrite (abstract #2391). 39th Lunar and Planetary Science Conference. CD-ROM.

Monnig O. E. 1963. The Bells, Texas, Meteorites. *Meteoritics* 2: 67.

Nagy B., Claus G., and Hennessy D. J. 1962. Organic particles embedded in minerals in Orgueil and Ivuna carbonaceous chondrites. *Nature* 193: 1129-1133.

Nakamura K., Zolensky M. E., Tomita S., Nakashima S., and Tomeoka K. 2002. Hollow organic globules in the Tagish Lake meteorite as possible products of primitive organic reactions. *International Journal of Astrobiology* 1: 179-189.

NakashimaS., Ohki S., and Ochiai S. 1989. Infrared microspectroscopy analysis of the chemical state and spatial distribution of hydrous species in minerals. *Geochemical Journal* 23: 57-64.

Pearson V. K., Sephton M. A., Kearsley A. T., Bland P. A., Franchi I. A., and Gilmour I. 2002. Clay mineral-organic matter relationships in the early solar system. *Meteoritics & Planetary Science* 37: 1829-1833.

Pflug H. D. 1984. Microvesicles in meteorites, a model of pre-biotic evolution. Naturwissenschaften 71: 531-533.

Pizzarello S., Cooper G. W., and Flynn G. J. 2006. The nature and distribution of the organic material in carbonaceous chondrites and interplanetary dust particles. In *Meteorites and the early solar system II*, edited by Lauretta D. S., Leshin L. A., and McSween H. Y., Jr. Tucson,

Arizona: The University of Arizona Press. pp. 625-651.

Rossignol-Strick M. and Barghoorn E. S. 1971. Extraterrestrial abiogenic organization of organic-matter − hollow spheres of Orgueil meteorite. *Space Life Sciences* 3: 89-107.

Salmon V., Derenne S., Lallier-Verges E., Largeau C., and Beaudoin B. 2000. Protection of organic matter by mineral matrix in a Cenomanian black shale. *Organic Geochemistry* 31: 463-474.

Socrates G. 2001. *Infrared and Raman characteristic group frequencies*, 3rd ed. Chichester, England: John Wiley & Sons, LTD.

Zolensky M. Barrett R., and Browning L. 1993. Mineralogy and composition of matrix and chondrules rims in carbonaceous chondrites. *Geochimica et Cosmochimica Acta* 57: 3123-3148.

Chapter 4

THERMAL STABILITIES OF ORGANIC MATTER IN CARBONACEOUS CHONDRITES AND EFFECTS OF MINERALS

Abstract

In order to elucidate effects of minerals on the thermal transformation of organic matter, thermal alteration on carbonaceous chondrites were simulated experimentally under micro FTIR spectroscopy with a heating stage. Both bulk and insoluble organic matter (IOM) of Murchison (CM2) and Orgueil (CI1) meteorites were heated in a heating stage from room temperature to 600ºC in an inert gas (Ar) flow. Thermal stability of organic matter was lower in the presence of minerals for Murchison, while thermal stability was higher in the presence of minerals for Orgueil. For the heating experiments under Ar flow and air of leonardite humic acid (LHA) with and without saponite, antigorite and olivine as analogs of carbonaceous chondrites, the thermal stability of LHA is higher with the presence of saponite. On the other hand, antigorite and olivine accelerate the decrease of aliphatic fractions, and decelerate the decrease of aromatic fractions. These mineral effects become dominant in oxidizing atmosphere. These results suggest that the thermal stability of chondritic organic matter depends on associated minerals. The thermal stability of organic matter with and without minerals provides a valuable insight into how parent body processes affect the overall structure of organic matter of carbonaceous chondrites.

4.1. Introduction

Carbonaceous chondrites are among the most studied objects from the solar system because of their primitive bulk compositions, and occurrence of primitive condensates and organic compounds. The CM and CI chondrites contain a few wt% of carbon mainly as solvent unextractable macromolecular matter (e.g., Botta and Bada 2002; Sephton 2002; Pizzarello et al. 2006), hereafter named as insoluble organic matter (IOM). IOM constitutes 70-95% of the total organic content in these meteorites (Hayatsu and Anders 1981). This material has been variously described as, an aromatic skeleton bearing functional groups such as −COOH and −OH (Anders et al. 1973), a highly condensed aromatic structure with carbonyl and other functional groups attached (Hayatsu et al. 1977) and a number of aromatic cores linked and decorated by short-branched aliphatic groups (Cronin et al. 1987). The IOM was modified by secondary processes on meteorite parent asteroids, such as aqueous alteration and thermal metamorphism. Low-temperature stepwise combustion up to 450ºC exhibited two organic components: a labile portion released between 250ºC and 350ºC and more stable portion released up to 450ºC (Kerridge et al. 1987). The labile portion can act

as a parent for the free aromatic hydrocarbons in meteorites (Sephton et al. 1998).

Several CM and CI chondrites experienced thermal metamorphism after the aqueous alteration (e.g., Zolensky et al. 2005; Tonui et al. in prep.). When the chondritic carbonaceous matter was heated in the parent asteroids, it became graphitic due to carbonization and "graphitization" reactions. Wdowiak et al. (1988) heated Orgueil IOM under vacuum at different temperatures and found that new weak aromatic features appeared along with the decrease of the aliphatic content by infrared spectroscopy. Micro Raman studies have shown that the molecular structures of IOM appear to correlate well with the petrologic type (Quirico et al. 2003; Bonal et al. 2006, 2007; Busemann et al. 2007). Solid-state ^{13}C nuclear magnetic resonance (NMR) spectroscopy of thermally altered CM2 chondrites shows that the aliphatic structures of the IOM could be modified in some way during thermal alteration, by being oxidized, aromatized, graphitized, or lost (Yabuta et al. 2005). Kitajima et al. (2002) used pyrolysis-gas chromatography coupled with mass spectrometry (pyr-GC/MS) to analyze the pyrolyzates of IOM from CM chondrites and determined their degrees of graphitization during thermal metamorphism. Naraoka et al. (2004) proposed an organic parameter of thermal alteration using carbon, hydrogen, and nitrogen concentrations of IOM.

The relationship between organic matter and the products of aqueous alteration such as clay minerals has been reported. Pearson et al. (2002) found that the meteoritic organic matter is strongly associated with clay minerals, using an osmium tetroxide (OsO_4) labeling technique that highlights the location of organic material within whole-rock samples. The authors suggested that clay mineral may have had an important trapping and possibly catalytic role in chemical evolution in the early solar system. Garvie and Buseck (2007) investigated carbon-clay assemblages in CI and Tagish Lake meteorites using transmission electron microscopy (TEM) and electron energy-loss spectroscopy (EELS).

On the other hand, the distribution of organic matter and relationship to clay minerals in sediments has received considerable attention. There is much evidence that an intimate association exists between clays and organic matter (Guggenberger and Kaiser 2003; Keil et al. 1994; Kennedy et al. 2002; Mayer 1999). Salmon et al. (2000) reported that sedimentary organic matter appears to be physically protected by clays due to sorptive protection mechanism, and suggested that adsorption of labile organic compounds onto minerals, might prevent their diagenetic degradation and promote their subsequent condensation into kerogen. Smectite clay is also known to have catalytic effects for carbon-carbon bond cleavage (Davis and Stanley 1982). However,

organic-mineral relationship of carbonaceous chondrites is poorly understood.

Fourier transform infrared (FTIR) spectroscopy is a non-destructive technique for organic functional groups, and has been successfully applied to organic matter in carbonaceous chondrites (Hayatsu et al. 1977; Wdowiak et al. 1988; Ehrenfreund et al. 1991, 1992; Murae 1994; Raynal et al. 2000; Flynn et al. 2001; Keller and Flynn 2001; Nakamura et al. 2002; Kissin 2003; Matrajt et al. 2004). Nakamura et al. (2003) conducted preliminary in-situ FTIR heating experiments of organic matter of carbonaceous chondrites and indicated varying thermal stabilities of different organic functional groups.

In this study, in-situ FTIR heating experiments of IOM and bulk Murchison and Orgueil meteorites have been performed in order to elucidate effects of minerals for thermal stability of organic matter. In addition, simulated heating experiments using humic acid with some minerals have been conducted in order to evaluate effects of specific minerals. I found that thermal stability of each functional group observed by infrared spectra was affected differently by coexisting minerals.

4.2. Samples

4.2.1. Carbonaceous Chondrite Samples

In order to study thermal stability of chondritic organic matter, two organic rich carbonaceous chondrites classified in different groups were used. Murchison (CM2) and Orgueil (CI1) meteorites were kindly provided by Dr. M. E. Zolensky at NASA Johnson Space Center. For bulk meteorite samples, matrix powders from freshly broken surfaces of the Murchison and Orgueil were pressed on a KBr plate with glass slides.

Murchison (CM2) fell in 1969 in Australia. Its matrix consists mainly of serpentine, tochilinite, Fe-Ni sulfides, carbonates, olivine and Fe-Ni metal (Zolensky and McSween 1988; Zolensky et al. 1993). Its total carbon content is 1.56-2.5 wt% (Kerridge 1985) and the insoluble carbon content is 0.83 wt% (Alexander et al. 2007). H/C and O/C ratios of the IOM are 0.588±0.016 and 0.183±0.003, respectively (Alexander et al. 2007). ^{13}C NMR estimates of carbon distribution of the IOM are 7.8-11.2% of CH_x, 12.3-8.9% of CH_xO, 14.2-18.2% of CO, and 65.7-61.7% of aromatic (total 100%) (Cody and Alexander 2005).

Orgueil (CI1) fell in 1864 in France. Its matrix consists mainly of serpentine, saponite, Fe oxides, Fe-Ni sulfides, carbonates and sulfates (Tomeoka and Buseck 1988; Zolensky et al. 1993). Its total carbon content is 2.71-3.75 wt% (Kerridge 1985) and

the insoluble carbon content is 2.00 wt% (Alexander et al. 2007). H/C and O/C ratios of the IOM are 0.673±0.014 and 0.181±0.002, respectively (Alexander et al. 2007). ^{13}C NMR estimates of carbon distribution of the IOM are 9.2-13.2% of CH_x, 17.6-13.6% of CH_xO, 8.5-12.5% of CO, and 64.7-60.7% of aromatic (total 100%) (Cody and Alexander 2005).

4.2.2. IOM Sample Preparation Procedures

Murchison (CM2) meteorite and Orgueil (CI1) meteorite (bulk) and their IOM were used to compare thermal stabilities of organic matter with and without mineral matrix.

The preparation procedures of IOM are as follows. All glassware used was sterilized by annealing in aluminum foil at 500ºC for 3 h. Murchison and Orgueil (0.7 g and 0.2 g, respectively) were broken using an alumina mortar and pestle. Soluble organic fractions from the powdered meteorite samples were extracted with organic solvent, a mixture of CH_2Cl_2/CH_3OH (9/1, v/v), with ultrasonication. The sample was then rinsed with 2 N HCl at room temperature. The extracted residue was shaken with 8 N HF/4 N HCl in a Teflon container at room temperature for more than 48 hours, followed by washing with 2 N HCl. This process was repeated several times. The demineralized residue was washed with water, methanol, dichloromethane, in that order, and was dried under vacuum. The powdered IOM was pressed on a KBr plate using a cleaned stainless spatula.

4.2.3. Simulated Meteoritic Materials

In order to elucidate effects of minerals on the thermal decomposition of chondritic organic matter, leonardite humic acid (LHA) was used as an analog of macromolecular organic matter in primitive carbonaceous chondrites. The H/C and O/C ratios and fractional concentration of aliphatic and aromatic moieties of LHA are relatively similar to those of chondrite IOM. Hence, LHA is expected to show similar thermal behavior to chondrite IOM. Synthetic saponite, natural antigorite and olivine were used as the representative matrix minerals. Details of materials used were as follows.

(1) Leonardite humic acid (LHA) standard: catalog number 1S104H, purchased from International Humic Substances Society (IHSS); H/C and O/C ratios are 0.70 and 0.37, respectively (IHSS, http://www.ihss.gatech.edu); ^{13}C NMR estimates of carbon distribution are 8% of carbonyl, 15% of carboxyl, 58% of

aromatic, 4% of acetal, 1% of heteroaliphatic, and 14% of aliphatic (total 100%) (IHSS, http://www.ihss.gatech.edu).

(2) Synthetic saponite (Sumecton SA®): $(Na,Mg)_{0.33}[(Si,Al)_4(Mg,Al)_3O_{10}(OH)_2]\cdot 4H_2O$; obtained from Kunimine Industries Co., Ltd. in fine powder form; Fe is not detected.

(3) Antigorite: $(Mg,Fe^{2+})_3Si_2O_5(OH)_4$; from Nakanochaya, Miyatsu, Kyoto, Japan; purchased from Nichika Corp. in fine powder form; Fe/Mg ratio is 0.04 (Uehara and Shirozu 1985).

(4) San Carlos olivine: $(Mg_{0.92},Fe_{0.08})_2SiO_4$; average grain size is approximately 7 μm; Fe/Mg ratio is 0.09 (Yamanoi 2008, Ph. D. Thesis).

LHA was mixed with saponite, antigorite and olivine with mixing ratio (wt.) of 45:55, 46:54 and 44:56, respectively, using an alumina mortar and pestle. These powdered samples were dispersed by MilliQ water then dropped on a CaF_2 plate and dried for an hour in an oven at around 50ºC.

4.3. Experimental Methods

4.3.1. TG-DTA Analysis

In order to examine thermal changes of organic matter which occurred during step heating experiments, thermogravimetric analysis (TG) and differential thermal analysis (DTA) were carried out simultaneously using a Rigaku ThermoPlus TG8110 instrument.

22.57 mg of LHA was weighed on a platinum crucible and heated from room temperature to 700ºC in a static air atmosphere. 43.65 mg of Murchison meteorite powder was weighed on a platinum crucible and heated from room temperature to 800ºC in Ar gas flow at the rate of 0.89 L/min. The heating rate was 10 ºC/min. Alumina (Al_2O_3) was used as a reference material.

4.3.2. In-Situ Heating Experiments under Micro FTIR

In order to elucidate thermal stabilities of chondritic organic matter and simulated organic materials, in-situ heating experiments under micro FTIR were conducted. Micro FTIR spectroscopy is a well-established technique for the identification of organic functional groups. In-situ observation of spectral changes during heating has been successfully performed by several authors (e.g., Rose et al. 1998; Nakamura et al. 2003; Okumura and Nakashima 2004).

A ceramic infrared light source, a Mercury-Cadmium-Telluride (MCT) detector

and a ×16 Cassegrainian mirror were used for the FTIR spectroscopy (Jasco FT-IR-620 + IRT30). 100 scans were accumulated with a wavenumber resolution of 4 cm^{-1}, in the wavenumber range of 4000-700 cm^{-1}.

All spectra were collected as absorbance (*Abs*) according to the following Lambert-Beer's law:

$$Abs = -\log_{10}\left(\frac{I}{I_0}\right) = \varepsilon dc \qquad (4\text{-}1)$$

I_0 and I are the background and sample infrared signal intensities, ε is the molar absorptivity, d is the thickness of the sample and c is the concentration of the component of interest.

Samples mounted on CaF_2 or KBr plates were set onto a heating stage (Linkam FTIR 600) and placed into the micro FTIR. The background spectra were collected on the sample-free area of the CaF_2 or KBr plate at room temperature. After measuring the sample spectra at room temperature, the samples were heated at 10 ºC/min from room temperature up to 600ºC using the heating stage under ambient air, and in an inert atmosphere of Ar. In the gas flow experiment, the sample was set between two CaF_2 windows of the heating stage and the low-oxygen condition for an anoxic atmosphere was maintained by flowing of Ar gas (99.99%) at 84 mL/min into the heating stage.

During the heating, sample spectra were collected from the same location at every 20ºC step. The temperature was kept constant during the collection of the sample spectra.

4.4. Results

4.4.1. TG-DTA Analysis

In order to study thermal changes of the samples during heating and to compare with in-situ infrared analyses, TG-DTA analyses were conducted.

The TG and DTA curves in air of leonardite humic acid (LHA) samples are shown in Fig. 4-1. The weight loss by TG of LHA is 72.66% during the step heating at 10 ºC/min up to 700ºC under air (Table 4-1).

The DTA curves of LHA showed a first exothermic peak at 342ºC and a second one at 442ºC. These results were consistent with the TG-DTA results on LHA samples of Francioso et al. (2005) which showed a first exothermic effect at 278-347ºC and a second one at 455-492ºC. According to the authors, the combustion reaction of the first exothermic peak was constantly lower than the second one, suggesting the presence

of a small proportion of carbohydrates and hydroxylated aliphatic structures. The more intense combustion reaction evidenced by the second peak is due to the cracking of higher molecular weight polynuclear systems.

The TG-DTA curves of the bulk Murchison meteorite are shown in Fig. 4-2. The weight loss of Murchison is 16.38% during step heating at 10 ºC/min up to 800ºC under Ar flow (Table 4-1). The DTA curve shows the baseline drift to the endothermic side, which is known to be an inevitable consequence of the gas flow at the sample cell (Shimoyama et al. 1991). Therefore, the curves are generally not good enough to show clear endothermic and/or exothermic peaks, and any comparison of the curves is not easy except for two peaks.

The curve of Murchison showed very broad exothermic peak over the temperature range of about 200-300ºC. These results were consistent with the TG-DTA results of Antarctic CM chondrites and were due partly to the degradation of insoluble organic matter (Shimoyama et al. 1991). An endothermic peak appeared at 419ºC was likely due to thermal decomposition of organic matter. A clear exothermic peak appeared at 683ºC. It is likely due to a change in inorganic phases rather than organic matter. It is known that magnetite had an exothermic peak around 600-700ºC, while calcite and dolomite do not show an endothermic or exothermic peak below 800ºC (Shimoyama et al. 1991). On the other hand, dehydration of serpentine is known to have an endothermic peak at 670ºC (Reddy et al. 1991). The endothermic peak at 660ºC of DTA curve of Murchison might be due to dehydration of serpentine.

Table 4-1. TG-DTA analysis of leonardite humic acid (LHA) and bulk Murchison meteorite.

Sample	Sample weight			Maximum temperature	Atmosphere
	Start [mg]	End [mg]	Weight loss [%]	[°C]	
LHA	22.57	6.17	72.66	700	Air
Murchison	43.65	36.50	16.38	800	Ar

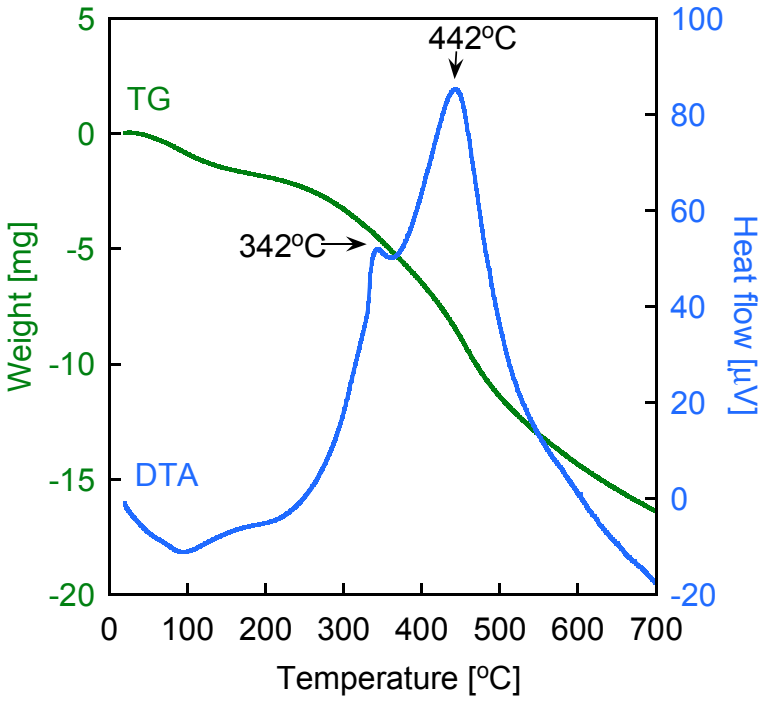

Fig. 4-1. TG-DTA curves in air atmosphere of leonardite humic acid (LHA).

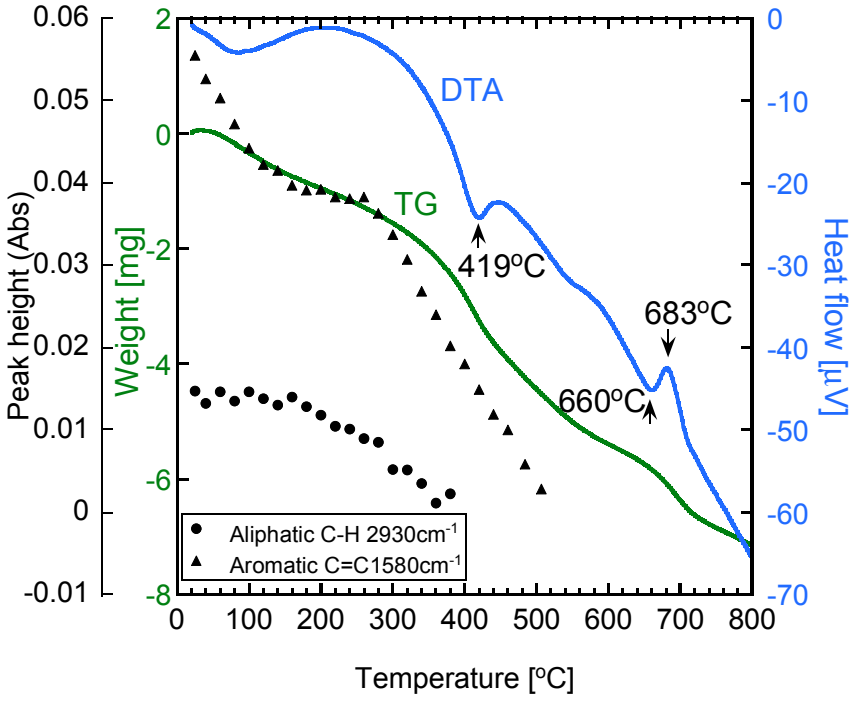

Fig. 4-2. TG-DTA curves in Ar flow of bulk Murchison meteorite, together with changes with temperature in infrared peak heights of aliphatic C−H and aromatic C=C observed by FTIR.

4.4.2. Heating Experiments of Carbonaceous Chondrites and the IOM

In order to evaluate thermal stability of chondritic organic matter with and without mineral, heating experiments of Murchison and Orgueil meteorites were conducted on their acid treated insoluble organic matter (IOM) and untreated meteorite powder (bulk).

The infrared absorption spectra of bulk meteorite of Murchison and Orgueil (Figs. 4-3a,c) showed some organic features at 2960 and 2870 cm^{-1} due to asymmetric and symmetric stretching vibrations of aliphatic CH_3, respectively, 2930 and 2855 cm^{-1} due to asymmetric and symmetric stretching vibrations of aliphatic CH_2, respectively, 1590 cm^{-1} shoulder due to aromatic C=C, and 1450 and 1375 cm^{-1} due to aliphatic C−H bending. Inorganic features appeared at 1030 cm^{-1} due to Si−O stretching vibration. The bands around 3400 cm^{-1} due to O−H stretching and 1640 cm^{-1} due to O−H bending were attributed to interlayer molecular water in phyllosilicates and/or water molecules loosely adsorbed on minerals. The 3675 cm^{-1} band of Orgueil and the broad 3550 cm^{-1} shoulder of Murchison were due to structural O−H stretching of phyllosilicates. In fact, serpentines are reported in the matrix of Murchison and Orgueil, and saponite is reported in the matrix of Orgueil (Zolensky and McSween 1988; Zolensky et al. 1993). The band around 1450 cm^{-1} of bulk Orgueil probably included absorption due to carbonates. The band at 2360 cm^{-1} is due to atmospheric CO_2.

Silicate features such as Si−O and structural O−H completely disappeared on the IOM spectra of Murchison and Orgueil (Figs. 4-3b,d). Organic features become recognizable at 1700 cm^{-1} due to C=O stretching and 1235 cm^{-1} due to C−O stretching, besides aliphatic C−H and aromatic C=C bands. The broad 3230cm^{-1} band of Murchison IOM was probably due to O−H stretching of alcohol, phenol and/or carboxyl groups. The 1140 and 1100 cm^{-1} bands of Murchison IOM were unknown but plausibly due to C−O and/or SO_2.

Fig. 4-4 showed spectra of Murchison and Orgueil (bulk and IOM) during step heating in Ar flow. Changes with temperature of peak heights at 2930 cm^{-1} due to aliphatic C−H, 1700 cm^{-1} due to C=O, and 1580 cm^{-1} due to aromatic C=C were determined for Murchison and Orgueil (bulk and IOM) during heating under Ar atmosphere (Figs. 4-5, 4-6 and 4-7). Peak heights were calculated with straight baseline correction at 2990-2890 cm^{-1} for 2930 cm^{-1}, 1800-1310 cm^{-1} for 1700 and 1680 cm^{-1} of IOM, and 1820-1480 cm^{-1} for 1700 and 1680 cm^{-1} of bulk meteorites.

The 2930 cm^{-1} band due to aliphatic C−H decreased from 100-200ºC to around 400-500ºC (Fig. 4-5). The 1700 cm^{-1} band due to C=O decreased from room temperature to around 400-600ºC (Fig. 4-6). The 1580 cm^{-1} due to aromatic C=C decreased from 300-400ºC to around 500-600ºC (Fig. 4-7). Apparent peak height

decreases around room temperature to ~100ºC of 1700 and 1580 cm^{-1} were probably due to decrease of water absorption band around 1640 cm^{-1}.

In order to compare thermal stabilities of chondritic organic matter with and without minerals (bulk and IOM), temperatures of peak disappearance T_{pd} were determined. Fig. 4-8 and Table 4-2 shows T_{pd} values at which baseline corrected peak heights became under the noise level (< 0.001). In inert atmosphere, T_{pd} of C=O and aliphatic C−H for bulk Murchison show lower value than for IOM, although aromatic C=C does not show significant difference between the presence and the absence of minerals assuming the uncertainty of T_{pd} as ± 20ºC. On the other hand, T_{pd} of C=O for Orgueil IOM shows clearly a lower value than that for bulk Orgueil, although T_{pd} of C=O for bulk is unclear due to limitation of temperature of the heating stage. Aliphatic C−H does not show a significant difference between the presence and the absence of minerals. Since aromatic C=C of bulk Orgueil and IOM showed its presence at 600ºC, the effect of minerals of the band is not clear. As a general trend, mineral assemblage of Orgueil appeared to inhibit decrease of IOM, while that of Murchison accelerated the decrease of IOM.

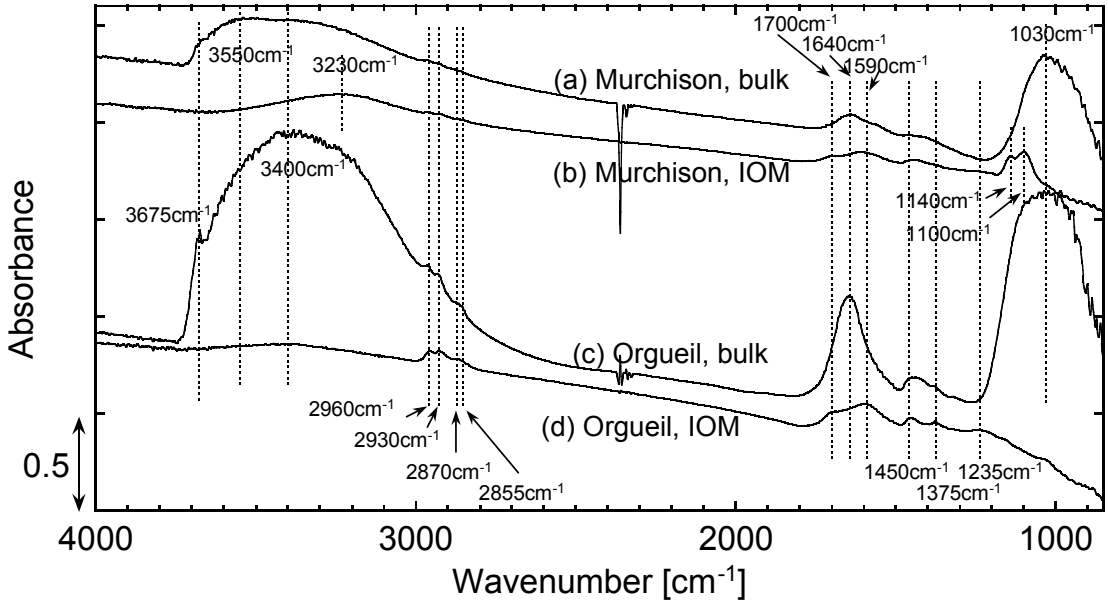

Fig. 4-3. Micro FTIR absorption spectra of Murchison (a) bulk meteorite and (b) IOM, and Orgueil (c) bulk meteorite and (d) IOM. The sample powders were pressed on KBr plates (< 1 mm thick). After collecting the background spectra on sample free regions of the same KBr plates, transmission spectra were collected with 100 × 100 μm^2 aperture at room temperature.

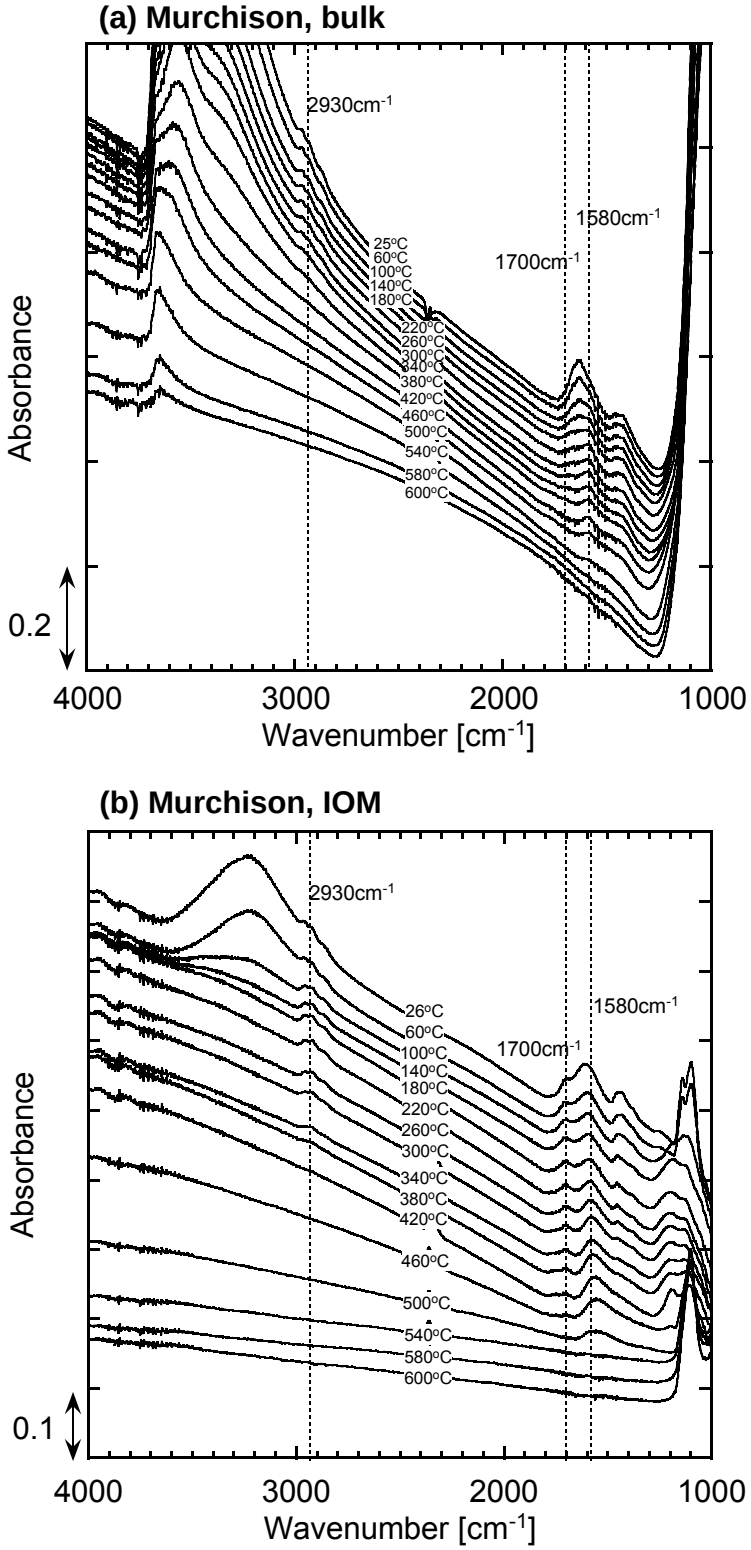

Fig. 4-4. Infrared spectral changes with temperature during the heating experiment under Ar flow. (a) Murchison bulk meteorite, (b) Murchison IOM, (c) Orgueil bulk meteorite, and (d) Orgueil IOM.

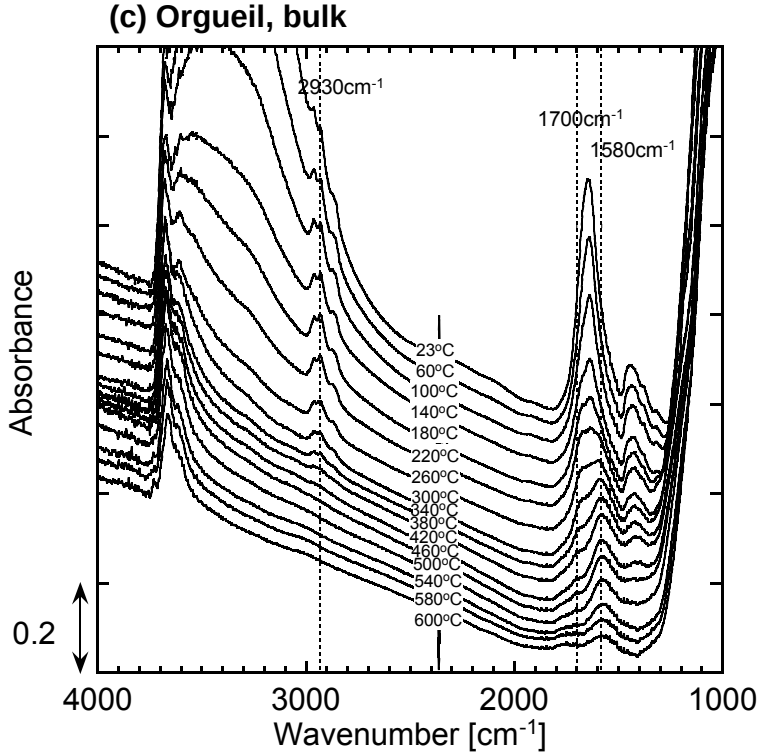

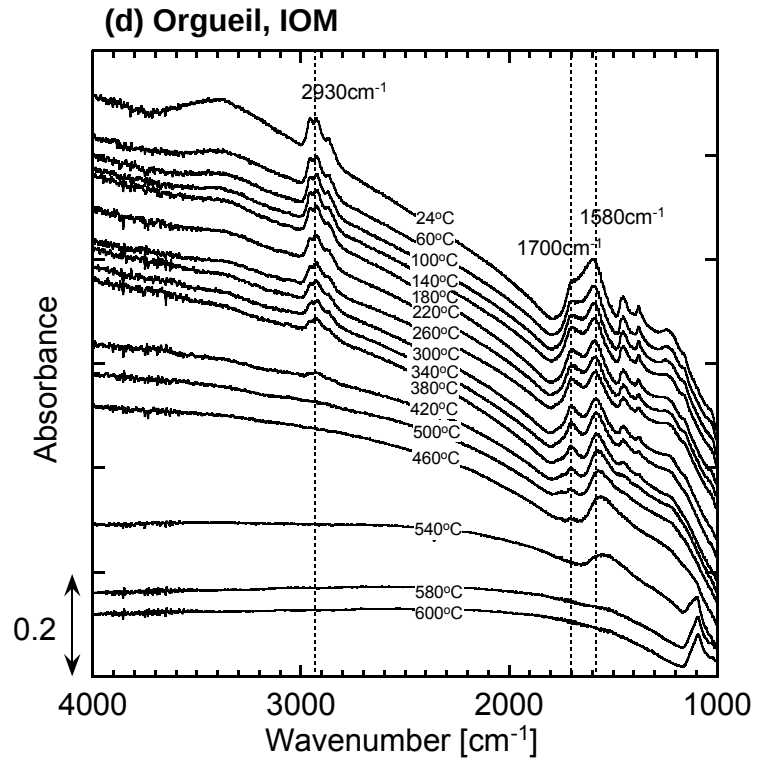

Fig. 4-4. (continued)

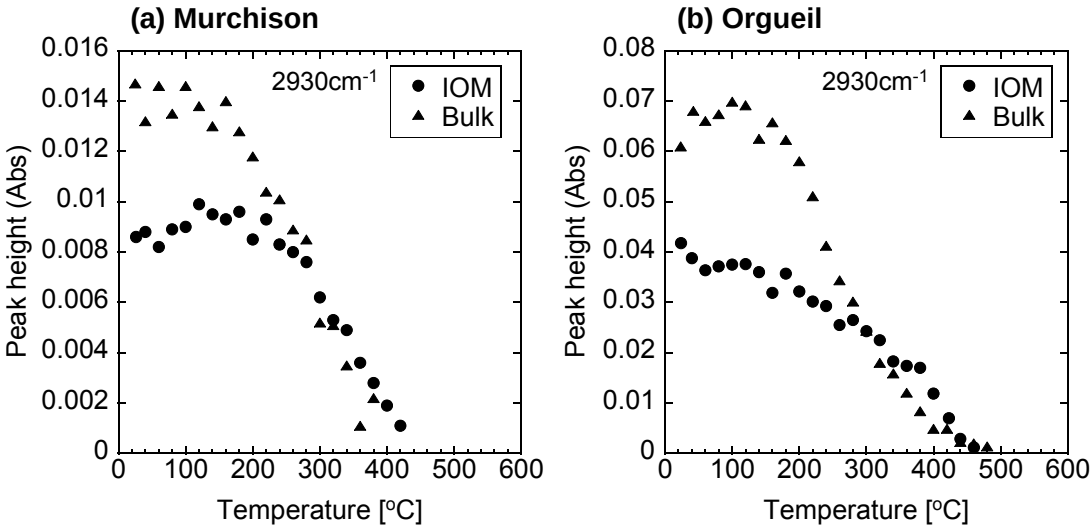

Fig. 4-5. Peak heights changes with temperature of aliphatic C−H at 2930 cm^{-1} during heating under Ar flow of (a) Murchison and (b) Orgueil.

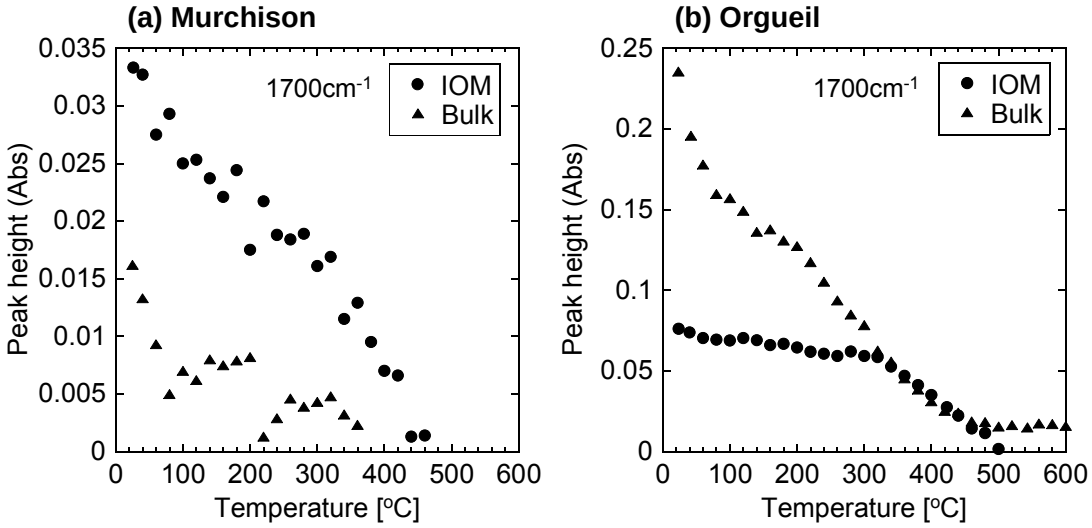

Fig. 4-6. Peak heights changes with temperature of C=O at 1700 cm^{-1} during heating under Ar flow of (a) Murchison and (b) Orgueil.

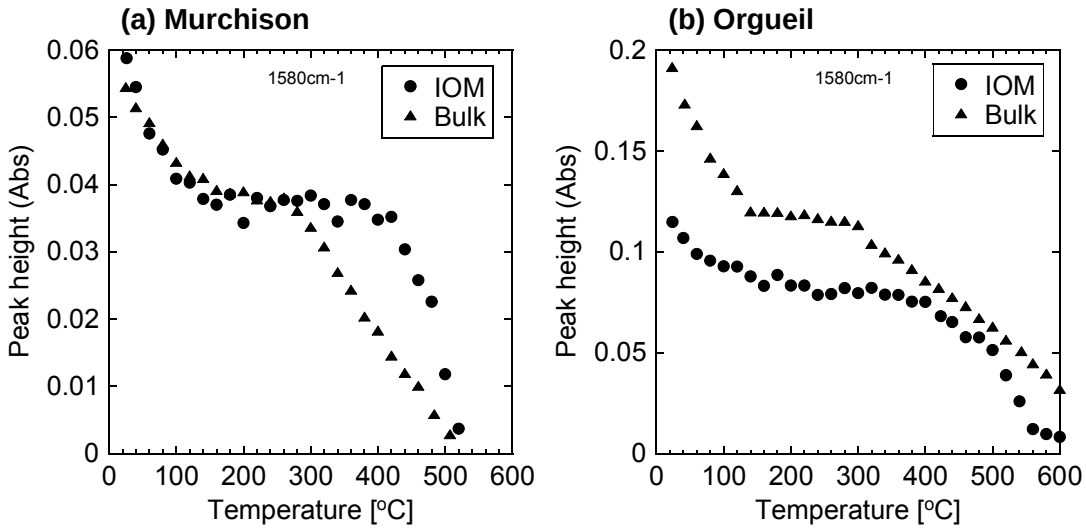

Fig. 4-7. Peak heights changes with temperature of aromatic C=C at 1580 cm^{-1} during heating under Ar flow of (a) Murchison and (b) Orgueil.

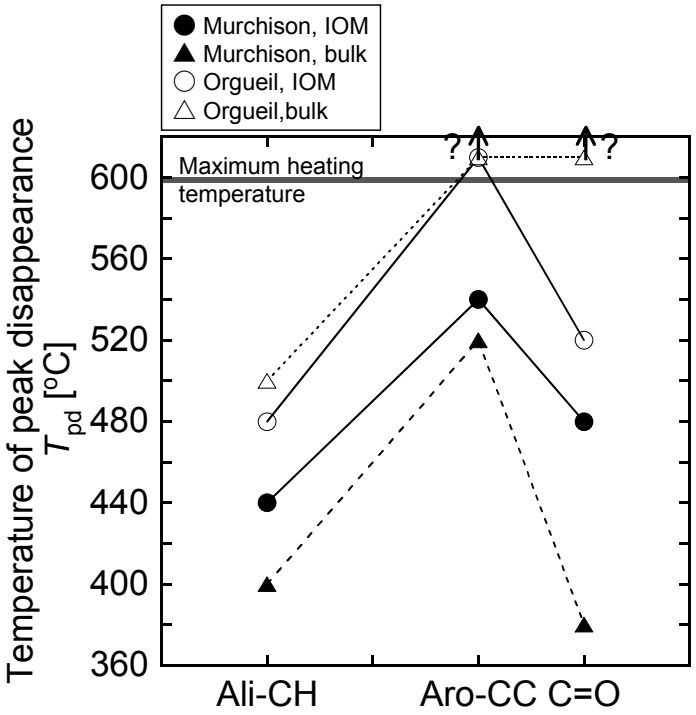

Fig. 4-8. Temperatures of peak disappearance T_{pd} determined for each functional group of Murchison and Orgueil (bulk and IOM) under Ar flow. The maximum heating temperature of the heating stage used here is 600ºC. Aromatic C=C of Orgueil IOM, and Aromatic C=C and C=O of bulk Orgueil showed band at 600ºC. Therefore T_{pd} of these bands are likely over 600ºC.

Table 4-2. Temperatures of peak disappearance T_{pd} of chondrites with and without minerals in Ar flow.

		Temperature of peak disappearance T_{pd} [°C]		
		Aliphatic C−H 2930 cm^{-1}	Aromatic C=C 1580 cm^{-1}	C=O 1700 cm^{-1}
Orgueil	Bulk	500	> 600	> 600
	IOM	480	> 600	520
Murchicon	Bulk	400	520	380
	IOM	440	540	480

4.4.3. Heating Experiments of Simulated Meteoritic Materials

In order to evaluate effects of coexisting minerals on the thermal stability of organic matter, heating experiments of leonardite humic acid (LHA, analog of chondritic IOM) were conducted with and without minerals (saponite, antigorite and olivine; representative matrix minerals of CM and CI chondrites; Zolensky et al. 1993).

The infrared absorption spectrum of LHA (Fig. 4-9a) showed a broad band around 3400 cm^{-1} due to water and hydroxyl O−H stretching vibrations, 2920 and 2850 cm^{-1} bands due to asymmetric and symmetric stretching vibrations of aliphatic CH_2, respectively, a 1705 cm^{-1} band due to C=O of COOH, a 1600 cm^{-1} band due to aromatic C=C, 1440 and 1380 cm^{-1} bands due to aliphatic C−H bending, and a 1230 cm^{-1} band due to C−O stretching (peak assignments are based on Socrates 2001). The infrared absorption spectra of LHA with minerals (saponite, antigorite and olivine) showed large bands due to Si−O stretching in the region 1200-900 cm^{-1} of silicates besides organic features of LHA (Figs. 4-9b-d). The infrared spectrum of LHA with saponite showed prominent 3400 and 1630 cm^{-1} bands due to O−H stretching and bending, respectively, mainly corresponding to interlayer water of saponite (Fig. 4-9b). The infrared spectrum of LHA with antigorite showed a 3670 cm^{-1} band and a shoulder at 3550 cm^{-1} due to structural O−H stretching of antigorite (Fig. 4-9c). A band at 2360 cm^{-1} was due to atmospheric CO_2.

Fig. 4-10 showed spectra of LHA during step heating in Ar flow. Changes with temperature of peak heights at 3070 cm^{-1} due to aromatic C−H, 2925 cm^{-1} due to aliphatic C−H, 1710 cm^{-1} due to C=O, and 1600 cm^{-1} due to aromatic C=C were determined for above samples (LHA, LHA+Sap, LHA+Ant and LHA+Oli) during heating under Ar (Fig. 4-11) and air (Fig. 4-12). Peak heights were calculated with

straight baseline correction at 3170-3020 cm^{-1} (≤ 360ºC) and 3170-3000 cm^{-1} (≥ 380ºC) for 3070 cm^{-1}, 3000-2870 cm^{-1} for 2925 cm^{-1}, 1800-1670 cm^{-1} for 1710 cm^{-1}, and 1670-1500 cm^{-1} for 1600 cm^{-1}.

The 3070 cm^{-1} band due to aromatic C−H which could not be well observed at room temperature, increased from room temperature to around 300-400ºC, then decreased to around 500-600ºC (Figs. 4-11a and 4-12a). The 2925 cm^{-1} band due to aliphatic C−H decreased from around 200-300ºC to around 400-500ºC (Figs. 4-11b and 4-12b). The 1710 cm^{-1} band due to C=O decreased from 100-150ºC to around 400-500ºC (Figs. 4-11c and 4-12c). The 1600 cm^{-1} due to aromatic C=C decreased from around 300ºC to around 500-600ºC (Figs. 4-11d and 4-12d).

In order to compare thermal stabilities of each sample, temperatures of peak disappearance T_{pd} were determined. Fig. 4-13 and Table 4-3, 4-4 shows T_{pd} at which calculated peak heights became under the noise level (< 0.001). In inert atmosphere, T_{pd} of aromatic C=C for LHA+Sap shows a higher value than that for LHA only, although T_{pd} of C=O for LHA+Sap seems lower than for LHA only. Aliphatic C−H and aromatic C−H do not show a significant difference between the presence and the absence of saponite. The uncertainty of T_{pd} is likely to be ± 20ºC which reflects dependence on baseline positions. T_{pd} values for LHA+Ant and LHA+Oli do not show a significant difference from LHA, except T_{pd} of C=O for LHA+Oli shows a lower value than that for LHA. It should be noted that the maximum heating temperature of the heating stage is 600ºC. Aromatic C−H and C=C of LHA+Sap Run 1, and aromatic C=C of LHA+Sap Run2 showed their presence at 600ºC. Therefore T_{pd} of these functional groups are likely over 600ºC.

On the other hand, in oxidizing atmosphere, T_{pd} values for LHA+Sap are higher than for LHA only on the all functional groups. T_{pd} values of aromatic C−H and C=C for LHA+Ant are higher than for LHA, while T_{pd} of aliphatic C−H is lower than LHA only. T_{pd} of C=O for LHA+Ant and LHA are the same values. T_{pd} value of aliphatic C−H for LHA+Oli is clearly lower than for LHA, and T_{pd} of aromatic C=C is clearly higher than for LHA only. T_{pd} of aromatic C−H for LHA+Oli Run2 shows a higher value than LHA. T_{pd} of C=O for LHA+Oli is similar to T_{pd} for LHA. Aromatic C−H of LHA+Ant Run2 and aromatic C=C of LHA+Sap Run2 showed their presence at 600ºC. Therefore T_{pd} of these functional groups are likely over 600ºC.

Overall, saponite appeared to inhibit decrease of all observed functional groups of LHA. Antigorite and olivine appeared to inhibit decrease of aromatic fraction, while accelerated decrease of aliphatic fraction. These effects were become dominant in oxidizing atmosphere.

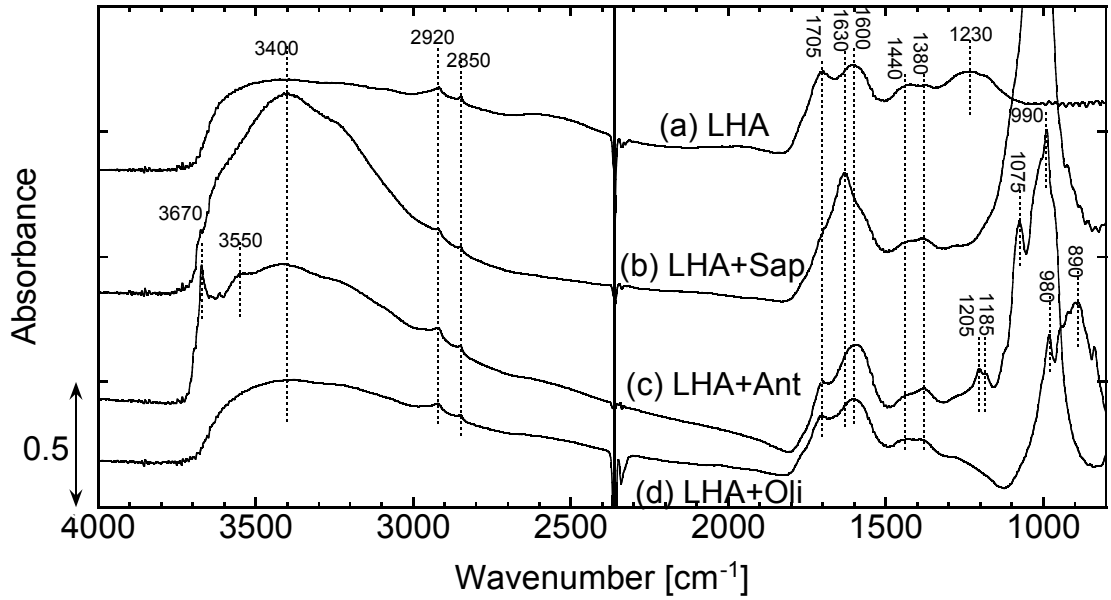

Fig. 4-9. Micro FTIR absorption spectra of (a) LHA, (b) LHA with saponite (LHA+Sap), (c) LHA with antigorite (LHA+Ant), and (d) LHA with olivine (LHA+Oli). The sample powders were diluted in water and dried on CaF_2 plates (1 mm thick). After collecting the background spectra on sample free regions of the same CaF_2 plates, transmission spectra were collected with 300 × 300 μm^2 (200 × 200 μm^2 for LHA+Oli) aperture at room temperature.

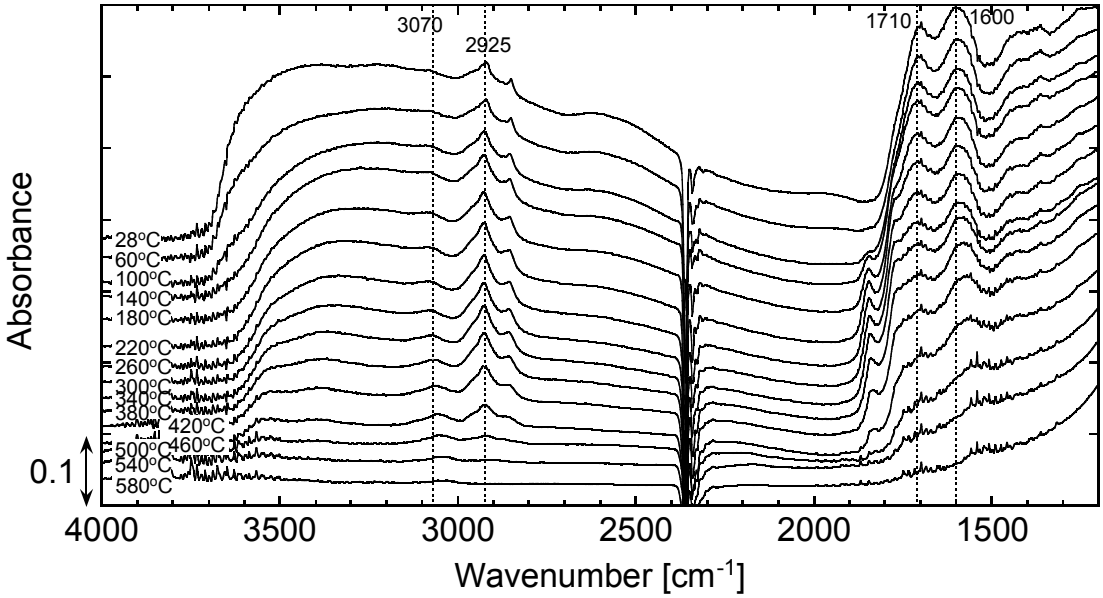

Fig. 4-10. Infrared spectral changes with temperature during the heating experiment of LHA under Ar flow.

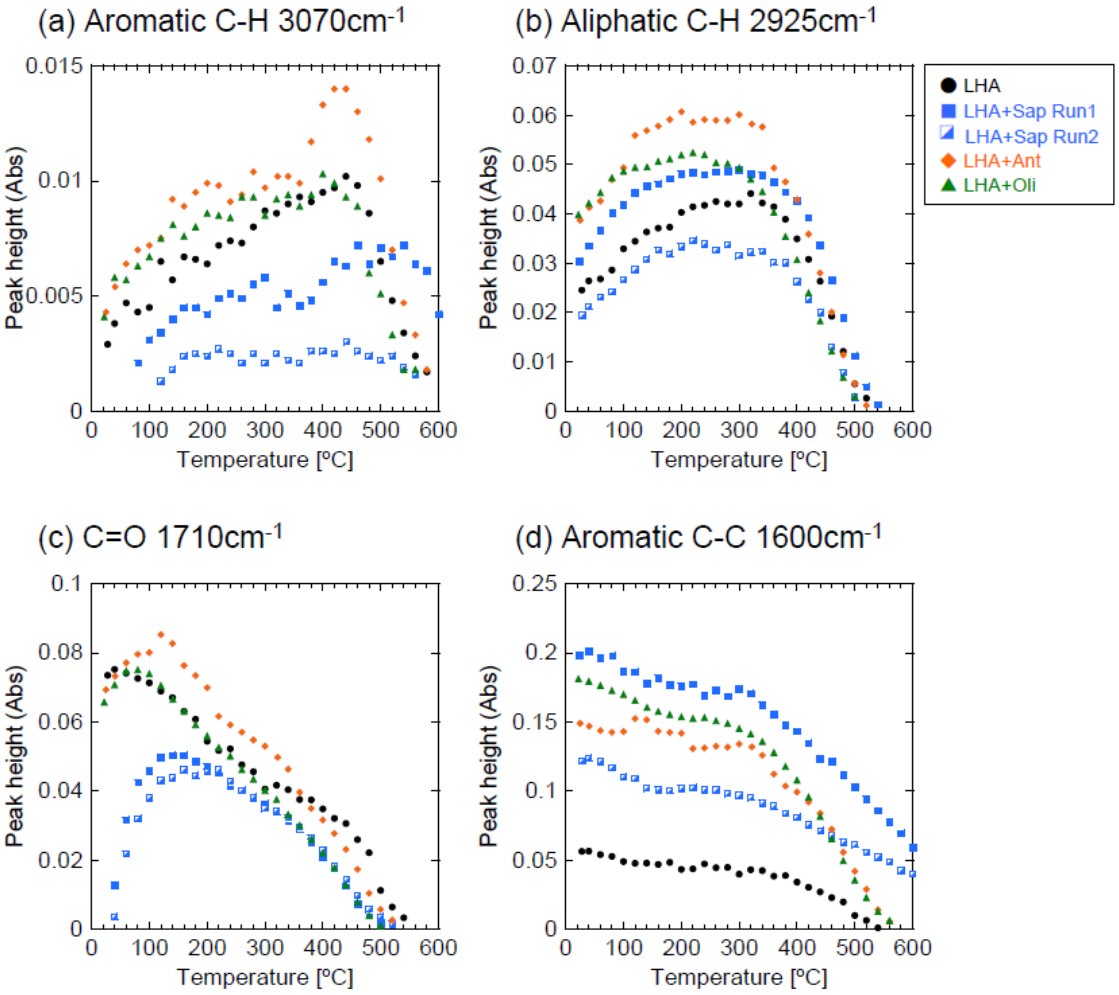

Fig. 4-11. Changes in peak heights upon heating of LHA, LHA+Sap, LHA+Ant and LHA+Oli under Ar flow. (a) Aromatic C−H at 3070 cm^{-1}, (b) Aliphatic C−H at 2925 cm^{-1}, (c) C=O at1710 cm^{-1},and (d) Aromatic C=C at 1600 cm^{-1}.

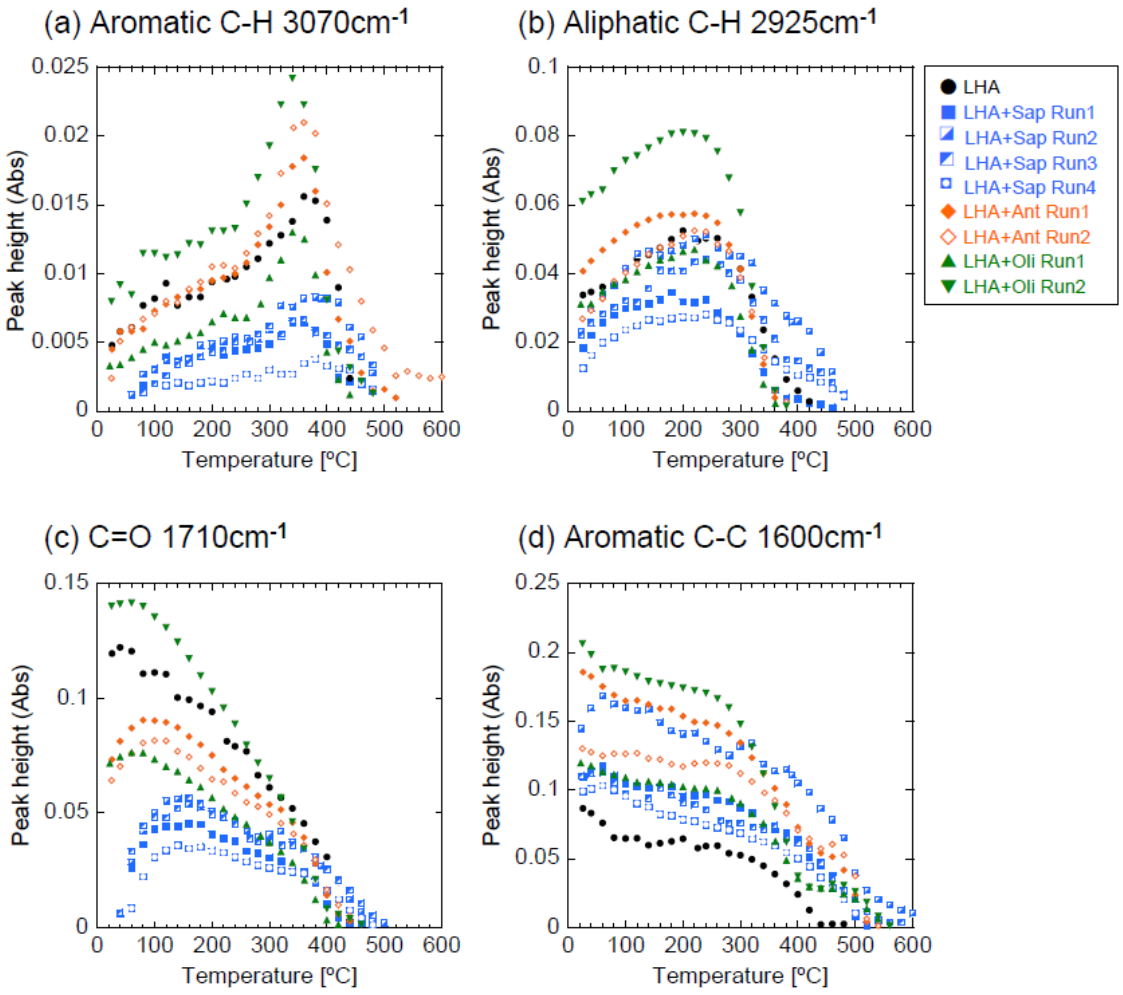

Fig. 4-12. Changes in peak heights upon heating of LHA, LHA+Sap, LHA+Ant and LHA+Oli under air. (a) Aromatic C−H at 3070 cm^{-1}, (b) Aliphatic C−H at 2925 cm^{-1}, (c) C=O at 1710 cm^{-1}, and (d) Aromatic C=C at 1600 cm^{-1}.

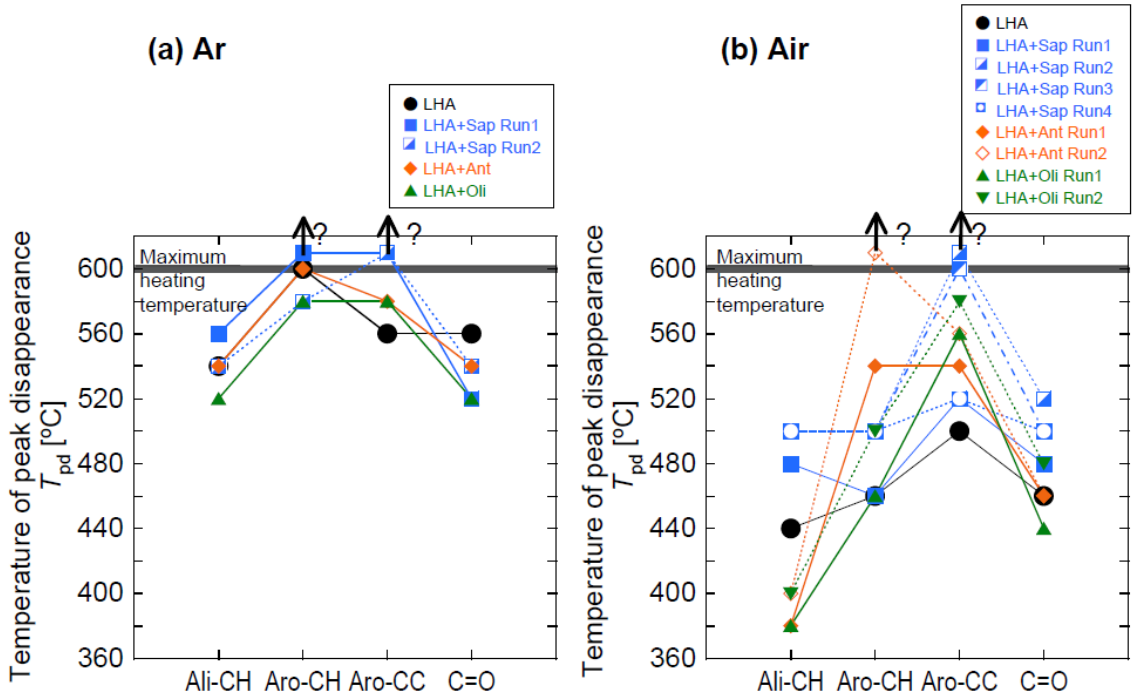

Fig. 4-13. Temperatures of peak disappearance T_{pd} determined for each functional group. (a) Heating experiments under atmospheric condition (air), and (b) heating experiments under Ar flow. The maximum heating temperature of the heating stage used here is 600ºC. Aromatic C−H and C=C of LHA+Sap Run1 and aromatic C=C of LHA+Sap Run2 in Ar, and aromatic C−H of LHA+Ant Run2 and aromatic C=C of LHA+Sap Run2 in air showed band at 600ºC. Therefore T_{pd} of these bands are likely over 600ºC.

Table 4-3. Temperatures of peak disappearance T_{pd} of LHA with and without minerals in air.

	Temperature of peak disappearance T_{pd} [°C]			
	Aliphatic C−H 2925 cm^{-1}	Aromatic C−H 3070 cm^{-1}	Aromatic C=C 1600 cm^{-1}	C=O 1710 cm^{-1}
LHA	540	600	560	560
LHA+Saponite Run1	560	> 600	> 600	520
LHA+Saponite Run2	540	580	> 600	540
LHA+Antigorite	540	600	580	540
LHA+Olivine	520	580	580	520

Table 4-4. Temperatures of peak disappearance T_{pd} of LHA with and without minerals in Ar flow.

	Temperature of peak disappearance T_{pd} [°C]			
	Aliphatic C−H 2925 cm^{-1}	Aromatic C−H 3070 cm^{-1}	Aromatic C=C 1600 cm^{-1}	C=O 1710 cm^{-1}
LHA	440	460	500	460
LHA+Saponite Run1	480	460	520	480
LHA+Saponite Run2	500	500	> 600	520
LHA+Saponite Run3	500	500	600	500
LHA+Saponite Run4	500	500	520	500
LHA+Antigorite Run1	380	540	540	460
LHA+Antigorite Run2	400	> 600	560	460
LHA+Olivine Run1	380	460	560	440
LHA+Olivine Run2	400	500	580	480

4.5. Discussion

4.5.1. Effects of Minerals for Thermal Decomposition of a Humic Acid

According to the TG-DTA curves of leonardite humic acid (LHA) (Figs. 4-1), decomposition of carbohydrates and hydroxylated aliphatic structures is likely to occur at around 350ºC, then the cracking of higher molecular weight polyaromatic structure is likely to take place at around 450ºC (Francioso et al. 2005). This is roughly consistent with in-situ IR heating experiments which show decreases of C=O and aliphatic C−H at around 200ºC to 400ºC (Figs. 4-12b,c), and decrease of aromatics at around 400ºC (Figs. 4-12a,d).

Table 4-5 summarizes the effects of minerals for thermal decomposition of LHA. On the heating experiments under ambient atmosphere, saponite inhibits decreases of all observed functional groups of LHA. Antigorite and olivine inhibit decrease of aromatic fraction, but accelerate decrease of aliphatic fraction. On the other hand, heating under inert atmosphere, saponite inhibits decrease of aromatic C=C but accelerate decrease of C=O. Olivine accelerates decrease of C=O.

Saponite seems to have sorptive preservation capacity of organic matter under oxidizing atmosphere. Humic acids are known to enter into interlayer sites of clay minerals from aqueous solution (Ohashi and Nakazawa 1996; Bosetto et al. 1997). Although this study was conducted under dry conditions, since LHA and saponite were dispersed by water before precipitation on CaF_2 plate, LHA might have partially entered

into interlayers of saponite. In addition, smectites including saponite have strong adsorption capacities for polar constituents of pyrolysates from kerogen, while hydrocarbons are not strongly adsorbed (Huizinga et al. 1987). The adsorption can be due to (1) hydrogen bonding between a COOH group and an oxygen sheet of silicate layers (Scheme 4-1), (2) direct linkage between the COOH group and an exchangeable cation (Scheme 4-2), (3) linkage between a COO^- group and an exchangeable cation through a water bridge (Scheme 4-3), and (4) direct linkage between a COO^- group and an exchangeable cation (Scheme 4-4) (Yariv 1996).

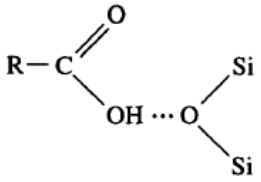

Scheme 4-1

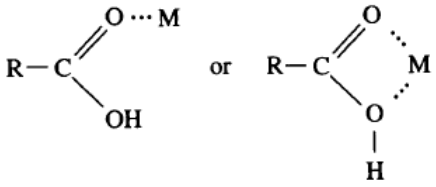

Scheme 4-2

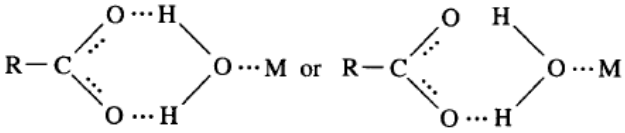

Scheme 4-3

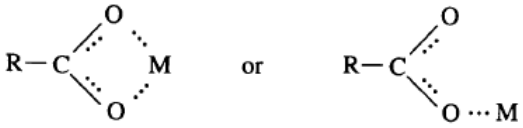

Scheme 4-4

However, sorptive preservation capacity of saponite seems to have reverse catalytic effects for C−C bond cleavage, since smectites are also known to have catalytic effects for carbon-carbon bond cleavage (Davis and Stanley 1982). Although the oxidative decomposition seems to be a dominant process rather than carbon-carbon bond cleavage under oxidizing atmosphere, saponite might show more catalytic effects for C−C bond cleavage than sorptive preservation of pyrolysates for LHA under an inert atmosphere. Furthermore, decrease of C=O is accelerated with the presence of

saponite under an inert atmosphere, since smectites are known to have a catalytic activity for decarboxylation (Jurg and Eisma 1964).

The roles of saponite are thus two-fold: it increases the retention of organic materials and it exerts a catalytic effect on their decomposition or cracking reactions, both through their adsorption to saponite.

Antigorite and olivine do not show significant preservation effects compared with those of saponite. One reason might be that the adsorption capacity for organic matter of antigorite is lower than that of smectite (Yariv 1996). Antigorite and olivine would rather have catalytic activities for cracking and decarboxylation, since decrease of aliphatic C−H and C=O is accelerated with the presence of antigorite and olivine in some cases.

Table 4-5. The effects of minerals for thermal decomposition of organic matter.

		Aliphatic C−H	Aromatic C−H	Aromatic C=C	C=O
LHA:	saponite	+	+	+	+
(in air)	antigorite	–	+	+	≈
	olivine	–	+	+	≈
LHA:	saponite	≈	≈	+	–
(in Ar flow)	antigorite	≈	≈	≈	≈
	olivine	≈	≈	≈	–
Chondritic IOM:	Orgueil	≈	ND	? *	+
(in Ar flow)	Murchison	–	ND	≈	–

+ : increase the temperature of peak dissappearance T_{pd}
≈ : no significant change
– : decrease the temperature of peak dissappearance T_{pd}
ND : not detected
* Both bulk and IOM bands remained at 600ºC, maximum heating temperature.

4.5.2. Effects of Minerals for Chondritic Organic Matter

In order to consider mineral effects on the organic matter alteration in chondrite parent bodies, I compare thermal stability of bulk chondrite and acid residual organic matter (IOM) without minerals and discuss the effects of minerals based on the above discussion of heating experiments on simulated chondritic materials.

According to the TG-DTA curves of bulk Murchison (Figs. 4-2), the degradation of IOM is likely to occur at around 200-300ºC, then the thermal decomposition of organic matter is likely to take place at around 420ºC (Shimoyama et al. 1991). This is

roughly consistent with in-situ IR heating experiments which show decreases of aliphatic C−H at around 200ºC to 300ºC (Figs. 4-12b,c), and decrease of aromatic C=C at around 300ºC to 500ºC (Figs. 4-12a,d). These results suggest that thermally labile portions such as aliphatic branches and bridges decompose at relatively low temperatures (200-300ºC), then refractory portions such as aromatic cores decompose at relatively high temperatures (300-500ºC). These results are also consistent with the low-temperature stepped combustion experiments of Kerridge et al. (1987). These authors detected two organic carbon components in the Murchison IOM released up to 450ºC. A labile component was released between 250ºC and 350ºC, while a second more stable component was released up to 450ºC.

Table 4-5 summarizes the effects of matrix minerals for thermal decomposition of organic matter in Murchison and Orgueil. Matrix minerals of Orgueil seem to inhibit decreases of C=O, under an inert atmosphere. Orgueil meteorite is known to contain saponite and serpentine as dominant fine-grained matrix phases (Tomeoka and Buseck 1988; Zolensky et al. 1993). Based on the mineral effects for LHA in Table 4-5, Orgueil organic matter might be protected by saponite in an inert atmosphere, while catalytic effects of saponite would be dominant on C=O of LHA in an inert atmosphere. This disagreement might be due to compositional deferences of C=O between Orgueil IOM and LHA. C=O in LHA occurs mainly as the form of COOH (Mao et al. 2000), while C=O in Orgueil IOM occurs as ketone, as well as COOR (i.e., carboxyl, where R = H and/or C) (Cody and Alexander 2005).

On the other hand, matrix minerals of Murchison seem to accelerate decreases of C=O and aliphatic C−H, under an inert atmosphere (Table 4-5). Murchison meteorite is known to contain serpentine as a dominant fine-grained matrix phase (Zolensky and McSween 1988; Zolensky et al. 1993). However serpentine (antigorite) do not show significant effect for thermal decrease of LHA under an inert atmosphere (Table 4-5). Antigorite used here has Fe/Mg ratio of 0.04 (Uehara and Shirozu 1985), while serpentine of Murchison has Fe/Mg ratio of 1.5 (Zolensky et al. 1993). Therefore, Fe^{2+} in serpentine of Murchison might induce decomposition of organic matter by oxidation/reduction reaction, since Fe^{2+} has stronger catalytic activity than Mg in decomposition of organic matter such as humic acids and coals (Martyniuk et al. 2001).

It should be noted that organic matter of bulk meteorites include, besides IOM, solvent soluble organic matter up to 30 wt%, which has been separated before HF/HCl treatment. The soluble organic matter is likely to be lost at relatively low temperature due to its low molecular weight nature, and does not affect temperatures of peak disappearance T_{pd}.

4.5.3. Chondrite Parent Body Processes

Most groups of chondritic meteorites experienced diverse styles of aqueous alteration to various degrees that resulted in the formation of hydrous and anhydrous minerals (Krot et al. 2006). The CM carbonaceous chondrites experienced low-temperature aqueous alteration to various degrees in an asteroidal setting that resulted in the formation of a variety of secondary phases, including phyllosilicates, magnetite, Fe,Ni-sulfides, and carbonates (e.g., Zolensky and McSween 1988; Zolensky et al. 1993). CI chondrites contain primarily phyllosilicates, oxides (primarily magnetite), sulfides, carbonates and sulfates, and CI matrix could have been derived from CM matrix material by further alteration (Zolensky and McSween 1988). Some CM chondrites subsequently experienced thermal metamorphism and partial dehydration (e.g., Tomeoka et al. 1989).

Most models assume an asteroid diameter of 100 km and an initial accretion temperature of 170-180 K (Brearley 2006). Melting of accreted water ice occurs as a result of heat released by the decay of ^{26}Al, which is typically assumed to have been accreted into the asteroid at initial $^{26}Al/^{27}Al$ ratios lower than $\sim 5 \times 10^{-5}$ (MacPherson et al. 1995). Alteration temperatures for CM2 chondrites are estimated by various authors as ~20ºC using mineral equilibria (DuFresne and Anders 1962), 1-25ºC using thermodynamic modeling of mineral assemblages (Zolensky et al. 1989), 0ºC by modeling of bulk-rock O-isotopic composition (Clayton and Mayeda 1999), and 80ºC by O-isotopic fractionation between structural bound water in phyllosilicates and calcite (Baker et al. 2002). Some thermally metamorphosed CM chondrites were heated to temperatures higher than 600ºC (Akai 1992). For CI1 chondrites, alteration temperatures are estimated as ~20ºC using mineral equilibria (DuFresne and Anders 1962), 50-150ºC using thermodynamic modeling of mineral assemblages (Zolensky et al. 1989), 100-150ºC using O-isotopic fractionation between carbonate and phyllosilicates (Clayton and Mayeda 1999).

The thermal stability of organic matter with and without the presence of minerals provide a valuable insight into how parent body processes affect the overall structure of organic matter of carbonaceous chondrites. Degradation of the macromolecular organic matter occurred during the aqueous alteration and soluble fractions were released (Sephton et al. 1998, 2003; Yabuta et al. 2007). Meteoritic organic matter is strongly associated with clay minerals, suggesting that these minerals may have had an important trapping and possibly catalytic role during molecular evolution in the early solar system (Pearson et al. 2002). This study is mainly consistent with this hypothesis

and suggests that saponite have both preservation effects for organic matter and catalytic effects for decomposing high molecular weight compounds into lower weight ones by heating experiments. If the thermal metamorphism occurred subsequent to the aqueous alteration, labile components might have been destroyed or transformed to more stable materials as metamorphism proceeded. Kitajima et al. (2002) indicate that graphitization of the carbonaceous matter progresses as temperature increases, and during graphitization, the organic matter has lost its labile portion. Dehydration of swelling clays could lead to decrease of preservation capacity for organic matter, especially for aliphatic and O-bearing compounds. Aromatic compounds seem to be less sensible to mineral phase changes (Table 4-5).

4.6. Conclusions

In order to elucidate effects of minerals on the thermal transformation of organic matter, simulation experiments of thermal alteration on carbonaceous materials were conducted under micro FTIR spectroscopy with a heating stage. These heating experiments provide the following conclusions.

1. For the heating experiments under Ar flow of bulk and insoluble organic matter (IOM) of Murchison (CM2) and Orgueil (CI1) meteorites, thermal stability of organic matter was lower in the presence of minerals for Murchison, while thermal stability was higher in the presence of minerals for Orgueil.
2. For the heating experiments under Ar flow and air of leonardite humic acid (LHA) with and without saponite, antigorite and olivine as analogs of carbonaceous chondrites, the thermal stability of LHA is higher with the presence of saponite. On the other hand, antigorite and olivine accelerate the decrease of aliphatic fractions, and decelerates the decrease of aromatic fractions. These mineral effects become dominant in oxidizing atmosphere.

These results suggest that the thermal stability of chondritic organic matter depends on associated minerals. If thermal metamorphism occurred subsequent to aqueous alteration, dehydration of swelling clays could lead to decrease of preservation capacity for organic matter. The thermal stability of organic matter with and without minerals provides a valuable insight into how parent body processes affect the overall structure of organic matter of carbonaceous chondrites.

References

Akai J. 1992. T-T-T diagram of serpentine and saponite, and estimation of metamorphic heating degree of Antarctic carbonaceous chondrites. *Proceedings of the NIPR Symposium on Antarctic Meteorites* 5: 120-135.

Alexander C. M. O'D., Fogel M., Yabuta H., and Cody G. D. 2007. The origin and evolution of chondrites recorded in the elemental and isotopic compositions of their macromolecular organic matter. *Geochimica et Cosmochimica Acta* 71: 4380-4403.

Anders E., Hayatsu R., and Studier M. H. 1973. Organic compounds in meteorites. *Science* 182: 781-790.

Baker L., Franchi I. A., Wright I. P., and Pillinger C. T. 2002. The oxygen isotopic composition of water from Tagish Lake: Its relationship to low-temperature phases and to other carbonaceous chondrites. *Meteoritics & Planetary Science* 37: 977-985.

Bonal L., Quirico E., Bourot-Denise M., Montagnac G. 2006. Determination of the petrologic type of CV3 chondrites by Raman spectroscopy of included organic matter. *Geochimica et Cosmochimica Acta* 70: 1849-1863.

Bonal L., Bourot-Denise M., Quirico E., Montagnac G., and Lewin E. 2007. Organic matter and metamorphic history of CO chondrites. *Geochimica et Cosmochimica Acta* 71: 1605-1623.

Bosetto M., Arfaioli P., Pantani O. L., and Ristori G. G. 1997. Study of the humic-like compounds formed from L-tyrosine on homoionic clays. *Clay Minerals* 32: 341-349.

Botta O. and Bada J. L. 2002. Extraterrestrial organic compounds in meteorites. *Surveys in Geophysics* 23: 411-467.

Brearley A. J. 2006. The action of water. In *Meteorites and the early solar system II*, edited by Lauretta D. S., Leshin L. A., and McSween H. Y., Jr. Tucson, Arizona: The University of Arizona Press. pp. 587-624.

Busemann H., Alexander C. M. O'D., and Nittler L. R. 2007. Characterization of insoluble organic matter in primitive meteorites by microRaman spectroscopy. *Meteoritics & Planetary Science* 42: 1387-1416.

Clayton R. N. and Mayeda T. K. 1999. Oxygen isotope studies of carbonaceous chondrites. *Geochimica et Cosmochimica Acta* 6: 2089-2104.

Cody G. D. and Alexander C. M. O'D. 2005. NMR studies of chemical structural variation of insoluble organic matter from different carbonaceous chondrite groups. *Geochimica et Cosmochimica Acta* 69: 1085-1097.

Cronin J. R., Pizzarello S., and Frye J. S. 1987. ^{13}C NMR spectroscopy of the insoluble carbon of carbonaceous chondrites. *Geochimica et Cosmochimica Acta* 51: 299-303.

Davis J. B. and Stanley J. P. 1982. Catalytic effect of smectite clays in hydrocarbon generation revealed by pyrolysis-gas chromatography. *Journal of Analytical and Applied Pyrolysis* 4:

227−240.

DuFresne E. R. and Anders E. 1962. On the chemical evolution of the carbonaceous chondrites. *Geochimica et Cosmochimica Acta* 26: 1085-1114.

Ehrenfreund P., Robert F., d'Hendecourt L., and Behar F. 1991. Comparison of interstellar and meteoritic organic matter at 3.4 microns. *Astronomy and Astrophysics* 252:712-717.

Ehrenfreund P., Robert F., and d'Hendecourt L. 1992. Similarity of the infrared spectrum of an Orgueil organic polymer with interstellar organic compounds in the line of sight towards IRS 7. *Advances in Space Research* 12: 53-56.

Flynn G. J., Keller L. P., Jacobsen C., and Wirick S. 2001. FTIR and carbon-XANES examination of organic carbon in Tagish Lake: Evidence for a moderately volatile organic component (abstract #1593). 32nd Lunar and Planetary Science Conference. CD-ROM.

Francioso O., Montecchio D., Gioacchini P., and Ciavatta C. 2005. Thermal analysis (TG-DTA) and isotopic characterization (C-13-N-15) of humic acids from different origins. *Applied Geochemistry* 20: 537-544.

Garvie L. A. J. and Buseck P. R. 2007. Prebiotic carbon in clays from Orgueil and Ivuna (CI), and Tagish Lake (C2 ungrouped) meteorites. *Meteoritics & Planetary Science* 42: 2111-2117.

Guggenberger G. and Kaiser K. 2003. Dissolved organic matter in soil: challenging the paradigm of sorptive preservation. *Geoderma* 113: 293-310.

Hayatsu R., Matsuoka S., Anders E., Scott R. G., and Studier M. H. 1977. Origin of organic matter in the early solar system – VII. The organic polymer in carbonaceous chondrites. *Geochimica et Cosmochimica Acta* 41: 1325-1339.

Hayatsu R. and Anders E. 1981. Organic-compounds in meteorites and their origins. *Topics in Current Chemistry* 99: 1-37.

Huizinga B. J., Tannenbaum E., and Kaplan I.R. 1987. The role of minerals in the thermal alteration of organic matter III. Generation of bitumen in laboratory experiments. *Organic Geochemistry* 11: 591-604.

Jurg J. W. and Eisma E. 1964. Petroleum hydrocarbons: Generation from fatty acid. *Science* 144: 1451−1452.

Keil R. G., Montlucon D. B., Prahl F. G., and Hedges J. I. 1994. Sorptive preservation of labile organic-matter in marine-sediments. *Nature* 370: 549-552.

Keller L. P. and Flynn G. J. 2001. Matrix Mineralogy of the Tagish Lake Carbonaceous Chondrite: TEM and FTIR Studies (abstract #1639). 32nd Lunar and Planetary Science Conference. CD-ROM.

Kennedy M. J., Pevear D. R., and Hill R. J. 2002. Mineral surface control of organic carbon in black shale. *Science* 295: 657-660.

Kerridge J. F. 1985. Carbon, hydrogen and nitrogen in carbonaceous chondrites: Abundances and

isotopic compositions in bulk samples. *Geochimica et Cosmochimica Acta* 49: 1707-1714.

Kerridge J. F., Chang S., and Ship R. 1987. Isotopic characterization of kerogen-like material in the Murchison carbonaceous chondrite. *Geochimica et Cosmochimica Acta* 51: 2527-2540.

Kissin Y. V. 2003. Hydrocarbon components in carbonaceous meteorites. *Geochimica et Cosmochimica Acta* 67: 1723-1735.

Kitajima F., Nakamura T., Takaoka N., and Murae T. 2002. Evaluating the thermal metamorphism of CM chondrites by using the pyrolytic behavior of carbonaceous macromolecular matter. *Geochimica et Cosmochimica Acta* 66: 163-172.

Krot A. N., Hutcheon I. D., Brearley A. J., Pravdivtseva O. V., Petaev M. I., and Hohenberg C. M. 2006. Timescales and settings for alteration of chondritic meteorites. In *Meteorites and the early solar system II*, edited by Lauretta D. S., Leshin L. A., and McSween H. Y., Jr. Tucson, Arizona: The University of Arizona Press. pp. 525-553.

MacPherson G. J., Davis A. M., and Zinner, E. K. 1995. The distribution of aluminum-26 in the early Solar System - A reappraisal. *Meteoritics* 30: 365-386.

Mao J. D., Hu W. G., Schmidt-Rohr K., Davies G., Ghabbour E. A., and Xing B. 2000. Quantitative characterization of humic substances by solid-state carbon-13 nuclear magnetic resonance. *Soil Science Society of America Journal* 64: 873-884.

Martyniuk H., Wiekowska J., and Lipman J. 2001. The study of influence of metal ions on thermal decomposition of humic acids. *Journal of Thermal Analysis And Calorimetry* 65: 711-721.

Matrajt G., Borg J., Raynal P. I., Djouadi Z., d'Hendecourt L., Flynn G., and Deboffle D. 2004. FTIR and Raman analyses of the Tagish Lake meteorite: Relationship with the aliphatic hydrocarbons observed in the Diffuse Interstellar Medium. *Astronomy and Astrophysics* 416: 983-990.

Mayer L. M. 1999. Extent of coverage of mineral surfaces by organic matter in marine sediments. *Geochimica et Cosmochimica Acta* 63: 207-215.

Murae T. 1994. FT-IR spectroscopic studies of major organic matter in carbonaceous chondrites using microscopic technique and comparison with terrestrial kerogen. *Proceedings of the NIPR Symposium on Antarctic Meteorites* 7:262-274.

Nakamura K., Zolensky M. E., Tomita S., Nakashima S., and Tomeoka K. 2002. Hollow organic globules in the Tagish Lake meteorite as possible products of primitive organic reactions. *International Journal of Astrobiology* 1: 179-189.

Nakamura K., Nakashima S., Shiota D., Zolensky M. E., and Keller L. P. 2003. In Situ Heating Behavior by Infrared Microspectroscopy of Organic Components in Tagish Lake Meteorite (abstract #1432). 34th Lunar and Planetary Science Conference. CD-ROM.

Naraoka H., Mita H., Komiya M., Yoneda S., Kojima H., and Shimoyama A. 2004. A chemical

sequence of macromolecular organic matter in the CM chondrites. *Meteoritics & Planetary Science* 39: 401-406.

Ohashi H. and Nakazawa H. 1996. The microstructure of humic acid-montmorillonite composites. *Clay Minerals* 31: 347-354.

Okumura S. and Nakashima S. 2004. Water diffusivity in rhyolitic glasses as determined by in situ IR spectroscopy. *Physics and Chemistry of Minerals* 31: 183-189.

Pearson V. K., Sephton M. A., Kearsley A. T., Bland P. A., Franchi I. A., and Gilmour I. 2002. Clay mineral-organic matter relationships in the early solar system. *Meteoritics & Planetary Science* 37: 1829-1833.

Pizzarello S., Cooper G. W., and Flynn G. J. 2006. The nature and distribution of the organic material in carbonaceous chondrites and interplanetary dust particles. In *Meteorites and the early solar system II*, edited by Lauretta D. S., Leshin L. A., and McSween H. Y., Jr. Tucson, Arizona: The University of Arizona Press. pp. 625-651.

Quirico E., Raynal P. I., and Bourot-Denise M. 2003. Metamorphic grade of organic matter in six unequilibrated ordinary chondrites. *Meteoritics & Planetary Science* 38: 795-811.

Raynal P. I., Quirico E., Borg J., Deboffle D., Dumas P., d'Hendecourt L., Bibring J. P., and Langevin Y. 2000. Synchrotron infrared microscopy of micron-sized extraterrestrial grains. *Planetary and Space Science* 48: 1329-1339.

Reddy B. R., Acharya S., Anand S., and Das R. P. 1991. Preparation and characterisation of magnesium sulphate heptahydrate from Kimberlite tailings. *Journal of Thermal Analysis* 37: 945-951.

Rose H. R., Smith D. R., and Vassallo A. M. 1998. Study of the oxidation of oil shale and kerogen by Fourier transform infrared emission spectroscopy. *Energy & Fuels* 12: 682-688.

Salmon V., Derenne S., Lallier-Verges E., Largeau C., and Beaudoin B. 2000. Protection of organic matter by mineral matrix in a Cenomanian black shale. *Organic Geochemistry* 31: 463-474.

Sephton M. A., Pillinger C. T., and Gilmour I. 1998. $\delta^{13}C$ of free and macromolecular aromatic structures in the Murchison meteorite. *Geochimica et Cosmochimica Acta* 62:1821-1828.

Sephton M. A. 2002. Organic compounds in carbonaceous meteorites. *Natural Product Reports* 19: 292-311.

Sephton M. A., Verchovsky A. B., Bland P. A., Gilmour I., Grady M. M., and Wright I. P. 2003. Investigating the variations in carbon and nitrogen isotopes in carbonaceous chondrites. *Geochimica et Cosmochimica Acta* 67: 2093-2108.

Shimoyama A., Komiya M., and Harada K. 1991. Release of organic compounds from some Antarctic CI and CM chondrites by laboratory heating. *Proceedings of the NIPR Symposium on Antarctic Meteorites* 4: 247-260.

Socrates G. 2001. *Infrared and Raman characteristic group frequencies*, 3rd ed. Chichester,

England: John Wiley & Sons, LTD.

Tomeoka K. and Buseck P. R. 1988. Matrix mineralogy of the Orgueil CI carbonaceous chondrite. *Geochimica et Cosmochimica Acta* 52: 1627-1640.

Tomeoka K., Kojima H., and Yanai K. 1989. Yamato-86720: A CM carbonaceous chondrite having experienced extensive aqueous alteration and thermal metamorphism. *Proceedings of the NIPR Symposium on Antarctic Meteorites* 2: 55-74.

Tonui E., Zolensky M. E., Hiroi T., Nakamura T., Lipschutz M. E., Wang M. -S., and Okudaira K. In preparation. Petrographic, chemical and spectroscopic evidence for thermal metamorphism in carbonaceous chondrites I: CI and CM chondrites. *Geochimica et Cosmochimica Acta*.

Uehara S. and Shirozu H. 1985. Variations in chemical composition and structural properties of antigorite. *Mineralogical Journal* 12: 299-318.

Wdowiak T. J., Flickinger G. C., and Cronin J. R. 1988. Insoluble organic material of the Orgueil carbonaceous chondrite and the unidentified infrared bands. *Astrophysical Journal* 328: L75-L79.

Yabuta H., Naraoka H., Sakanishi K., Kawashima H. 2005. Solid-state ^{13}C NMR characterization of insoluble organic matter from Antarctic CM2 chondrites: Evaluation of the meteoritic alteration level. *Meteoritics & Planetary Science* 40: 779-787.

Yabuta H., Williams L. B., Cody G. D., Alexander C. M. O'D., and Pizzarello S. 2007. The insoluble carbonaceous material of CM chondrites: A possible source of discrete organic compounds under hydrothermal conditions. *Meteoritics & Planetary Science* 42:37-48.

Yamanoi Y. 2008. Color change processes of volcanic materials by spectro-colorimetry and in-situ high temperature visible spectroscopy. Ph.D. thesis, Osaka University, Toyonaka, Osaka, Japan.

Yariv S. 1996. Thermo-IR-spectroscopy analysis of the interactions between organic pollutants and clay minerals. *Thermochimica Acta* 274: 1-35.

Zolensky M. and McSween H.Y., Jr. 1988. Aqueous alteration. In *Meteorites and Early Solar System*, edited by Kerridge J. R. and Matthews M. S. Tucson, Arizona: The University of Arizona Press. pp. 114-143.

Zolensky M. E., Bourcier W. L., and Gooding J. L. 1989. Aqueous alteration on the hydrous asteroids − Results of EQ3/6 computer-simulations. *Icarus* 78: 411-425.

Zolensky M. Barrett R., and Browning L. 1993. Mineralogy and composition of matrix and chondrules rims in carbonaceous chondrites. *Geochimica et Cosmochimica Acta* 57: 3123-3148.

Zolensky M. E., Abell P. A., and Tonui E. K. 2005. Metamorphosed CM and CI carbonaceous chondrites could be from the breakup of the same earth-crossing asteroid (abstract #2084).

36th Lunar and Planetary Science Conference. CD-ROM.

Chapter 5

THERMAL DECOMPOSITION KINETICS OF ORGANIC MATTER IN CARBONACEOUS CHONDRITE BY MICRO FTIR

Abstract

In order to evaluate kinetic parameters for thermal decomposition of organic matter, in-situ heating experiments of bulk and insoluble organic matter (IOM) of Murchison (CM2) meteorite were conducted under micro FTIR combined with a heating stage. Bulk and IOM of Murchison are heated at 160-300ºC isothermally in the heating stage under Ar gas flow and air for several hours. Infrared spectra are collected in-situ during heating. The decrease rate of aliphatic C−H peak heights is much faster in air than in Ar flow. Decreases of aliphatic C−H peak heights in Ar flow are well fitted with Ginstling-Brounshtein three dimensional diffusion model, and the rate constants for decreases of aliphatic C−H were determined. Activation energies and frequency factors are estimated from these rate constants at different temperatures using Arrhenius equation. The activation energy and frequency factor for bulk Murchison under Ar flow are 72 ± 6 kJ/mol and 48 s^{-1}, respectively, while these for Murchison IOM under Ar flow are 107 ± 3 kJ/mol and 5.2×10^4 s^{-1}, respectively. Activation energy values of aliphatic C−H decrease are larger for IOM than bulk of Murchison. Hence, the mineral assemblage of Murchison meteorite might have catalytic effects for the organic matter decomposition. The time scales for metamorphism can be estimated for given temperatures with aliphatic C−H peak heights, otherwise temperatures of metamorphism can be estimated for given time scales. The rate of organic decomposition might be variable with changes of mineral assemblages during aqueous alteration and/or thermal metamorphism.

5.1. Introduction

Carbonaceous chondritic meteorites contain abundant carbon up to a few wt%, which exists predominantly in the form of insoluble organic matter (IOM) (e.g., Botta and bada 2002). The unusually heavy H and N isotopic compositions of some IOM suggest a chemical connection to the protosolar interstellar medium or cold regions of the outer protoplanetary disk (Busemann et al. 2006; Alexander et al. 2007). After accretion of the meteorite parent bodies, IOM was subjected to thermal metamorphism and/or aqueous alteration in their parent bodies (Huss et al. 2006; Brearley 2006). The effects of this parent body process are evident in structural features of the IOM, such as the relative abundances of aromatic and aliphatic moieties, functional groups and bonding (Cody and Alexander 2005); the H, C, and N abundances and isotopic compositions (Alexander et al. 1998, 2007; Busemann et al. 2006; Pearson et al. 2006);

the amounts of pyrolysates that may be generated upon flash heating (Kitajima et al. 2002).

In order to quantify the extent of alteration of IOM, there have been considerable recent efforts directed at using micro Raman spectral analysis for the purpose of ranking chondritic IOM. For example, the studies of Quirico et al. (2003), Bonal et al. (2006, 2007), and Busemann et al. (2007) all reveal that the spectral characteristics by micro Raman spectroscopy appear to coarsely record the molecular structural evolution of chondritic organic matter that accompanies parent body metamorphism. Busemann et al. (2007), for example, showed that the line width of the Raman D band correlated with the parent body maximum temperature estimates derived from mineralogical indicators and could be used as a straightforward estimation of these temperatures.

More recently, Cody et al. (2008) demonstrated that the development of the intensity of a 1s−σ* exciton observed using carbon X-ray absorption near edge structure (XANES) spectroscopy appears to correlate well with other estimates of the thermal metamorphism of the chondritic parent bodies. Cody et al. (2008) showed that laboratory heating experiments could be used to follow the development of the exciton intensity as a function of temperature and time, thus allowing the construction of a simple kinetic expression capable of calculating effective temperatures assuming a duration of 10^7 years of parent body heating. These experiments reveal that modification of IOM is a kinetically controlled process.

It is important to note that in the work of Cody et al. (2008), the changes observed involved a change in bulk electronic properties of the IOM, and only a single kinetic expression was used. Therefore, an independent estimate of time was needed in order to establish temperature. It is likely, however, that different parent bodies have different bulk chemistry, dimensions and likely different thermal histories. For example, Sears et al. (1991) pointed out that CO chondrites might have experienced lower temperatures, but for longer periods than the same petrologic type ordinary chondrites. Enhanced and additional kinetic studies of thermal processing of organic matter may further help sorting out the thermal history of the parent bodies.

The temperatures of aqueous alteration and thermal metamorphism have been estimated by numerous authors using various ways, for example, O-isotopic composition (Clayton and Mayeda 1999), mineral assemblages and thermodynamic modeling (Zolensky et al. 1989, 1993), and Cr-spinel/olivine thermometer (Wlotzka 1985, 1987). However obtaining well resolved timescale estimates of chondritic meteorites is limited to using short-lived isotope chronologies (^{26}Al-^{26}Mg, ^{53}Mn-^{53}Cr, ^{129}I-^{129}Xe) of the secondary minerals. Employing the kinetic response of meteoritic

organic matter to temperature and time could be used as a new sensitive indicator of parent body alteration time scale.

In this study, I conducted in-situ heating experiments of IOM and bulk of Murchison meteorite under Fourier transform infrared (FTIR) microspectroscopy to estimate kinetic parameters for thermal decomposition of aliphatic C−H groups. These data may constrain temperature and time scales of meteorite parent body processes.

5.2. Samples

5.2.1. Carbonaceous Chondrite Samples

For kinetic analysis of thermal stability of organic matter in carbonaceous chondrites, an organic rich carbonaceous chondrite, Murchison (CM2) meteorite was used. Murchison was kindly provided by Dr. M. E. Zolensky at NASA Johnson Space Center. For bulk meteorite samples, matrix powders from freshly broken surfaces of the Murchison were pressed on a KBr plate with glass slides.

Murchison (CM2) fell in 1969 in Australia. Its matrix consists mainly of serpentine, tochilinite, Fe-Ni sulfides, carbonates, olivine and Fe-Ni metal (Zolensky and McSween 1988; Zolensky et al. 1993). Its total carbon content is 1.56-2.5 wt% (Kerridge 1985) and the insoluble carbon content is 0.83 wt% (Alexander et al. 2007). H/C and O/C ratios of the IOM are 0.588 ± 0.016 and 0.183 ± 0.003, respectively (Alexander et al. 2007). ^{13}C NMR estimates of carbon distribution of the IOM are 7.8-11.2% of CH_x, 12.3-8.9% of CH_xO, 14.2-18.2% of CO, and 65.7-61.7% of aromatic (total 100%) (Cody and Alexander 2005).

5.2.2. IOM Sample preparation procedures

The IOM of the Murchison meteorite was used for comparison. The preparation procedures of IOM are as follows. All glassware used was sterilized by annealing in aluminum foil at 500ºC for 3 h. Murchison (0.7 g) were broken using an alumina mortar and pestle. Soluble organic fractions from the powdered meteorite sample was extracted with organic solvent, a mixture of CH_2Cl_2/CH_3OH (9/1, v/v), with ultrasonication. The sample was then rinsed with 2 N HCl at room temperature. The extracted residue was shaken with 8 N HF/4 N HCl in a Teflon container at room temperature for more than 48 hours, followed by washing with 2 N HCl. This process was repeated several times. The demineralized residue was washed with water, methanol, dichloromethane, in that order, and was dried under vacuum. The powdered

IOM was pressed on a KBr plate with a spatula.

5.3. Experimental Methods

5.3.1. In-Situ Heating Experiments under Micro FTIR

In order to elucidate thermal stabilities of chondritic organic matter, in-situ heating experiments under micro FTIR were conducted. Micro FTIR spectroscopy is a well-established technique for the identification of organic functional groups. In-situ observation of spectral changes during heating has been successfully performed by several authors (e.g., Rose et al. 1998; Nakamura et al. 2003; Okumura and Nakashima 2004).

A ceramic infrared light source, a Mercury-Cadmium-Telluride (MCT) detector and a ×16 Cassegrainian mirror were used for the FTIR spectroscopy (Jasco FT-IR-620 + IRT30). 100 or 256 scans were accumulated with a wavenumber resolution of 4 cm^{-1}, in the wavenumber range of 4000-700 cm^{-1}.

All spectra were collected as absorbance (*Abs*) according to the following Lambert-Beer's law:

$$Abs = -\log_{10}\left(\frac{I}{I_0}\right) = \varepsilon dC \qquad (5\text{-}1)$$

I_0 and I are the background and sample IR signal intensities, ε is the molar absorptivity, d is the thickness of the sample and C is the concentration of the component of interest.

Samples mounted on KBr plates were set onto a heating stage (Linkam FTIR 600) and placed into the micro FTIR. The background spectra were collected on the sample-free area of the KBr plate at room temperature. After measuring the sample spectra at room temperature, the samples were heated at 100 ºC/min from room temperature to target temperatures using the heating stage under ambient air, in an inert atmosphere of Ar (99.99%). In the gas flow experiment, the sample was set between two CaF_2 windows of the heating stage and the low-oxygen condition for an anoxic atmosphere was maintained by flowing of Ar gas (99.99%) at 84 mL/min into the heating stage. The target temperatures were kept for three to nine hours to collect spectra at the same locations at every 120 or 240 seconds. The target temperatures were 160-300ºC since labile portions of organic matter decompose around 200-300ºC.

5.4. Results

5.4.1. Isothermal Heating of Bulk Murchison Meteorite

Fig. 5-1 is a typical change in IR spectra of bulk Murchison meteorite during the heating experiment. Fig. 5-2 shows changes in peak height of 2930 cm^{-1} (aliphatic C−H) determined with linear baseline at 2990-2890 cm^{-1}, with elapsed heating time under Ar flow at different temperatures. Peak height normalized by the value at $t = 0$ sec (Abs_0) was used as the vertical axis because the amount of organic matter in the analyzed area was not completely equal among each run and this caused variation in the initial peak height (Abs_0). The decrease rates of aliphatic C−H increased with temperatures. The reproducibility was confirmed by the duplicate experiments at 260ºC (Fig. 5-2).

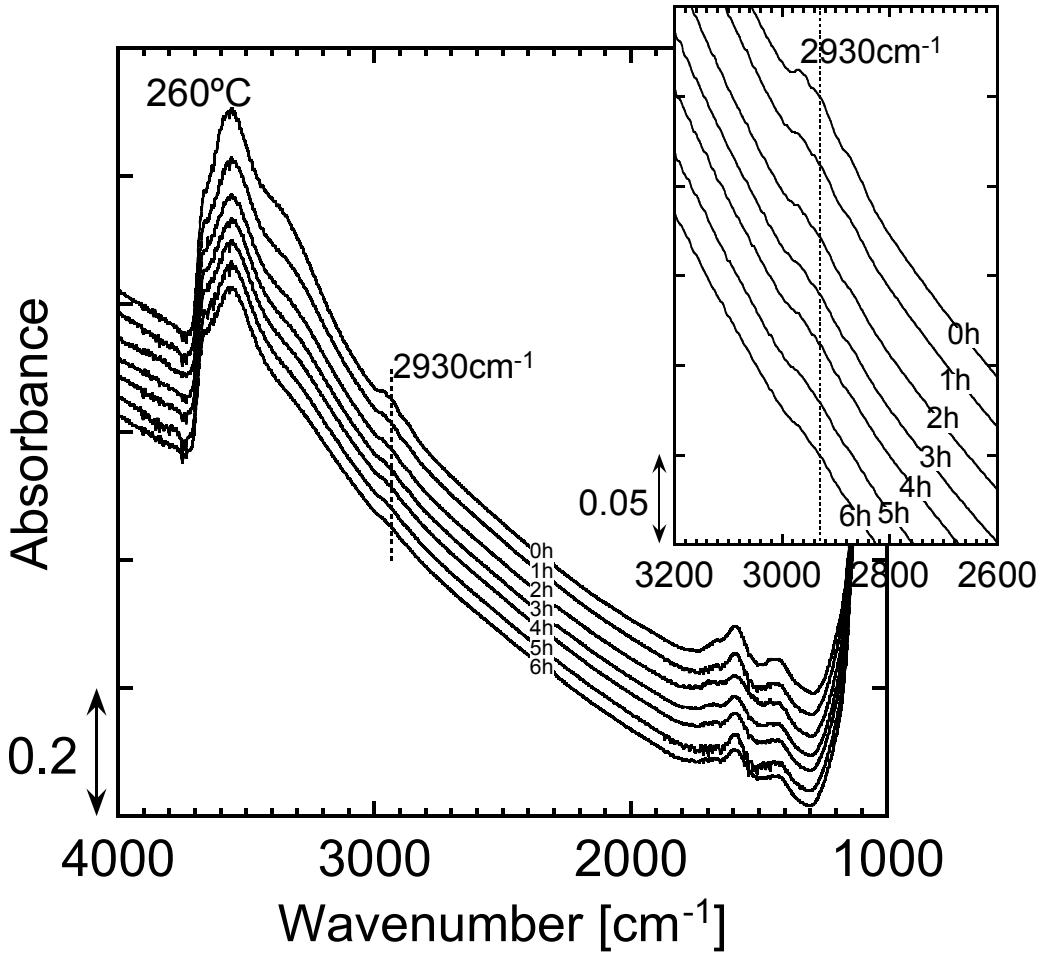

Fig. 5-1. Infrared spectral changes with time during the heating experiments of bulk Murchison meteorite under Ar flow at 260ºC.

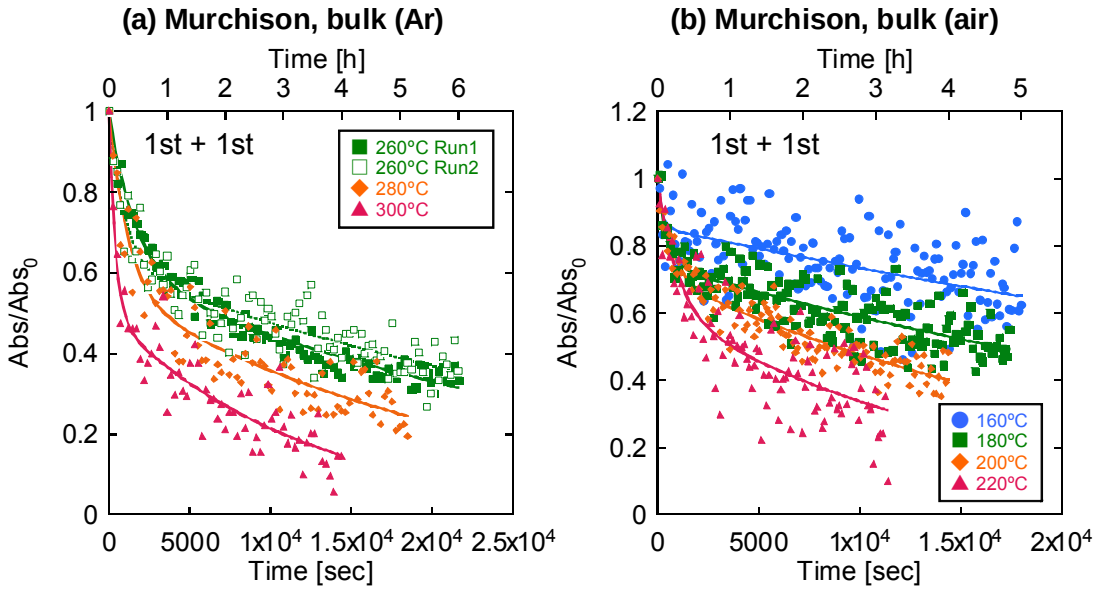

Fig. 5-2. The decrease with time of the peak height of aliphatic C−H (2930 cm^{-1}) normalized to that at t = 0 sec (Abs_0) during the heating experiments of bulk Murchison meteorite. (a) 2 runs under Ar flow at 260ºC, 280ºC and 300ºC. (b) Under air at 160ºC, 180ºC, 200ºC and 220ºC. The fitting curves were based on the combination of two first-order reaction model (eq. 5-6) (see 5.4.4).

5.4.2. Isothermal Heating of Murchison IOM

Fig. 5-3 is a typical change in infrared spectra of Murchison IOM during the heating experiment. Fig. 5-4 shows changes in peak height of 2930 cm^{-1} (aliphatic C−H) determined with linear baseline at 2990-2890 cm^{-1}, with elapsed heating time under Ar flow at different temperatures. Peak height normalized by the value at t = 0 sec (Abs_0) was used as the vertical axis because the amount of organic matter in the analyzed area was not completely equal among each run and this caused variation in the initial peak height (Abs_0). The decrease rates of aliphatic C−H increased with temperatures (Fig. 5-4).

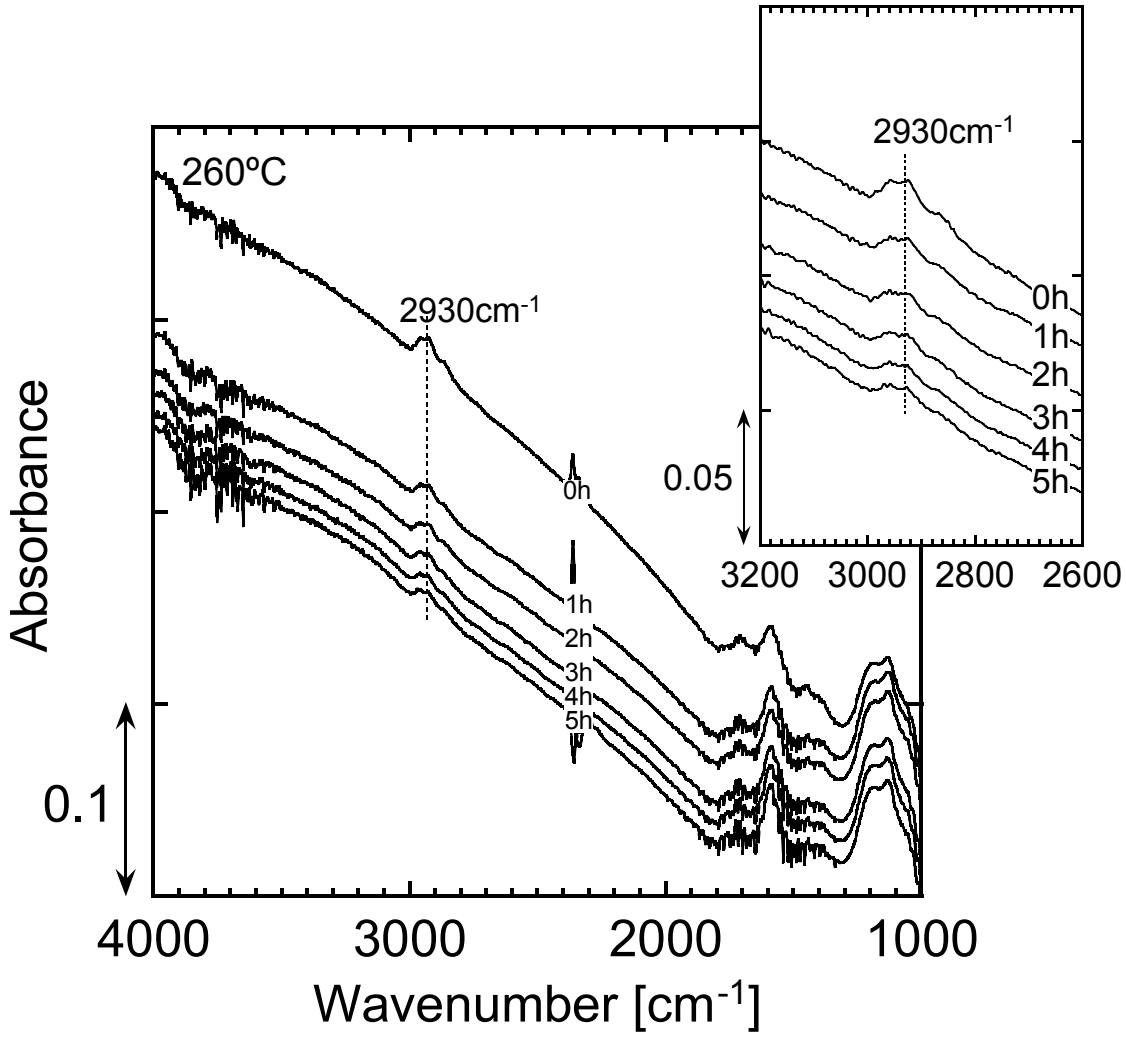

Fig. 5-3. Infrared spectral changes with time during the heating experiments of Murchison IOM under Ar flow at 260°C.

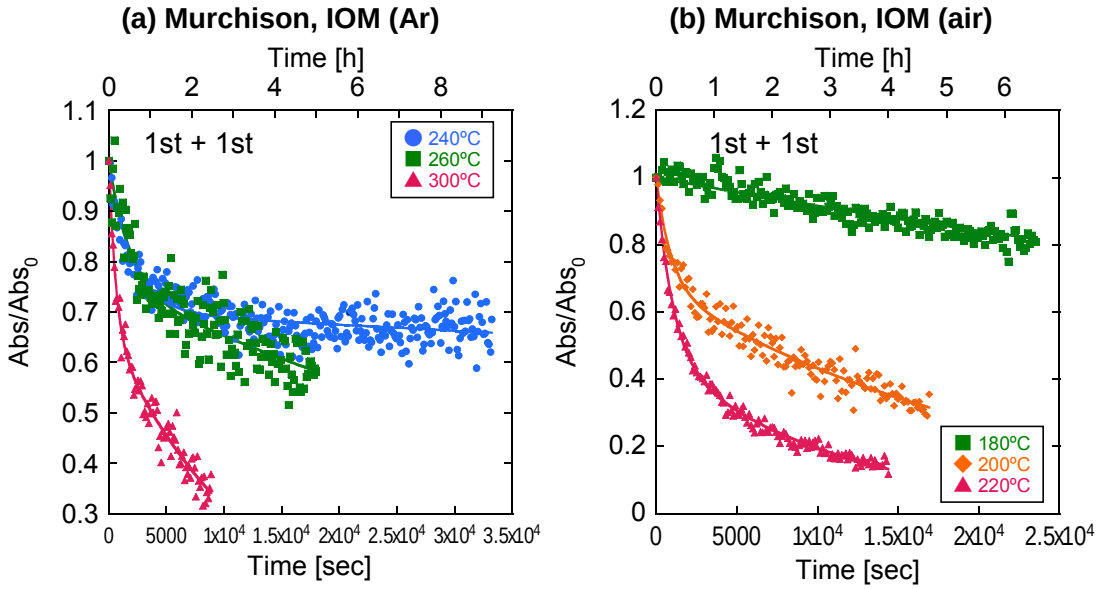

Fig. 5-4. The decrease with time of the peak height of aliphatic C−H (2930 cm^{-1}) normalized to that at t = 0 sec (Abs_0) during the heating experiments of Murchison IOM. (a) Under Ar flow at 240°C, 260°C and 300°C. (b) Under air at 180°C, 200°C and 220°C. The fitting curves were based on the combination of two first-order reaction model (eq. 5-6) (see 5.4.4).

5.4.3. Kinetic approach

Thermal durability of aliphatic C−H in chondritic organic matter was evaluated on the basis of kinetic analysis on the infrared spectral changes with time in order to evaluate a precise and independent thermal history.

The pyrolysis process of organic matter may be represented by the following reaction scheme:

$$A_{(solid)} \rightarrow B_{(solid)} + C_{(volatile)}$$

The rate of conversion, dx/dt may be expressed by the commonly used equation in decomposition kinetics for solid materials (Vyazovkin and Wight 1997).

$$\frac{dx}{dt} = kf(x) \qquad (5\text{-}2)$$

and

$$g(x) = \int_0^x \frac{dx}{f(x)} = kt \qquad (5\text{-}3)$$

where x is the degree of reaction progress defined by

$$x = \frac{Abs_0 - Abs}{Abs_0} \qquad (5\text{-}4)$$

where $f(x)$ and $g(x)$ are conversion functions, t is the time, and k is the rate constant. The temperature dependence of the rate constant k is often modeled successfully by the Arrhenius equation:

$$k = A\exp\left(-\frac{E_a}{RT}\right) \qquad (5\text{-}5)$$

where E_a is the activation energy, A the frequency factor, R the gas constant, and T the temperature.

Possible $f(x)$ and $g(x)$ forms and related mechanisms are listed in Table 5-1 (Aboulkas et al. 2008). By fitting these equations to the plot of $g(x)$ versus time, rate constants k can be determined. These rate constants k were then plotted versus inverse of temperature T (Arrhenius diagram) and activation energy E_a, and frequency factor A values were determined by fitting the data with the Arrhenius equation (5-5).

On the other hand, a combination of two first-order reactions is also used for simulating isothermal degradation of organic matter (e.g., Rajeshwar 1981; Dogan and Uysal 1996; Khraisha 1998), and is expressed as follows:

$$\frac{C}{C_0} = a\exp(-k_1 t) + (1-a)\exp(-k_2 t) \qquad (5\text{-}6)$$

where C is the concentration, C_0 is the initial concentration, k_1, k_2 is the rate constant ($k_1 > k_2$), t is the time, and a is the quantitative ratio of the labile fraction to the refractory fraction. Since the molar absorption coefficient and the sample thickness are constant within each experimental run, C in the above equation can be converted to Abs according to Lambert-Beer's Law (eq. 5-1).

$$\frac{C}{C_0} = \frac{Abs}{Abs_0} \qquad (5\text{-}7)$$

Using Arrehnius equation (eq. 5-5), the activation energies E_1 and E_2 for the rapid process (k_1) and the slow process (k_2), respectively, and frequency factor A values were determined.

Table 5-1. Algebraic expressions of functions of the most common reaction mechanisms operating in solid-state reactions (Aboulkas et al. 2008).

Mechanism	$f(x)$	$g(x)$
Power law (P2)	$2x^{1/2}$	$x^{1/2}$
Power law (P3)	$3x^{2/3}$	$x^{1/3}$
Power law (P4)	$4x^{3/4}$	$x^{1/4}$
Avarami-Erofe'ye (A2)	$2(1-x)[-\ln(1-x)]^{1/2}$	$[-\ln(1-x)]^{1/2}$
Avarami-Erofe'ye (A3)	$3(1-x)[-\ln(1-x)]^{2/3}$	$[-\ln(1-x)]^{1/3}$
Avarami-Erofe'ye (A4)	$4(1-x)[-\ln(1-x)]^{3/4}$	$[-\ln(1-x)]^{1/4}$
Contracting area (R2)	$2(1-x)^{1/2}$	$1-(1-x)^{1/2}$
Contracting volume (R3)	$3(1-x)^{2/3}$	$1-(1-x)^{1/3}$
One-dimensional diffusion (D1)	$1/2x$	x^2
Two-dimensional diffusion (D2)	$[-\ln(1-x)]^{-1}$	$[(1-x)\ln(1-x)] + x$
Three-dimensional diffusion, Jander (D3)	$3(1-x)^{2/3}/[2(1-(1-x)^{1/3})]$	$[1-(1-x)^{1/3}]^2$
Ginstling-Brounshtein (D4)	$3/2((1-x)^{-1/3}-1)$	$1-(2x/3)-(1-x)^{2/3}$
First-order (F1)	$(1-x)$	$-\ln(1-x)$
Second-order (F2)	$(1-x)^2$	$(1-x)^{-1}-1$
Third-order (F3)	$(1-x)^3$	$[(1-x)^{-2}-1]/2$

5.4.4. The Kinetics of Thermal Degradation

In order to determine rate constants k, the plot of $g(x)$ (calculated by eq. 5-3) vs. time were fitted various kinetic model equations (Table 5-1, Aboulkas et al. 2008). The calculated fitting lines to aliphatic C−H decrease of bulk Murchison under Ar flow and air, Murchison IOM under Ar flow and air were presented in Figs. 5-5, 5-6, 5-7 and 5-8. The obtained rate constants k and correlation coefficients r were summarized in Table 5-2, 5-3, 5-4 and 5-5. Figs. 5-9, 5-10, 5-11 and 5-12 show Arrhenius diagrams for the rate constants k [s^{-1}] as a function of temperature T [K]. The obtained activation energies E_a [kJ·mol^{-1}] and frequency factor A [s^{-1}] were summarized in Table 5-2, 5-3, 5-4 and 5-5.

As a result, the best fitted model function for the bulk Murchison under Ar flow was found to be two dimensional diffusion model (D2) and Ginstling-Brounshtein's three dimensional diffusion model (D4) which had the largest average correlation coefficient r values of 0.89 (Table 5-2). Apparent activation energy E_a and frequency factor A using D2 model were estimated as 68 ± 6 kJ/mol and ~76 s^{-1} by Arrhenius

equation (eq. 5-3), respectively. E_a and A using D4 model were estimated as 72 ± 6 kJ/mol and ~48 s^{-1}, respectively (Table 5-2).

The best fitted model function for the bulk Murchison under air was found to be contracting area (R2) and volume (R3) models (r = 0.74). Apparent activation energy E_a and frequency factor A using R2 model were 16 ± 4 kJ/mol and ~2.2 × 10^{-3} s^{-1}, respectively. E_a and A using R3 model were 17 ± 5 kJ/mol and ~1.7 × 10^{-3} s^{-1}, respectively (Table 5-3).

The best fitted model function for the Murchison IOM under Ar flow was found to be one-dimensional diffusion (D1), two-dimensional diffusion (D2), Jander's three dimensional diffusion (D3), and Ginstling-Brounshtein's three dimensional diffusion (D4) models (r = 0.82). Apparent activation energy E_a and frequency factor A using D1 model were 99 ± 2 kJ/mol and ~6.6 × 10^4 s^{-1}, respectively. E_a and A using D2 model were 105 ± 3 kJ/mol and ~1.3 × 10^5 s^{-1}, respectively. E_a and A using D3 model were 111 ± 4 kJ/mol and ~1.6 × 10^5 s^{-1}, respectively. E_a and A using D4 model were 107 ± 3 kJ/mol and ~5.2 × 10^4 s^{-1}, respectively (Table 5-4).

The best fitted model function for the Murchison IOM under air was found to be second-order reaction model (F2) (r = 0.95). Apparent activation energy E_a and frequency factor A were estimated as 175 ± 34 kJ/mol and ~2.1 × 10^{15} s^{-1}, respectively (Table 5-5).

However, in most cases, the largest r value was different for each temperature. Therefore, the reaction mechanism cannot be defined by fitting correlation. Since chondritic organic matter is a complex heterogeneous mixture of organic compounds, its decomposition includes a very complex reaction, or group of reactions, that results in the formation of different types of products. Obtained apparent kinetic parameters of aliphatic C−H decrease should be considered as only rough indicators for long term prediction.

On the other hand, kinetic studies on degradation of terrestrial organic matter (kerogen) often use a mechanism of two first order reactions to describe the decomposition of kerogen (e.g., Rajeshwar 1981; Dogan and Uysal 1996; Khraisha 1998);

$$\text{Kerogen} \xrightarrow{k_1} \text{Bitumen} + \text{Gas}$$
$$\text{Bitumen} \xrightarrow{k_2} \text{Oil} + \text{Gas} + \text{residue}$$

where the bitumen product refers to lower molecular weight components which are vaporizable. The same mechanism might also be applied to chondritic IOM which is commonly referred to as 'kerogen-like' material.

The fitting results of the combination of two first-order reactions were shown in

Fig. 5-2 and 5-4. All the fitting curves agreed with experimental data. The estimated rate constants (k_1 and k_2) were listed in Table 5-6. Fig. 5-13 showed Arrhenius diagrams for the rate constants k_1, k_2 [s^{-1}] as a function of temperature T [K]. The obtained activation energies E_1, E_2 [$kJ \cdot mol^{-1}$] and frequency factor A_1, A_2 [s^{-1}] were summarized in Table 5-7. The linearity of Arrhenius plots using the combination of two first-order reactions (Fig. 5-13) was relatively lower than those of single reaction models (Figs. 5-9, 5-10, 5-11 and 5-12). Moreover, apparent activation energy E_1 for bulk Murchison under air was found to be minus value, which is not realistic.

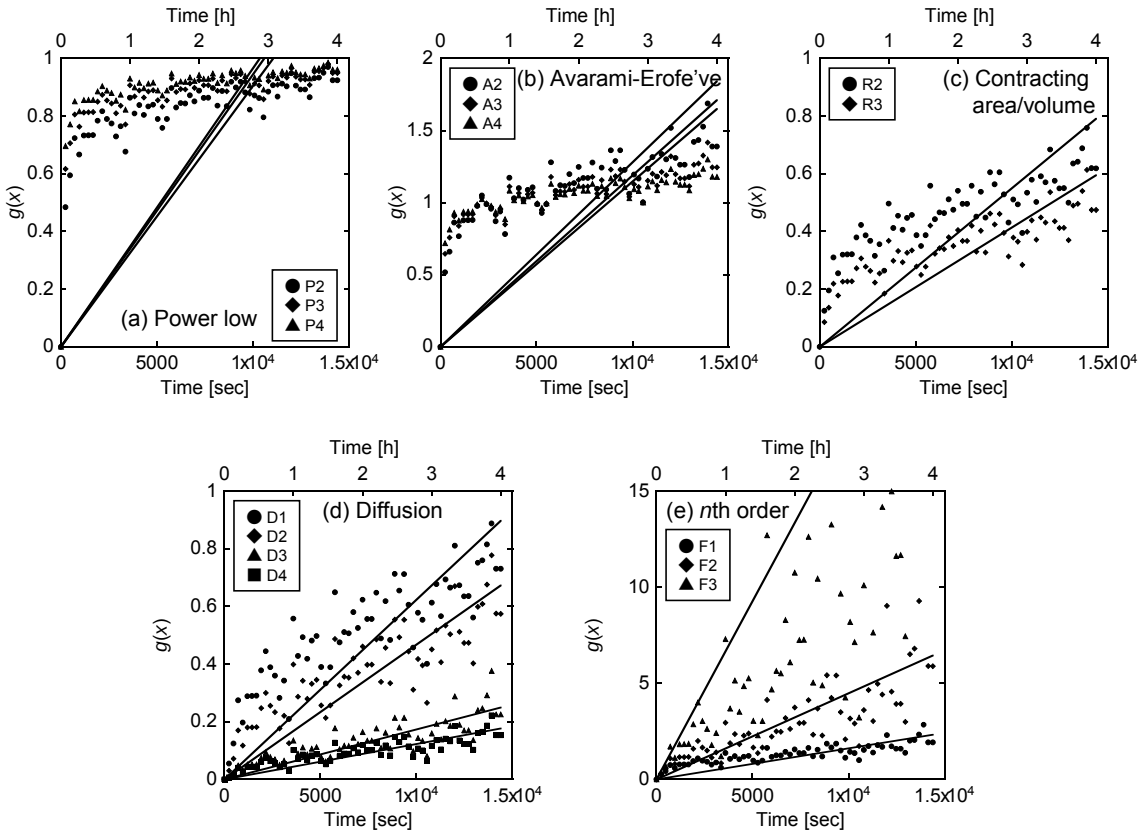

Fig. 5-5. Fitting results of aliphatic C−H decrease of bulk Murchison meteorite in Ar flow at 300ºC by various kinetic models listed in Table 5-1; (a) power law (P2, P3, P4), (b) nuclei growth models by Avarami-Erofe'ye (A2, A3, A4), (c) contracting area (R2) and contracting volume (R3), (d) one-dimensional diffusion (D1), two-dimensional diffusion (D2), and three-dimensional diffusion by Jander (D3) and Ginstling-Brounshtein (D4), (e) first-order (F1), second-order (F2) and third-order (F3) reactions. The rate constant *k* values were determined as listed in Table 5-2.

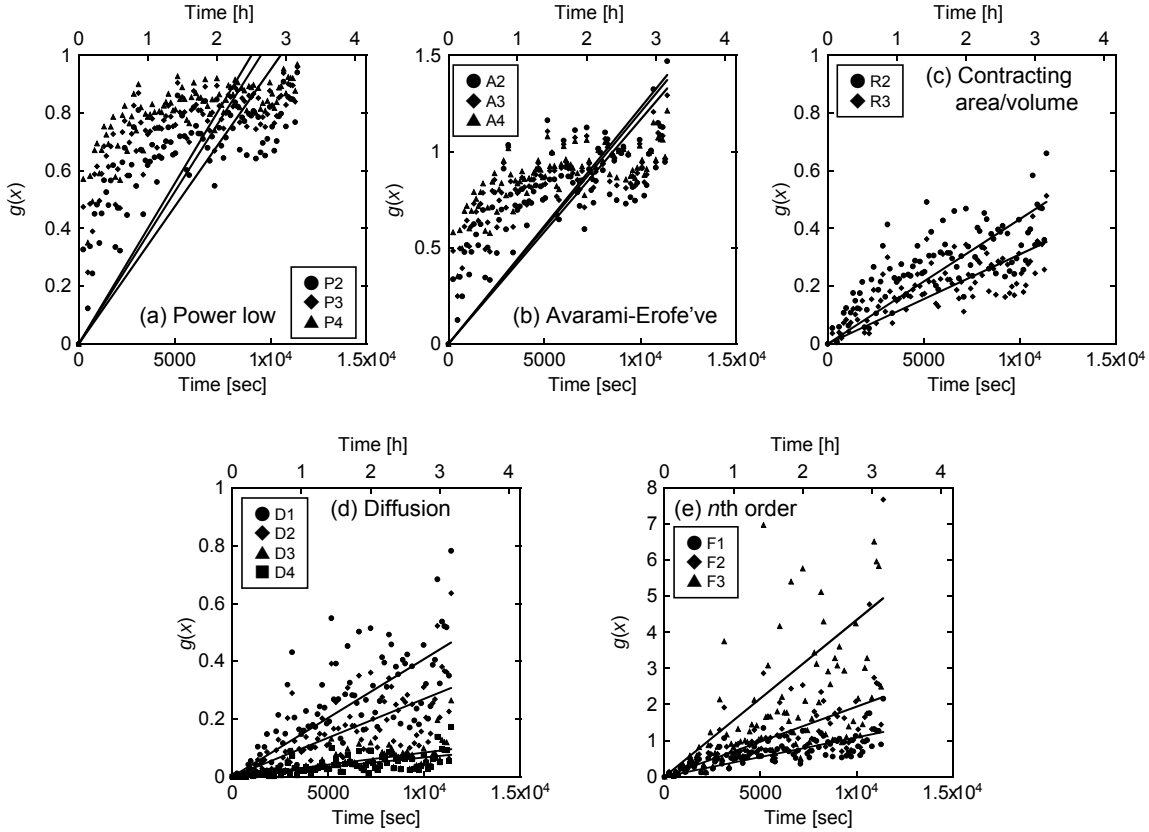

Fig. 5-6. Fitting results of aliphatic C−H decrease of bulk Murchison meteorite in air at 220ºC by various kinetic models listed in Table 5-1. The rate constant *k* values were determined as listed in Table 5-3.

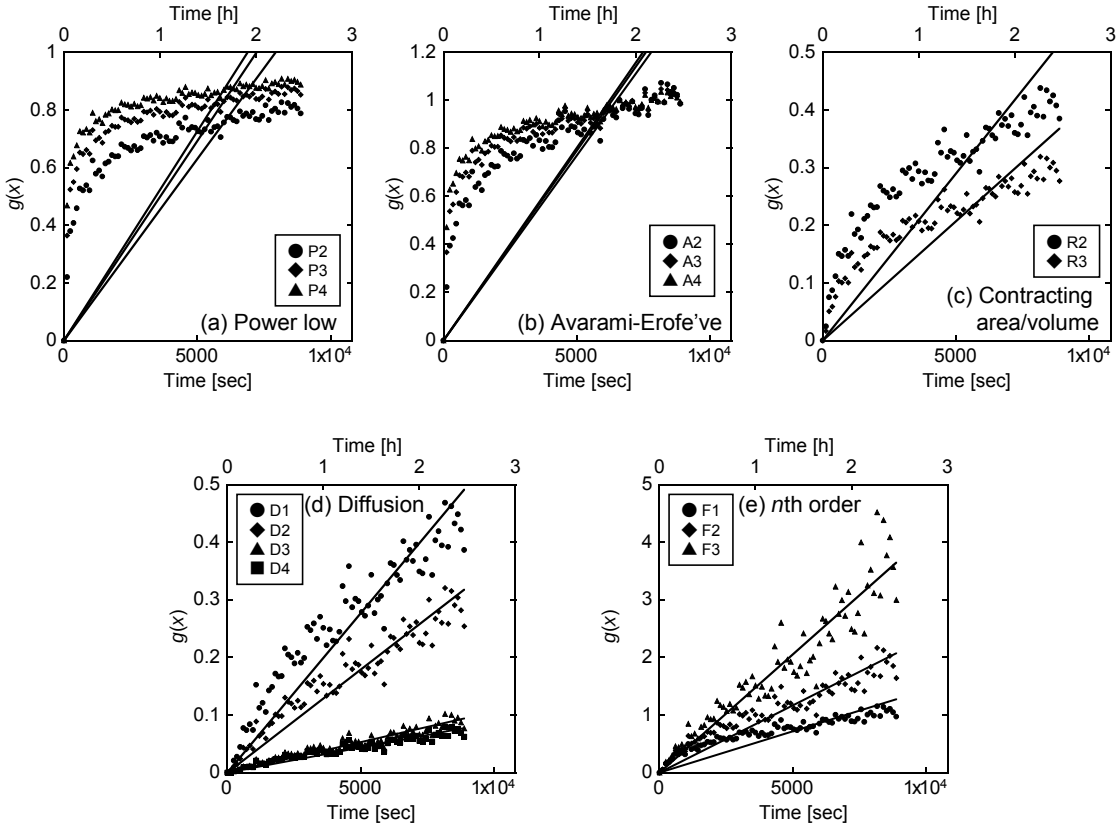

Fig. 5-7. Fitting results of aliphatic C−H decrease of Murchison IOM in Ar flow at 300ºC by various kinetic models listed in Table 5-1. The rate constant *k* values were determined as listed in Table 5-4.

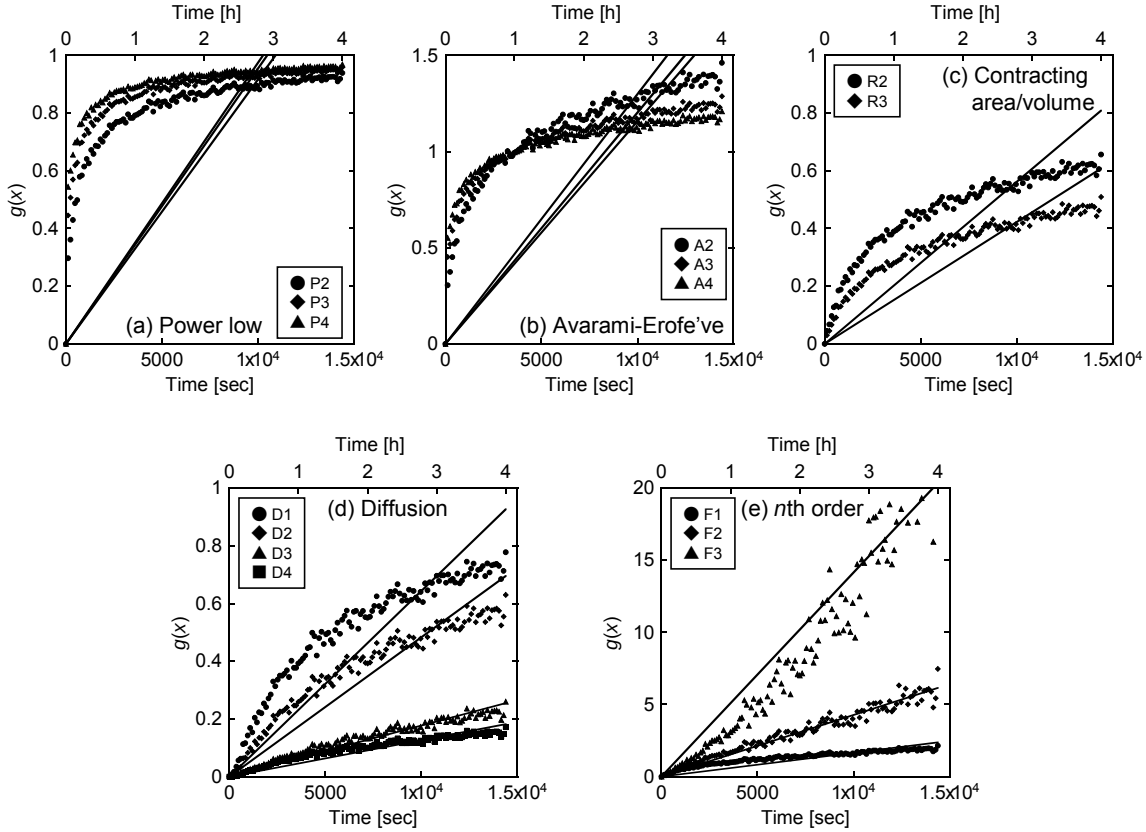

Fig. 5-8. Fitting results of aliphatic C−H decrease of Murchison IOM in air at 220ºC by various kinetic models listed in Table 5-1. The rate constant *k* values were determined as listed in Table 5-5.

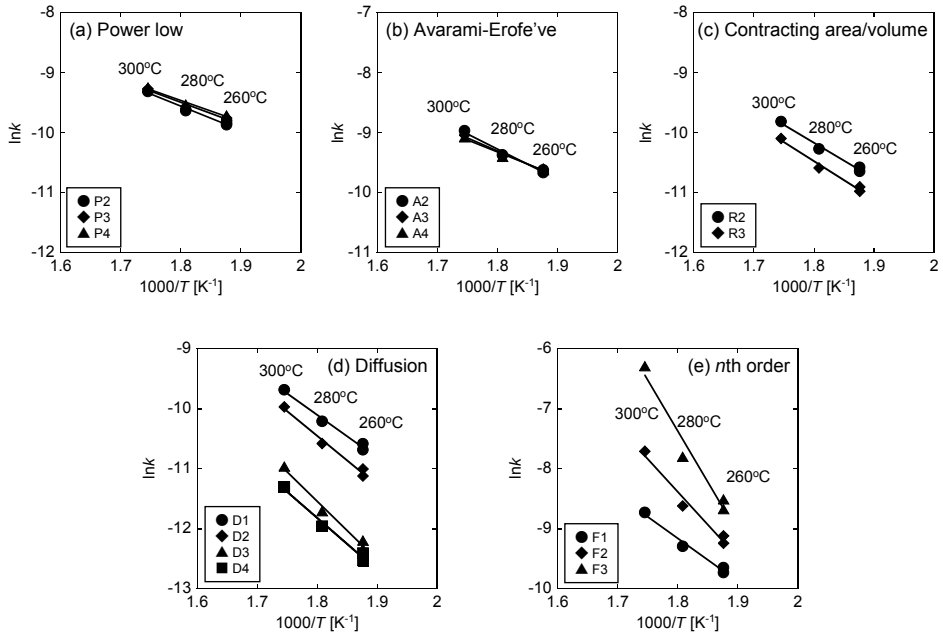

Fig. 5-9. Arrhenius diagrams of aliphatic C−H decrease of bulk Murchison meteorite in Ar flow for various kinetic models listed in Table 5-1; (a) power law (P2, P3, P4), (b) nuclei growth models by Avarami-Erofe'ye (A2, A3, A4), (c) contracting area (R2) and contracting volume (R3), (d) one-dimensional diffusion (D1), two-dimensional diffusion (D2), and three-dimensional diffusion by Jander (D3) and Ginstling-Brounshtein (D4), (e) first-order (F1), second-order (F2) and third-order (F3) reactions. Activation energy E_a values and frequency factor A were estimated as listed in Table 5-2.

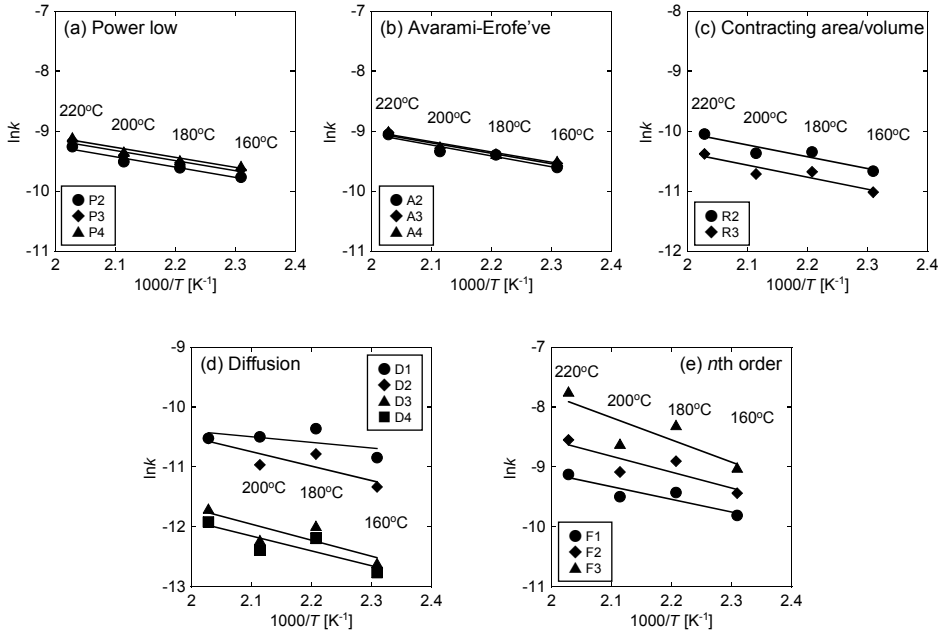

Fig. 5-10. Arrhenius diagrams of aliphatic C−H decrease of bulk Murchison meteorite in air for various kinetic models listed in Table 5-1. Activation energy E_a values and frequency factor A were estimated as listed in Table 5-3.

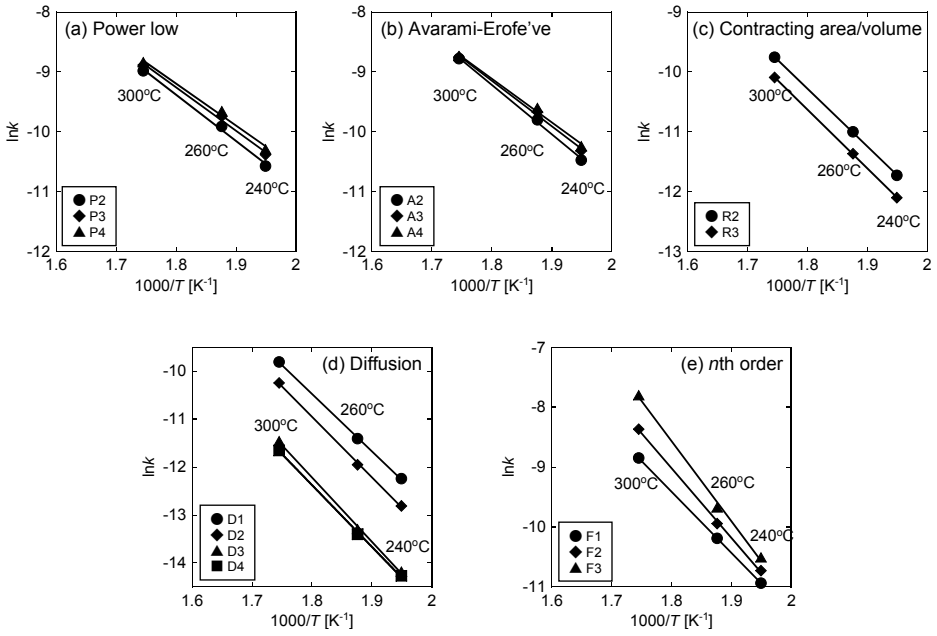

Fig. 5-11. Arrhenius diagrams of aliphatic C−H decrease of Murchison IOM in Ar flow for various kinetic models listed in Table 5-1. Activation energy E_a values and frequency factor A were estimated as listed in Table 5-4.

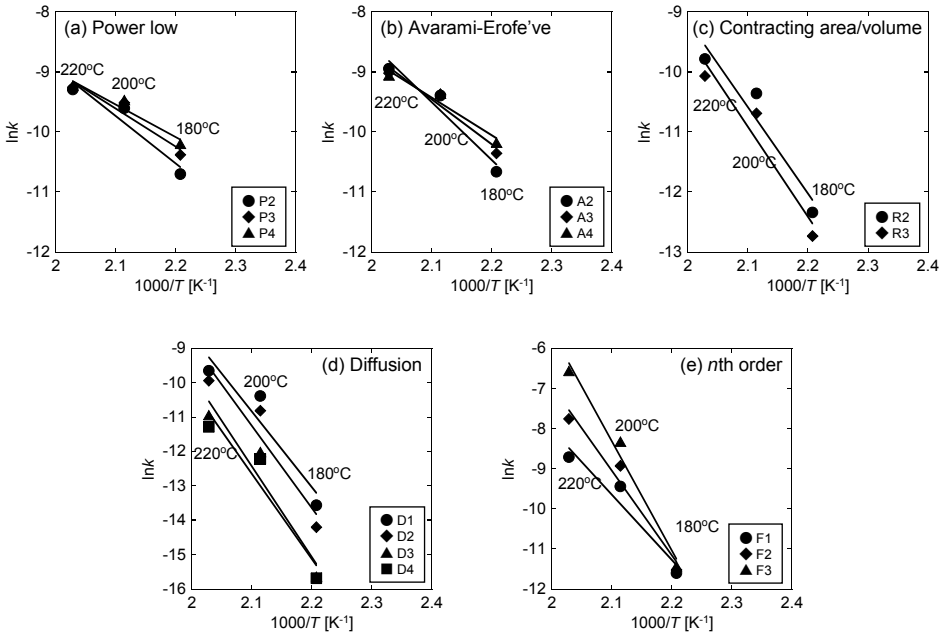

Fig. 5-12. Arrhenius diagrams of aliphatic C−H decrease of Murchison IOM in air for various kinetic models listed in Table 5-1. Activation energy E_a and frequency factor A values were estimated as listed in Table 5-5.

Table 5-2. Kinetic parameters for aliphatic C−H decrease of bulk Murchison in Ar flow using various kinetic models listed in Table 5-1.

Mechanism	260°C Run1		260°C Run2		280°C		300°C		Average			
	k [s^{-1}]	r	k [s^{-1}]	r	k [s^{-1}]	r	k [s^{-1}]	r	r	A [s^{-1}]	E_a [kJ•mol^{-1}]	r
P2	5.3E-05	0.79	5.2E-05	0.72	6.6E-05	0.73	9.0E-05	0.70	0.74	1.0E-01	34 ± 3	0.99
P3	5.8E-05	0.71	5.7E-05	0.64	7.0E-05	0.66	9.5E-05	0.61	0.65	5.8E-02	31 ± 3	0.99
P4	6.1E-05	0.63	6.0E-05	0.57	7.3E-05	0.59	9.7E-05	0.63	0.61	4.4E-02	29 ± 3	0.99
A2	6.6E-05	0.86	6.4E-05	0.79	8.6E-05	0.82	1.3E-04	0.80	0.82	8.3E-01	42 ± 4	0.99
A3	6.7E-05	0.79	6.5E-05	0.72	8.4E-05	0.76	1.2E-04	0.75	0.75	2.3E-01	36 ± 3	0.99
A4	6.8E-05	0.73	6.6E-05	0.66	8.3E-05	0.70	1.1E-04	0.65	0.68	1.2E-01	33 ± 3	0.99
R2	2.6E-05	0.91	2.4E-05	0.83	3.5E-05	0.85	5.5E-05	0.17	0.69	1.8E+00	50 ± 4	0.99
R3	1.8E-05	0.92	1.7E-05	0.84	2.5E-05	0.86	4.1E-05	0.86	0.87	2.5E+00	53 ± 5	0.99
D1	2.5E-05	0.94	2.3E-05	0.85	3.7E-05	0.87	6.2E-05	0.88	0.88	1.6E+01	59 ± 5	0.99
D2	1.7E-05	0.95	1.5E-05	0.85	2.5E-05	0.87	4.7E-05	0.88	0.89	7.6E+01	68 ± 6	0.99
D3	5.0E-06	0.95	4.4E-06	0.84	8.2E-06	0.87	1.7E-05	0.87	0.88	4.3E+02	81 ± 7	0.99
D4	**4.1E-06**	**0.95**	**3.6E-06**	**0.85**	**6.4E-06**	**0.87**	**1.2E-05**	**0.88**	**0.89**	**4.8E+01**	**72 ± 6**	**0.99**
F1	6.4E-05	0.93	5.9E-05	0.84	9.2E-05	0.87	1.6E-04	0.87	0.88	4.3E+01	60 ± 6	0.99
F2	1.1E-04	0.95	9.7E-05	0.84	1.8E-04	0.86	4.5E-04	0.76	0.85	8.0E+04	91 ± 10	0.99
F3	2.0E-04	0.95	1.7E-04	0.80	4.1E-04	0.82	1.9E-03	0.53	0.77	1.2E+10	141 ± 19	0.98

Table 5-3. Kinetic parameters for aliphatic C−H decrease of bulk Murchison in air using various kinetic models listed in Table 5-1.

Mechanism	160°C		180°C		200°C		220°C		Average				
	k [s^{-1}]	r	k [s^{-1}]	r	k [s^{-1}]	r	k [s^{-1}]	r	r	A [s^{-1}]	E_a [kJ•mol^{-1}]		r
P2	5.7E-05	0.49	6.7E-05	0.59	7.4E-05	0.80	9.5E-05	0.74	0.66	3.0E-03	14	± 2	0.98
P3	6.5E-05	0.44	7.3E-05	0.49	8.3E-05	0.73	1.1E-04	0.64	0.57	3.0E-03	14	± 2	0.97
P4	6.9E-05	0.39	7.6E-05	0.42	8.7E-05	0.66	1.1E-04	0.67	0.53	3.1E-03	14	± 2	0.97
A2	6.7E-05	0.52	8.3E-05	0.69	8.8E-05	0.85	1.2E-04	0.75	0.70	4.4E-03	15	± 3	0.97
A3	7.2E-05	0.48	8.4E-05	0.60	9.3E-05	0.79	1.2E-04	0.69	0.64	3.9E-03	14	± 2	0.97
A4	7.5E-05	0.44	8.4E-05	0.52	9.5E-05	0.74	1.2E-04	0.71	0.60	3.8E-03	14	± 2	0.97
R2	**2.3E-05**	**0.54**	**3.2E-05**	**0.75**	**3.1E-05**	**0.89**	**4.3E-05**	**0.77**	**0.74**	**2.2E-03**	**16**	**± 4**	**0.94**
R3	**1.6E-05**	**0.54**	**2.3E-05**	**0.76**	**2.2E-05**	**0.89**	**3.1E-05**	**0.76**	**0.74**	**1.7E-03**	**17**	**± 5**	**0.93**
D1	2.0E-05	0.54	3.2E-05	0.78	2.8E-05	0.90	2.7E-05	0.71	0.73	2.0E-04	8	± 8	0.55
D2	1.2E-05	0.53	2.1E-05	0.78	1.7E-05	0.89	2.7E-05	0.71	0.73	3.4E-03	20	± 8	0.86
D3	3.4E-06	0.52	6.3E-06	0.78	4.9E-06	0.89	8.3E-06	0.66	0.71	1.7E-03	22	± 10	0.84
D4	2.9E-06	0.53	5.1E-06	0.78	4.2E-06	0.89	6.7E-06	0.69	0.72	9.8E-04	21	± 9	0.85
F1	5.5E-05	0.54	8.1E-05	0.77	7.5E-05	0.89	1.1E-04	0.74	0.73	7.6E-03	18	± 6	0.91
F2	8.0E-05	0.52	1.4E-04	0.77	1.1E-04	0.89	1.9E-04	0.61	0.70	3.9E-02	22	± 9	0.87
F3	1.2E-04	0.49	2.5E-04	0.76	1.8E-04	0.86	4.3E-04	0.43	0.64	6.8E-01	31	± 14	0.84

Table 5-4. Kinetic parameters for aliphatic C−H decrease of Murchison IOM in Ar flow using various kinetic models listed in Table 5-1.

Mechanism	240°C		260°C		300°C		Average			
	k [s^{-1}]	r	k [s^{-1}]	r	k [s^{-1}]	r	r	A [s^{-1}]	E_a [kJ•mol^{-1}]	r
P2	2.6E-05	0.57	5.0E-05	0.78	1.3E-04	0.80	0.72	9.1E+01	64 ± 4	1.00
P3	3.1E-05	0.52	5.9E-05	0.64	1.4E-04	0.71	0.63	4.4E+01	60 ± 5	1.00
P4	3.4E-05	0.48	6.4E-05	0.68	1.5E-04	0.65	0.60	3.1E+01	58 ± 5	1.00
A2	2.8E-05	0.59	5.5E-05	0.80	1.5E-04	0.87	0.76	2.8E+02	69 ± 3	1.00
A3	3.3E-05	0.55	6.3E-05	0.69	1.6E-04	0.80	0.68	9.4E+01	63 ± 4	1.00
A4	3.6E-05	0.51	6.8E-05	0.71	1.6E-04	0.73	0.65	5.4E+01	60 ± 5	1.00
R2	8.1E-06	0.63	1.7E-05	0.84	5.8E-05	0.93	0.80	1.2E+03	80 ± 1	1.00
R3	5.6E-06	0.64	1.2E-05	0.85	4.1E-05	0.93	0.80	1.2E+03	82 ± 1	1.00
D1	4.8E-06	0.64	1.1E-05	0.86	5.5E-05	0.96	0.82	6.6E+04	99 ± 2	1.00
D2	2.7E-06	0.64	6.5E-06	0.86	3.6E-05	0.96	0.82	1.3E+05	105 ± 3	1.00
D3	7.0E-07	0.64	1.7E-06	0.86	1.1E-05	0.96	0.82	1.6E+05	111 ± 4	1.00
D4	**6.4E-07**	**0.64**	**1.5E-06**	**0.86**	**8.7E-06**	**0.96**	**0.82**	**5.2E+04**	**107 ± 3**	**1.00**
F1	1.8E-05	0.64	3.8E-05	0.85	1.4E-04	0.94	0.81	8.2E+03	85 ± 0	1.00
F2	2.2E-05	0.64	4.8E-05	0.86	2.3E-04	0.96	0.82	1.5E+05	97 ± 3	1.00
F3	2.7E-05	0.64	6.3E-05	0.85	4.1E-04	0.94	0.81	5.6E+06	111 ± 6	1.00

Table 5-5. Kinetic parameters for aliphatic C−H decrease of Murchison IOM in air using various kinetic models listed in Table 5-1.

Mechanism	180°C		200°C		220°C		Average				
	k [s^{-1}]	r	k [s^{-1}]	r	k [s^{-1}]	r	r	A	E_a [kJ•mol^{-1}]		r
P2	2.2E-05	0.90	6.7E-05	0.82	9.2E-05	0.76	0.83	9.4E+02	66	± 19	0.96
P3	3.1E-05	0.75	7.4E-05	0.75	9.5E-05	0.69	0.73	4.0E+01	53	± 15	0.96
P4	3.7E-05	0.82	7.7E-05	0.69	9.7E-05	0.62	0.71	6.1E+00	45	± 12	0.97
A2	2.3E-05	0.90	8.3E-05	0.89	1.3E-04	0.89	0.89	4.5E+04	80	± 20	0.97
A3	3.2E-05	0.76	8.5E-05	0.83	1.2E-04	0.84	0.81	5.2E+02	62	± 15	0.97
A4	3.8E-05	0.83	8.6E-05	0.78	1.2E-04	0.78	0.80	4.2E+01	52	± 12	0.97
R2	4.4E-06	0.93	3.2E-05	0.93	5.6E-05	0.92	0.93	3.2E+08	119	± 35	0.96
R3	3.0E-06	0.93	2.3E-05	0.93	4.2E-05	0.93	0.93	8.0E+08	124	± 35	0.96
D1	1.3E-06	0.89	3.1E-05	0.95	6.4E-05	0.94	0.93	2.5E+15	183	± 61	0.95
D2	6.8E-07	0.88	2.0E-05	0.96	4.8E-05	0.96	0.93	9.8E+16	199	± 62	0.95
D3	1.6E-07	0.88	6.1E-06	0.95	1.8E-05	0.98	0.94	5.2E+18	219	± 63	0.96
D4	1.5E-07	0.88	4.9E-06	0.96	1.3E-05	0.97	0.94	1.3E+17	206	± 63	0.96
F1	9.1E-06	0.93	7.9E-05	0.94	1.6E-04	0.96	0.94	4.4E+10	135	± 35	0.97
F2	**9.9E-06**	**0.93**	**1.3E-04**	**0.95**	**4.3E-04**	**0.98**	**0.95**	**2.1E+15**	**175**	**± 34**	**0.98**
F3	1.1E-05	0.93	2.4E-04	0.93	1.4E-03	0.95	0.94	1.9E+21	226	± 30	0.99

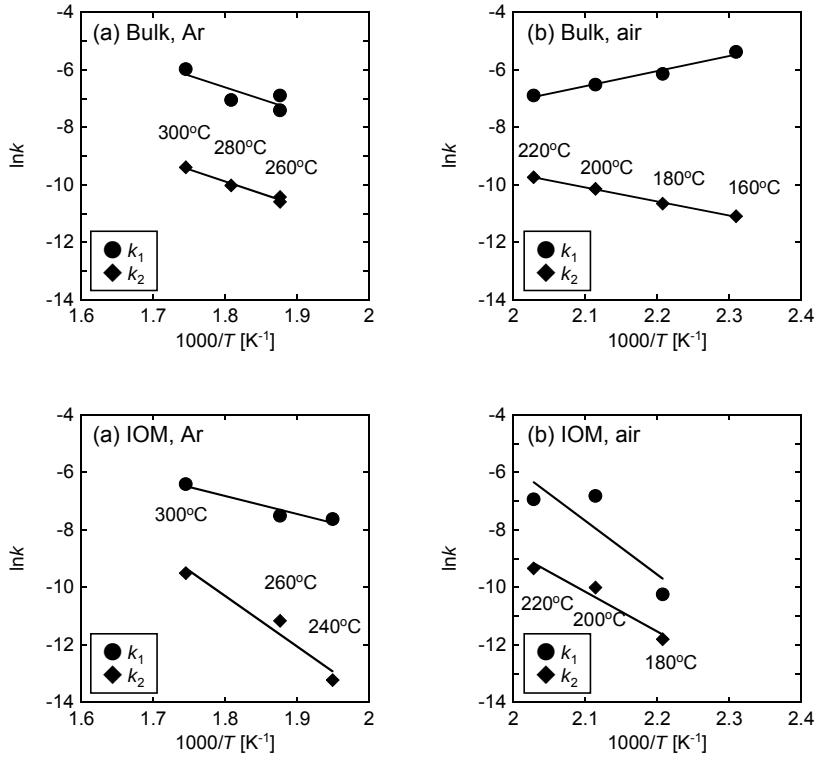

Fig. 5-13. Arrhenius diagrams for the combination of two first-order reaction model of aliphatic C−H decrease of (a) bulk Murchison in Ar flow, (b) bulk Murchison in air, (c) Murchion IOM in Ar flow, and (d) Murchison IOM in air. Activation energy E_a values and frequency factor A were estimated as listed in Table 5-5. The rate constant k values were determined as listed in Table 5-6 by fitting eq. 5-6 as shown in Fig. 5-2 and 5-4.

Table 5-6. Rate constants and ratio of the labile fraction (k_1) to the refractory fraction (k_2) for aliphatic C−H decrease of Murchison (bulk and IOM) using the combination of two first-order reaction models.

	a	Error	k_1 [s^{-1}]	Error	k_2 [s^{-1}]	Error	r
Bulk, Ar							
260°C Run1	0.40	0.02	6.1E-04	5.7E-05	3.0E-05	2.0E-06	0.98
260°C Run2	0.39	0.02	1.0E-03	1.8E-04	2.5E-05	2.6E-06	0.92
280°C	0.44	0.03	8.7E-04	1.7E-04	4.4E-05	5.7E-06	0.93
300°C	0.50	0.03	2.6E-03	5.9E-04	8.4E-05	8.7E-06	0.93
Bulk, Air							
160°C	0.14	0.02	4.6E-03	4.9E-03	1.5E-05	2.2E-06	0.57
180°C	0.25	0.01	2.2E-03	6.0E-04	2.4E-05	1.9E-06	0.84
200°C	0.29	0.02	1.5E-03	2.7E-04	4.0E-05	2.6E-06	0.93
220°C	0.39	0.06	1.0E-03	3.2E-04	5.9E-05	1.3E-05	0.85
IOM, Ar							
240°C	0.30	0.01	4.9E-04	3.3E-05	1.8E-06	4.2E-07	0.88
260°C	0.25	0.02	5.5E-04	8.9E-05	1.4E-05	2.0E-06	0.92
300°C	0.34	0.02	1.7E-03	1.8E-04	7.5E-05	4.3E-06	0.98
IOM, Air							
180°C	0.05	3.96	3.6E-05	1.2E-03	7.5E-06	5.2E-05	0.92
200°C	0.32	0.01	1.1E-03	1.2E-04	4.5E-05	1.9E-06	0.98
220°C	0.53	0.01	9.8E-04	3.8E-05	8.8E-05	2.7E-06	1.00

Table 5-7. Activation energies and frequency factors for aliphatic C−H decrease of Murchison (bulk and IOM) using the combination of two first-order reaction models.

	A_1 [s^{-1}]	E_1 [kJ•mol^{-1}]	r	A_2 [s^{-1}]	E_2 [kJ•mol^{-1}]	r
Bulk, Ar	3.4E+03	68 ± 30	0.85	1.9E+02	70 ± 8	0.99
Bulk, Air	2.2E-08	−44 ± 5	0.99	1.2E+00	41 ± 1	1.00
IOM, Ar	8.5E+01	52 ± 14	0.96	1.9E+09	146 ± 33	0.98
IOM, Air	5.6E+13	156 ± 91	0.86	1.7E+08	115 ± 28	0.97

5.5. Discussion

5.5.1. Reaction Models for Aliphatic C-H Decrease of Murchison

Although reaction pathways for the thermal degradation of organic matter in Murchison meteorite are still unclear, possible major reactions in air can be considered to be first oxidation and then breaking of chemical bonds. Possible reaction models for the aliphatic C−H decrease can be written as the following;

Partial oxidation: $R{-}CH_2{-}CH_3 \xrightarrow{+O_2} R{-}CH_2{-}COOH \longrightarrow R{-}CH_3 + CO_2$

Bond breaking: $R{-}CH_2{-}CH_2{-}CH_3 \longrightarrow R{-}CH_2\bullet + \bullet CH_2{-}CH_3$

Meanwhile, Cody and Alexander (2005) proposed chemical oxidation which has taken place during parent body aqueous alteration, based on mineralogical and organic chemical aspects;

$$R{-}CH\bullet{-}R' \xrightarrow{+\bullet OH} R{-}CH(OH){-}R' \xrightarrow{+\bullet OH,\,-H_2O} R{-}C(OH)\bullet{-}R'$$

$$\xrightarrow{+\bullet OH,\,-H_2O} R{-}(C{=}O){-}R' \xrightarrow{+\bullet OH} R{-}(C{=}O){-}OH + \bullet R' \xrightarrow{+\bullet OH} H_2CO_3 + \bullet R$$

However, possibility of above aqueous chemical oxidation is uncertain, since the heating experiments in my study were conducted in dry condition.

As a whole, activation energies for IOM are higher than those for bulk Murchison (Table 5-2 to 5-5). Therefore, mineral assemblages of Murchison meteorite might have catalytic effects for the organic matter decomposition. Karabakan and Yurum (1998) reported the mineral matrix of oil shale kerogen affected the activation energy of pyrolysis. The authors suggested that pyrolysis reactions were catalyzed by alkaline earth metal cations in carbonates and inhibited by silicates. Since both carbonates and silicates were known to present in Murchison (Zolensky and McSween 1988; Zolensky et al. 1993), the catalytic effect of the carbonates seemed to be greater than the inhibition effect of the silicates. However, it is not clear that these catalytic and inhibitive effects for terrestrial kerogen can also be applied for chondrite IOM.

5.5.2. Reaction Controlling Mechanisms

In general, reaction controlling mechanism is evaluated by fitting of the experimental results. There were several probable mechanisms for aliphatic C−H decrease of Murchison meteorite for each experimental condition (Table 5-2 to 5-5). It should be noted that the decrease rate is much faster in air than in low oxygen condition (Ar flow). Therefore, reaction mechanisms might be different between heating in air and in Ar.

Judging from correlation coefficient *r* values, the most probable mechanisms in Table 5-1 for aliphatic C−H decrease in Ar flow are D2 and D4 for bulk Murchison, D1-D4 and F2 for IOM. Rate-determining process of aliphatic C−H decrease in low oxygen condition is likely to be diffusion of decomposition products and/or oxygen. Since three-dimensional diffusion seems more probable than one- or two- dimensional diffusion, Ginstling-Brounshtein three-dimensional diffusion model (D4) is likely to give the best expression for aliphatic C−H decrease of Murchison in low oxygen condition. The activation energies are 72 ± 6 kJ/mol for bulk Murchison and 107 ± 3 kJ/mol for IOM. These results are consistent with the experimental result of Aboulkas et al. (2008) that the most probable model for the pyrolysis process of oil shale kerogen agrees with D4 diffusion model and has activation energy of 80 kJ/mol determined by thermogravimetric analysis in an inert atmosphere.

On the other hand, rate-determining process of aliphatic C−H decrease in air is likely to be different between bulk Murchison and IOM. The most probable mechanisms in Table 1 are R2 and R3 for bulk Murchison, and F2 for IOM. For bulk Murchison, contracting area (R2) or contracting volume (R3) is likely to be controlling mechanisms. The activation energies are 16 ± 4 kJ/mol for R2 and 17 ± 5 kJ/mol for R3. For Murchison IOM, second-order reaction gives the best expression for aliphatic C−H decrease, and the activation energy is 175 ± 34 kJ/mol.

However, correlation coefficients *r* of contracting area/volume (R2-R3), diffusion (D1-D4) and 'order' reactions (F1-F3) do not show much difference in each experimental condition. The largest *r* values are different for each temperature. Therefore only fitting correlation coefficient could not give the best determination of the reaction mechanisms. Nonetheless, power law (P2-P4) and Avarami-Erofe'ev nuclei growth models (A2-A4) can be ruled out for all the experimental conditions. Since chondritic organic matter is a complex heterogeneous mixture of organic compounds, single reaction mechanism cannot give an expression of the aliphatic C−H decrease of Murchison meteorite.

An example of combination of multiple reactions is a combination of two first-order reactions. This model is commonly used for kinetics of thermal decomposition of oil shale kerogen (e.g., Rajeshwar 1981; Dogan and Uysal 1996; Khraisha 1998). Since chondritic IOM comprises at least two components: a more labile portion and a refractory material (Sephton et al. 1998), the combination of two first-order reactions might be applicable for organic matter in Murchison. This model seems probable for the aliphatic C−H decrease in most experimental conditions except bulk Murchison in air which has minus E_1 value.

For the aliphatic C−H decrease of IOM in Ar, the lower values of activation energy of stage 1 indicate that the decomposition of organic matter involves the breaking of relatively weak chemical bonds, while the higher values of stage 2 indicate the decomposition of much stronger chemical bonds. Bulk Murchison in Ar and IOM in air did not show much difference of activation energy between stage 1 and 2 due to the large error (Table 5-7). Determined activation energies (E_1, E_2) seem to be appropriate compared with terrestrial kerogen values (Table 5-8; Rajeshwar 1981; Dogan and Uysal 1996; Khraisha 1998).

However, the uncertainty of parameter determined by the combination of two first-order reactions should be larger than that for a single mechanism. Since fitting equation has three unknown parameters for each experimental decrease curve while single mechanism models have only one unknown parameter.

In order to estimate thermal processing on chondrite parent bodies, I employ kinetic parameters (E_a and A) of Murchison meteorite (bulk and IOM) determined by Ginstling-Brounshtein three-dimensional diffusion (D4) mechanism under low oxygen conditions. D4 mechanism showed best fits for both $g(x)$ versus time plots and Arrhenius diagrams (Figs. 5-5, 5-7, 5-9 and 5-11; Table 5-2 and 5-4). In addition, the single mechanism fittings show smaller error values of activation energies than that of the combination of two first-order reactions. Applications for the parent body processes are discussed in the following section.

Table 5-8. Literature data sets of activation energies by two first-order reactions (E_1, E_2) for decomposition of oil shale kerogen determined by thermogravimetric analyses.

Reference	Atmosphere	E_1 [kJ•mol^{-1}]	E_2 [kJ•mol^{-1}]
Rajeshwar (1981)	N_2	27.40 to 108.10	116.48 to 209.50
Dogan and Uysal (1996)	He	12.6 to 19.8	12.5 to 43.4
Khraisha (1998)	N_2	43.5 to 48.2	55.9 to 71.3

5.5.3. Time Scales and Temperatures for Thermal Processing of Carbonaceous Chondrites

If the time-temperature history of a given chondritic parent body were known, then these kinetic data could be used to put chondrites of different petrologic type in a spatial context, i.e., in terms of a radial distance from parent body center.

Heating time t can be expressed with temperature T and normalized peak height of aliphatic C−H ($C/C_0 = 1 - x$) using estimated activation energy E_a and frequency factor A, by $g(x)$ (5-3) and Arrhenius equation (5-5);

$$At = g(x) \cdot \exp\left(\frac{E_a}{RT}\right) \qquad (5\text{-}8)$$

I employ Ginstling-Brounshtein three-dimensional diffusion (D4) mechanism, then equation 5-8 yields;

$$At = \left[\frac{1}{3} + \frac{2}{3} \cdot \frac{C}{C_0} - \left(\frac{C}{C_0}\right)^{\frac{2}{3}}\right] \cdot \exp\left(\frac{E_a}{RT}\right) \qquad (5\text{-}9)$$

The time scale for metamorphism can be estimated for given temperature with aliphatic C−H peak height by equation 5-9. Otherwise, temperatures of metamorphism can be estimated for given time scales. Fig. 5-14 shows aliphatic C−H peak height decreases with time for individual temperatures calculated by equation 5-9 using kinetic parameters (E_a and A) of Murchison (bulk and IOM) estimated by the heating experiments in low oxygen condition (Ar flow).

According to the calculation, aliphatic C−H of bulk Murchison almost disappears for ~3 years at 100ºC. At 500ºC, aliphatic C−H disappears for ~9 minutes. The aliphatic C−H of Murchison would disappear for one million years even at 0ºC. This estimation seems to be too fast, assuming that aqueous alteration of CM chondrites have occurred for periods of ~7.5 ± ~2 m.y., at the temperature range of 0ºC to 80ºC (Brearley 2006). Since the heating experiments were conducted at dry conditions, direct application for aqueous alteration might be difficult. Further studies are needed to estimate kinetic parameters for wet conditions.

On the other hand, aliphatic C−H of Murchison IOM disappears for ~200 years at 100ºC, for ~2 minutes at 500ºC. At 0ºC and 80ºC, aliphatic C−H disappears for ~70 m.y. and ~1000 years, respectively. Assuming alteration of ~7.5 ± ~2 m.y., alteration temperatures could be calculated to be less than 13 ± 13ºC (where the temperature uncertainty reflects the error in the experimentally determined values of A and E_a). However the estimated temperature does not include the effects of minerals and aqueous fluid.

Over ~300ºC, aliphatic C−H decrease without mineral (IOM) is slower than with mineral (bulk) (Fig. 5-15). It is considered to be due to the catalytic effects of minerals. Therefore, the rate of organic decomposition might be variable with changes of mineral assemblages during aqueous alteration and/or thermal metamorphism.

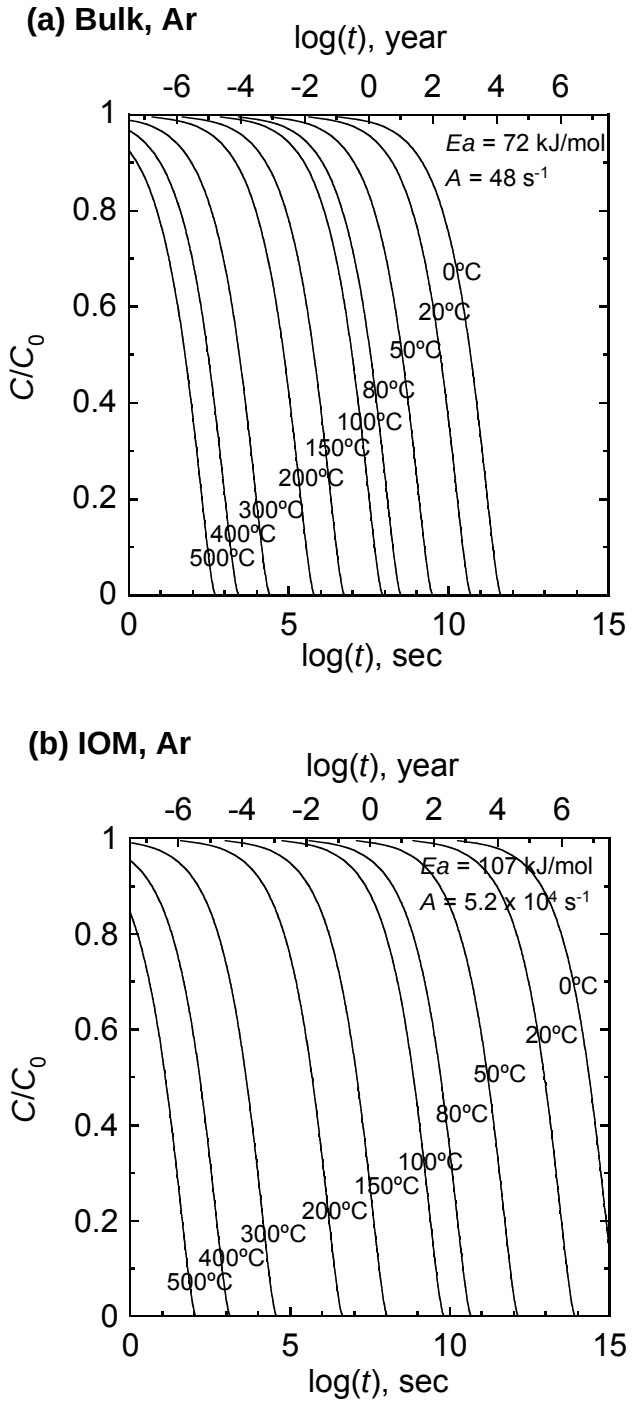

Fig. 5-14. Aliphatic C−H peak height decrease with time for individual temperatures calculated with kinetic parameters of Murchison (a) bulk and (b) IOM, heating in low oxygen condition (Ar flow).

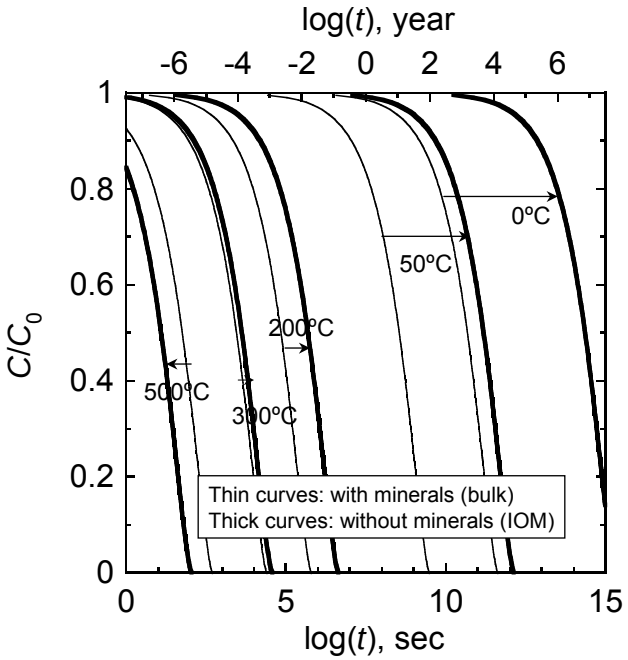

Fig. 5-15. Difference of the aliphatic C−H peak height decrease rates with and without minerals.

5.6. Conclusions

In order to evaluate kinetic parameters for thermal decomposition of organics, in-situ heating experiments of bulk and insoluble organic matter (IOM) of Murchison (CM2) meteorite were conducted under micro FTIR combined with a heating stage. A series of experiments provides the following results.

1. The decrease rate of aliphatic C−H peak heights is much faster in air than in Ar flow, suggesting that reaction mechanisms might be different between heating in air and in Ar.
2. Activation energy values of aliphatic C−H decrease are larger for IOM than bulk of Murchison. Hence, the mineral assemblage of Murchison meteorite might have catalytic effect for the organic matter decomposition. The rate of organic decomposition might be varied with change of mineral assemblage during aqueous alteration and/or thermal metamorphism.
3. Decreases with time of aliphatic C−H peak heights in Ar flow are well fitted with Ginstling-Brounshtein three dimensional diffusion model (D4). The activation energy and frequency factor for bulk Murchison under Ar flow are 72 ± 6 kJ/mol and ~48 s^{-1}, respectively, while those for Murchison IOM under Ar

flow are 107 ± 3 kJ/mol and ~5.2 × 10^4 s^{-1}, respectively.

4. The time scale for metamorphism can be estimated for a given temperature with aliphatic C−H peak height, or the temperature of metamorphism can be estimated for a given time scale. For example, aliphatic C−H of bulk Murchison would almost disappear for ~3 years at 100ºC.

These in-situ heating experiments provide us a new insight into the thermal stability of organic matter in carbonaceous chondrites during thermal processes on their parent bodies.

References

Aboulkas A., El Harfi K., and El Bouadili A. 2008. Kinetic and mechanism of Tarfaya (Morocco) oil shale and LDPE mixture pyrolysis. *Journal of Materials Processing Technology* 206: 16-24.

Alexander C. M. O'D., Russell S. S., Arden J. W., Ash R. D., Grady M. M., and Pillinger C. T. 1998. The origin of chondritic macromolecular organic matter: A carbon and nitrogen isotope study. *Meteoritics & Planetary Science* 33: 603-622.

Alexander C. M. O'D., Fogel M., Yabuta H., and Cody G. D. 2007. The origin and evolution of chondrites recorded in the elemental and isotopic compositions of their macromolecular organic matter. *Geochimica et Cosmochimica Acta* 71: 4380-4403.

Bonal L., Quirico E., Bourot-Denise M., Montagnac G. 2006. Determination of the petrologic type of CV3 chondrites by Raman spectroscopy of included organic matter. *Geochimica et Cosmochimica Acta* 70: 1849-1863.

Bonal L., Bourot-Denise M., Quirico E., Montagnac G., and Lewin E. 2007. Organic matter and metamorphic history of CO chondrites. *Geochimica et Cosmochimica Acta* 71: 1605-1623.

Botta O. and Bada J. L. 2002. Extraterrestrial organic compounds in meteorites. *Surveys in Geophysics* 23: 411-467.

Brearley A. J. 2006. The action of water. In *Meteorites and the early solar system II*, edited by Lauretta D. S., Leshin L. A., and McSween H. Y., Jr. Tucson, Arizona: The University of Arizona Press. pp. 587-624.

Busemann H., Young A. F., Alexander C. M. O., Hoppe P., Mukhopadhyay S., and Nittler L. R. 2006. Interstellar chemistry recorded in organic matter from primitive meteorites. *Science* 312: 727-730.

Busemann H., Alexander C. M. O'D., and Nittler L. R. 2007. Characterization of insoluble organic matter in primitive meteorites by microRaman spectroscopy. *Meteoritics & Planetary Science* 42: 1387-1416.

Clayton R. N. and Mayeda T. K. 1999. Oxygen isotope studies of carbonaceous chondrites. *Geochimica et Cosmochimica Acta* 6: 2089-2104.

Cody G. D. and Alexander C. M. O'D. 2005. NMR studies of chemical structural variation of insoluble organic matter from different carbonaceous chondrite groups. *Geochimica et Cosmochimica Acta* 69: 1085-1097.

Cody G. D., Alexander C. M. O'D., Yabuta H., Kilcoyne A. L. D., Araki T., Ade H., Dera P., Fogel M., Militzer B., Mysen B. O. 2008. Organic thermometry for chondritic parent bodies. *Earth and Planetary Science Letters* 272: 446-455.

Dogan O. M. and Uysal B. Z. 1996. Non-isothermal pyrolysis kinetics of three Turkish oil shales. *Fuel* 75: 1424-1428.

Huss G. R., Rubin A. E., and Grossman J. N. 2006. Thermal metamorphism in chondrites. In *Meteorites and the early solar system II*, edited by Lauretta D. S., Leshin L. A., and McSween H. Y., Jr. Tucson, Arizona: The University of Arizona Press. pp. 567-586.

Karabakan A. and Yürüm Y. 1998. Effect of the mineral matrix in the reactions of oil shales: 1. Pyrolysis reactions of Turkish Göynük and US Green River oil shales. *Fuel* 77: 1303-1309.

Kerridge J. F. 1985. Carbon, hydrogen and nitrogen in carbonaceous chondrites: Abundances and isotopic compositions in bulk samples. *Geochimica et Cosmochimica Acta* 49: 1707-1714.

Khraisha, Y. H. 1998. Kinetics of Isothermal Pyrolysis of Jordan Oil Shales. E*nergy Conversion and Management* 39: 157-165.

Kitajima F., Nakamura T., Takaoka N., and Murae T. 2002. Evaluating the thermal metamorphism of CM chondrites by using the pyrolytic behavior of carbonaceous macromolecular matter. *Geochimica et Cosmochimica Acta* 66: 163-172.

Nakamura K., Nakashima S., Shiota D., Zolensky M. E., and Keller L. P. 2003. In Situ Heating Behavior by Infrared Microspectroscopy of Organic Components in Tagish Lake Meteorite (abstract #1432). 34th Lunar and Planetary Science Conference. CD-ROM.

Okumura S. and Nakashima S. 2004. Water diffusivity in rhyolitic glasses as determined by in situ IR spectroscopy. *Physics and Chemistry of Minerals* 31: 183-189.

Pearson V. K., Sephton M. A., and Gilmour I. 2006. Molecular and isotopic indicators of alteration in CR chondrites. *Meteoritics & Planetary Science* 41: 1291-1303.

Quirico E., Raynal P. I., and Bourot-Denise M. 2003. Metamorphic grade of organic matter in six unequilibrated ordinary chondrites. *Meteoritics & Planetary Science* 38: 795-811.

Rajeshwar K. 1981. The kinetics of the thermal-decomposition of Green River oil-shale kerogen by non-isothermal thermogravimetry. *Thermochimica Acta* 45: 253-263.

Rose H. R., Smith D. R., and Vassallo A. M. 1998. Study of the oxidation of oil shale and kerogen by Fourier transform infrared emission spectroscopy. *Energy & Fuels* 12: 682-688.

Sears D. W. G., Batchelor J. D., Lu J., and Keck B. D. 1991. Metamorphism of CO and CO-like

chondrites and comparisons with type 3 ordinary chondrites. *Proceedings of the NIPR Symposium on Antarctic Meteorites* 4: 319-343.

Sephton M. A., Pillinger C. T., and Gilmour I. 1998. $\delta^{13}C$ of free and macromolecular aromatic structures in the Murchison meteorite. *Geochimica et Cosmochimica Acta* 62:1821-1828.

Vyazovkin S. and Wight C. A. 1997. Kinetics in solids. *Annual Review of Physical Chemistry* 48: 125-149.

Wlotzka F. 1985. Olivine-spinel and olivine-ilmenite thermometry in chondrites of different petrologic type (abstract). In *Lunar and Planetary Science XVI*, Lunar and Planetary Institute, Houston. pp. 918-919.

Wlotzka F. 1987. Equilibration temperatures and cooling rates of chondrites − A new approach (abstract). *Meteoritics* 22: 529-531.

Zolensky M. and McSween H.Y., Jr. 1988. Aqueous alteration. In *Meteorites and Early Solar System*, edited by Kerridge J. R. and Matthews M. S. Tucson, Arizona: The University of Arizona Press. pp. 114-143.

Zolensky M. E., Bourcier W. L., and Gooding J. L. 1989. Aqueous alteration on the hydrous asteroids − Results of EQ3/6 computer-simulations. *Icarus* 78: 411-425.

Zolensky M. Barrett R., and Browning L. 1993. Mineralogy and composition of matrix and chondrules rims in carbonaceous chondrites. *Geochimica et Cosmochimica Acta* 57: 3123-3148.

Chapter 6

SUMMARY AND IMPLICATIONS

6.1. Summary

6.1.1. Background and Objectives

Carbonaceous chondrite meteorites contain up to a few wt% carbon. These meteorites are known to be the most primitive meteorites and contain records of the early solar system. The larger fraction of the organic carbon (70-99%) is a complex insoluble organic matter (IOM), while the other fraction (< 30%) is numerous soluble organic compounds. Since IOM is generally obtained from meteorite powders after repeated extractions with solvents and demineralization by concentrated hydrofluoric and hydrochloric acids or CsF, their spatial distribution in chondrite textures has not been well known. Recent studies on chondritic organics by scanning electron microscope (SEM) and transmission electron microscopy/electron energy-loss spectroscopy (TEM-EELS) without this extraction suggest the association of carbonaceous materials with phyllosilicate minerals (e.g., Pearson et al. 2002; Garvie and Buseck 2007). However, very little is known on the nature of microscopic organic matter and their interaction with minerals.

Structural changes of chondritic graphitic materials have been used to evaluate parent body thermal metamorphism. Recently, Cody et al. (2008) demonstrated that the development of the intensity of a $1s-\sigma^*$ exciton observed using carbon X-ray absorption near edge structure (XANES) spectroscopy appeared to correlate well with other estimated degrees of the thermal metamorphism of the chondritic parent bodies. These experiments revealed that modification of IOM is a kinetically controlled process. Enhanced and additional kinetic studies of thermal processing of organic matter may further help sorting out the thermal history of the parent bodies.

I first aim to elucidate spatial relationship of organic matter and inorganic phases, then effects of minerals on thermal transformation of organic matter. Finally, I evaluate thermal processing on chondrite parent bodies by kinetic studies of chondritic organic matter using Fourier transform infrared (FTIR) spectroscopy, which is a non-destructive technique for organic components and minerals.

First I checked organic contamination of carbonaceous chondrites for FTIR microspectroscopic analyses. Second, I conducted mapping of chondrite by high resolution infrared imaging technique using near-field infrared (NFIR) microspectroscopy for microscopic and spatial characterization of chondritic organic matter. Third, I conducted heating experiments of IOM and bulk meteorite to elucidate roles of mineral phases for thermal stability of organic matter. Finally, I conducted heating experiments of carbonaceous chondrite to estimate kinetic parameters using

infrared bands. Kinetic data sets were applied to estimate temperature and time scales for parent body processes of chondritic meteorites. This technique would be a new alternative method to estimate alteration temperatures, which are conventionally given by thermal stabilities of minerals.

6.1.2. Organic Contamination during Storage of Carbonaceous Chondrites for Micro FTIR Measurements

Organic contamination (~2965 and ~1260 cm^{-1} peaks) on the samples pressed on Al plates during storage was found on Tagish Lake (C2) and Murchison (CM2) carbonaceous chondrites containing abundant hydrous minerals by Fourier transform infrared (FTIR) microspectroscopy (Fig. 6-1). On the other hand, anhydrous chondrite (Moss, CO3) was not contaminated. This contamination occurred within one day of storage, when the samples pressed on Al were stored within containers including silicone rubber mats. Volatile molecules having similar peaks to the contaminants were detected by long-path gas cell FTIR measurements for the silicone rubber mat. Rapid adsorption of the volatile contaminants also occurred when silica gel and hydrous minerals such as serpentine were stored in containers including silicone rubber, silicone grease or adhesive tape. However, they did not show any contamination when stored in glass and polystyrene containers without these compounds. Therefore, precious astronomical samples such as meteorites, interplanetary dust particles (IDPs) and mission returned samples from comets, asteroids and Mars, should be measured by micro FTIR within one day of storage in glass containers without silicone rubber, silicone grease or adhesive tape.

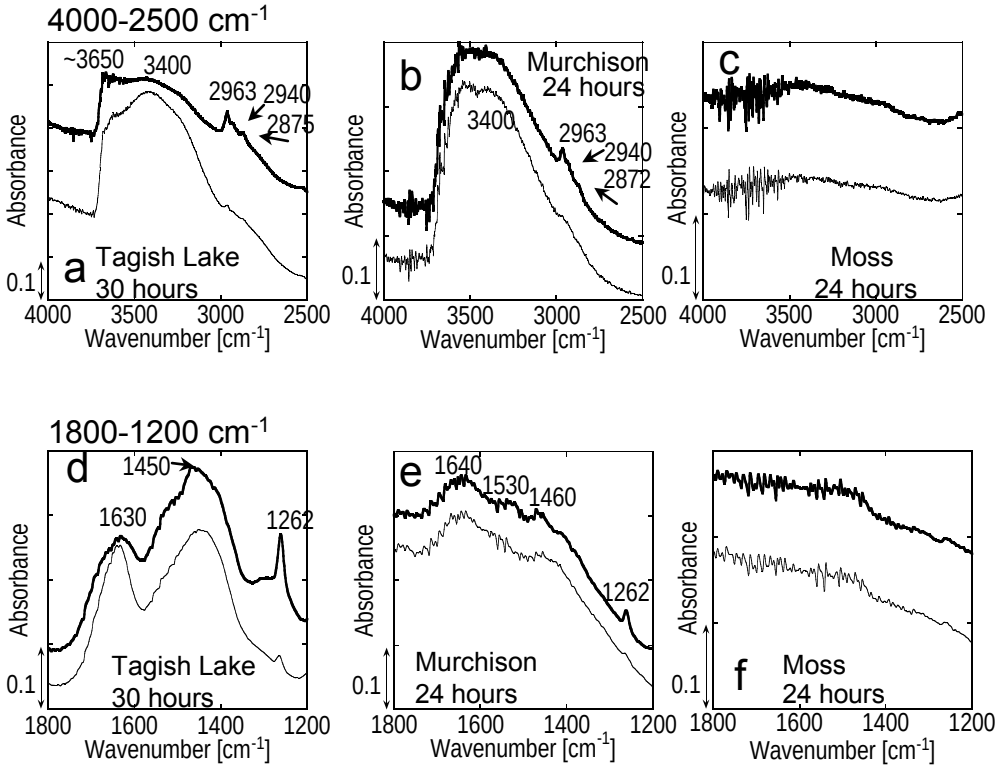

Fig. 6-1. Infrared transmission-reflection spectra of (a-c) 4000-2500 cm^{-1} and (d-f) 1800-1200 cm^{-1} regions of the samples pressed on Al plates before (thin curves) and after (thick curves) storage in the polystyrene tray with the silicone rubber mat for 24-30 hours. (a, d) Tagish Lake meteorite, (b, e) Murchison meteorite, and (c, f) Moss meteorite.

6.1.3. Organic Matter Distribution Using a Near-Field Infrared (NFIR) Microspectroscopy in a Carbonaceous Chondrite

In order to study organic matter distribution and mineral association at the submicron scale spatial resolution, the Bells (CM2) carbonaceous chondrite has been studied using a NFIR spectroscopy, which has been developed to enable infrared spectral mapping beyond the optical diffraction limit of conventional FTIR microspectroscopy. NFIR spectral mapping of the Bells 300 nm thick sections on the Al plate showed ~1 μm aliphatic C−H rich areas which were considered to represent the organic rich areas, while phyllosilicates were ubiquitously distributed. One of the aliphatic C−H rich portions (~1 μm) in other slices of Bells might contain C−O bonds (Fig. 6-2). These results suggest that different organic functional groups are heterogeneously distributed in a few μm scale, and some of these might correspond to

organic globules found in several carbonaceous chondrites. The NFIR imaging method can provide submicron spatial distribution of organic functional groups and their association with minerals.

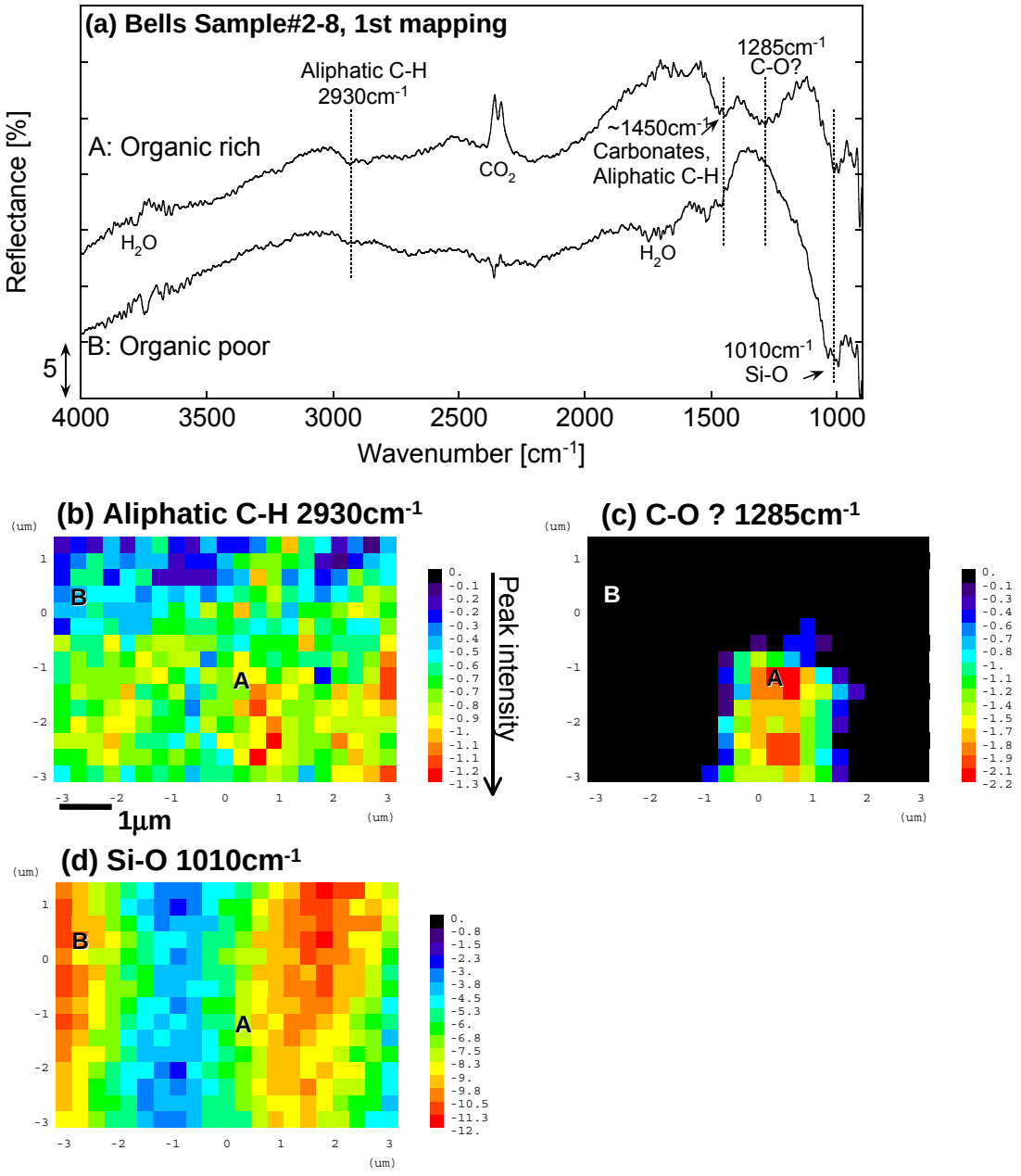

Fig. 6-2. (a) Representative NFIR spectra of Bells Sample#2-8 for an organic-rich point (mark A in **b-d**), and a organic-poor point (mark B in **b-d**). (b-d) NFIR spectral mapping of the band depths of Bells Sample#2-8, (b) 2930 cm^{-1} due to aliphatic C−H, (c) 1285 cm^{-1} probably due to organic C−O, (d) 1010 cm^{-1} due to Si−O.

6.1.4. Thermal stabilities of organic matter in carbonaceous chondrites and effects of minerals

In order to elucidate effects of minerals on the thermal transformation of organic matter, thermal alteration on carbonaceous materials were simulated experimentally under micro FTIR spectroscopy with a heating stage. Both bulk and IOM samples of Murchison (CM2) and Orgueil (CI1) meteorites were heated in the heating stage from room temperature to 600ºC in an inert gas (Ar) flow. Infrared spectra were collected at every 20ºC under the micro FTIR spectroscopy. Thermal stability of organic matter was lower in the presence of minerals than IOM for Murchison, while thermal stability was higher in the presence of minerals than IOM for Orgueil (Fig. 6-3). Similarly, heating experiments were conducted using leonardite humic acid (LHA) with and without saponite, antigorite and olivine as analogs of carbonaceous chondrites, under Ar flow and air. The thermal stability of LHA is higher with saponite. On the other hand, antigorite and olivine accelerate the decrease of aliphatic fractions, and decelerates the decrease of aromatic fractions. These effects were dominant in oxidizing atmosphere. These results suggest that thermal stability of organic matter depend on coexisting minerals.

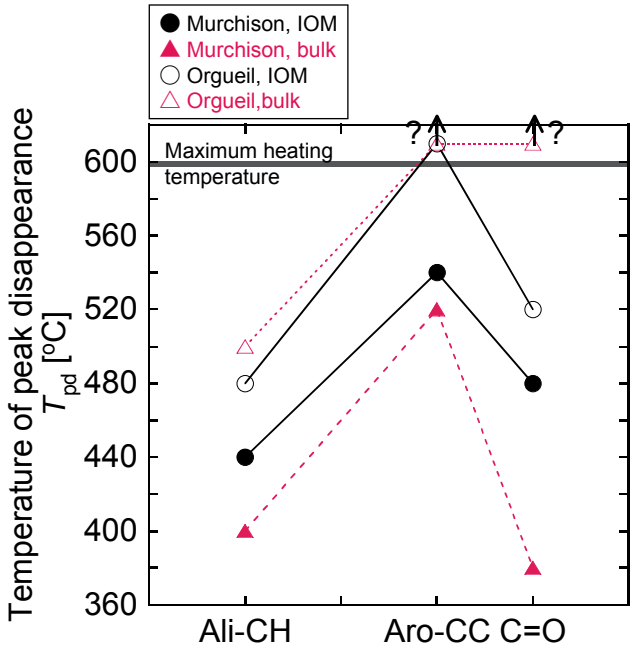

Fig. 6-3. Temperatures of peak disappearance T_{pd} determined for each functional group of Murchison and Orgueil (bulk and IOM) under Ar flow. The maximum heating temperature of the heating stage used here is 600ºC. Aromatic C=C of Orgueil IOM, and Aromatic C=C and C=O of bulk Orgueil showed band at 600ºC. Therefore T_{pd} of these bands are likely over 600ºC.

6.1.5. Kinetic studies on thermal decomposition of organic matter in carbonaceous chondrites

In order to evaluate kinetic parameters for thermal decomposition of organic matter, in-situ heating experiments of bulk and IOM of Murchison (CM2) meteorite were conducted under micro FTIR combined with a heating stage. Bulk and IOM of Murchison grains are heated at 160-300ºC isothermally in the heating stage under Ar gas flow and air for several hours. Infrared spectra are collected in-situ during heating. Decreases of aliphatic C−H peak heights with time at each temperature are well fitted with Ginstling-Brounshtein three dimensional diffusion model (D4), and the rate constants for decreases of aliphatic C−H were determined (Fig. 6-4a). Activation energies and frequency factors are estimated from these rate constants at different temperatures using Arrhenius equation (Fig. 6-4b). The activation energy and frequency factor for bulk Murchison under Ar flow are 72 ± 6 kJ/mol and ~48 s^{-1}, respectively, while these for Murchison IOM under Ar flow are 107 ± 3 kJ/mol and ~5.2 × 10^4 s^{-1}, respectively. The time scales for metamorphism can be estimated for given temperatures with aliphatic C−H peak heights, otherwise temperatures of metamorphism can be estimated for given time scales. The rate of aliphatic C−H decrease of Murchison is different between organic matter without mineral (IOM) and with mineral (bulk). The rate of organic decomposition might be variable with changes of mineral assemblages during aqueous alteration and/or thermal metamorphism.

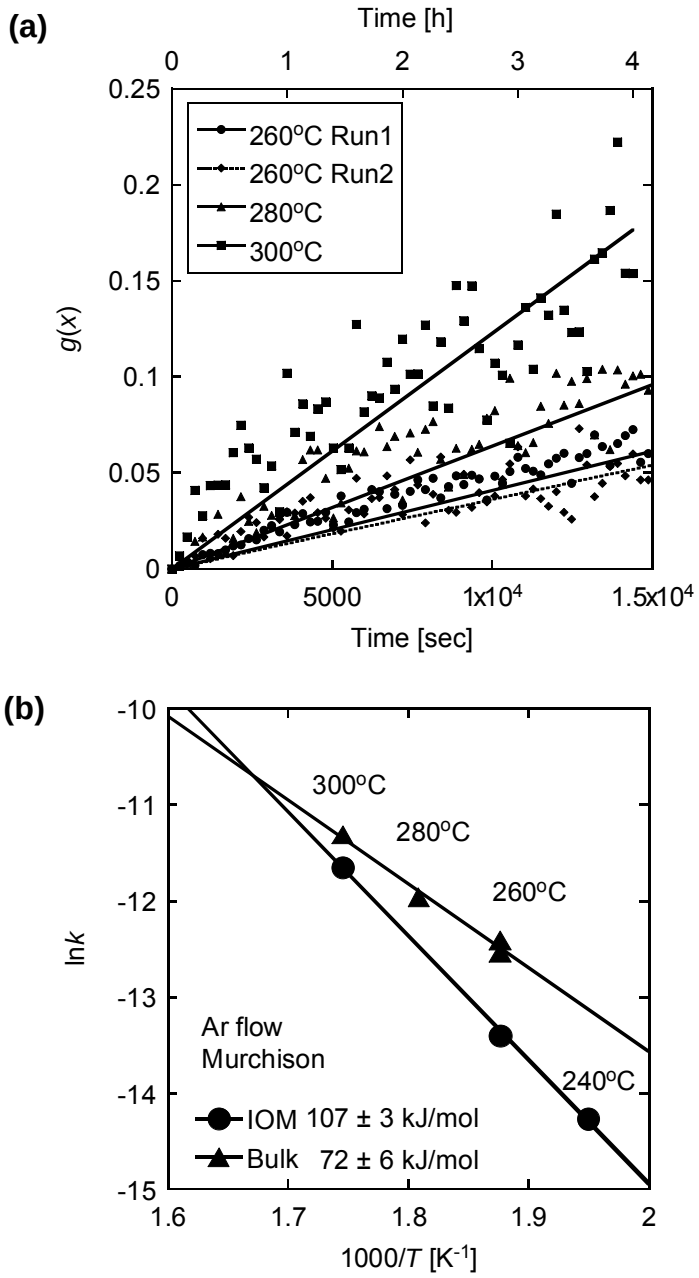

Fig. 6-4. (a) Fitting results of aliphatic C−H decrease of bulk Murchison meteorite in Ar flow by Ginstling-Brounshtein three-dimensional diffusion model. (b) Arrhenius diagrams of aliphatic C−H decrease of Murchison bulk and IOM in Ar flow for Ginstling-Brounshtein three dimensional diffusion (D4) model.

6.2. Implications and Future Perspectives for Thermal Processes of Carbonaceous Chondrites

Kinetic heating experiments indicateed that the organic matter in Murchison

meteorite decreases faster with minerals (bulk) than without minerals (IOM). Step heating experiments using simulated materials suggest that the tendency is likely to vary with coexisting minerals. For example, organic matter in Orgueil is likely to decrease slower with minerals (bulk) than without minerals (IOM), due to the presence of saponite.

The NFIR mapping results suggested the association of COOH containing organic moieties with phyllosilicates. However, further improvement of the present NFIR method is needed to elucidate detailed association of specific functional groups and mineral species for the mineral effects on the organic decomposition.

Kinetic heating experiments allow us to constrain the time and temperature range of thermal changes of organic matter in carbonaceous chondrites by using obtained kinetic parameters such as rates and activation energies. Fig. 6-5 shows constraints of temperature T and time t for the survival of organic matter in Murchison with and without minerals, using the following equation:

$$At = g(x) \cdot \exp\left(\frac{E_a}{RT}\right) \qquad (6\text{-}1)$$

where $g(x)$ is the conversion function, x the degree of reaction progress ($0 \leq x \leq 1$), A the frequency factor, E_a the activation energy, and R the gas constant. For example, aliphatic C−H decrease by half is within ~4 months and to zeto within ~3 years at 100ºC in the presence of Murchison mineral assemblage. Without minerals, aliphatic C−H decrease by half is within ~20 years and aliphatic C−H is lost within ~200 years at 100ºC (Fig. 6-5).

By the constraints on time scale for alteration, the depth limit of parent body could be estimated. According to a temperature profile of CM like parent body calculated by Grimm and McSween (1989), melting of ice, aqueous alteration, and initiation of dehydration all take place within 1 m.y., assuming the diameter of 100 km (Fig. 6-6). The temperature profile at 1 m.y. is shown in Fig. 6-6a. The temperature should be under 300K for aliphatic C−H of Murchison (IOM) to survive for 1 m.y. (Fig. 6-6b). The aliphatic C−H survival zone is restricted at $r > 48$ km (< 2 km in depth) to keep under 300K for 1 m.y.

However, above estimation is based on the dry heating experiment of organic matter of Murchison. Since presence of water should affect the decrease rate of organic matter, kinetic heating experiments in the presence of water are needed. Furthermore, these kinetic experiments for another primitive carbonaceous chondrite such as CI and CR are needed, in order to evaluate kinetic parameters for organic matter with different mineral assemblages. Although this study uses the decrease of aliphatic

C−H, decrease rates of other functional groups should give different profiles of thermal history. Hence other functional group analyses are needed including Raman spectroscopic parameters such as D band width.

Recently, Cody et al. (2008) demonstrated that the development of the intensity of a 1s−σ* exciton observed using carbon XANES spectroscopy appeared to correlate well with degrees of the thermal metamorphism of the chondritic parent bodies. Cody et al. (2008) showed that laboratory heating experiments could be used to follow the development of the exciton intensity as a function of temperature and time, thus allowing for the construction of a simple kinetic expression capable of calculating effective temperatures assuming a duration of 10^7 years of parent body heating. These experiments reveal that modification of IOM is a kinetically controlled process. It is important to note that in the work of Cody et al. (2008), the changes observed involved a change in bulk electronic properties of the IOM, and only a single kinetic expression was tested. An independent estimate of time is needed in order to establish temperature.

It is likely, however, different parent bodies have different bulk chemistry and different thermal histories. For example, Sears et al. (1991) pointed out that CO chondrites might have experienced lower temperatures, but for longer periods than the same petrologic type ordinary chondrites. Enhanced and additional kinetic studies of thermal processing of organic matter may further help sorting out the thermal history of the parent bodies. In addition, spatial distribution of organic matter with minerals observed by NFIR spectroscopy may help understanding associations and roles of minerals on the parent body processes.

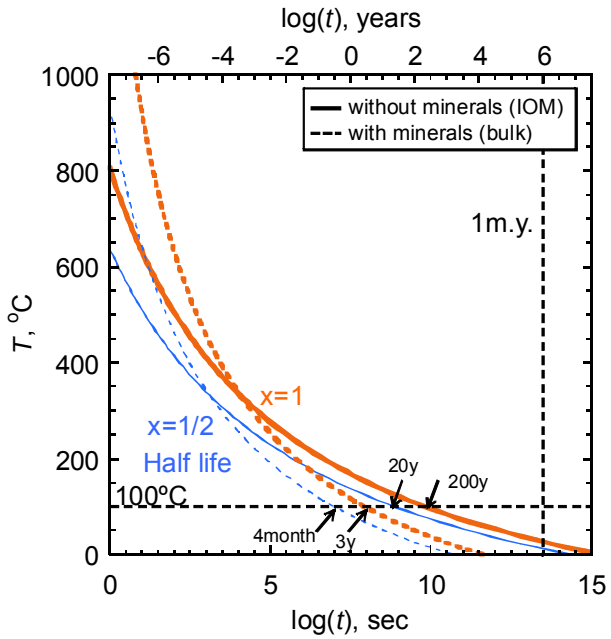

Fig. 6-5. Temperature and time limits for Murchison aliphatic C−H survival. Thin curves show decrease by half and thick curves show complete depletion, respectively. Solid curves are without mineral assemblages (IOM), and dashed curves are with mineral assemblages (bulk), respectively.

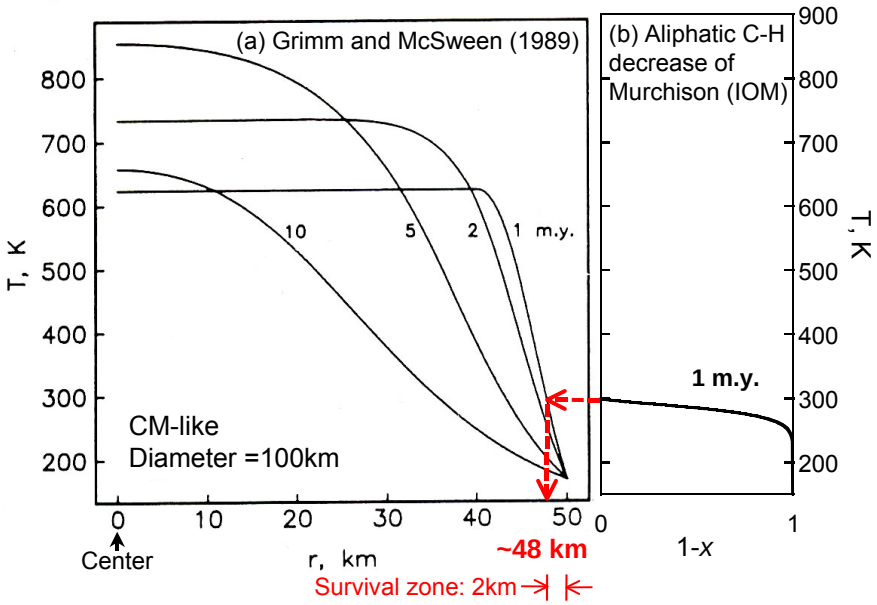

Fig. 6-6. Estimation of the aliphatic C−H survival zone using temperature profiles of Grimm and McSween (1989). (a) Temperature profiles of CM-like parent body assuming 100 km in diameter by Grimm and McSween (1989). (b) Temperature profile of aliphatic C−H decrease of Murchison (IOM) for 1 m.y., the y axis (temperature, K) is set to the same scale as that of (a).

6.3. Simulations Using Estimated Kinetic Parameters

Fig. 6-7 shows time-temperature-transformation (T-T-T) diagram (Fig. 6-5) now with errors. The diagram might be limited in the temperature range until about ~400ºC considering phase transitions of minerals. Murchison matrix consists mainly of serpentine, tochilinite, Fe-Ni sulfides, carbonates, olivine and Fe-Ni metal (Zolensky and McSween 1988; Zolensky et al. 1993). Serpentine is known to decompose into olivine and enstatite above ~750ºC, however transitional structure appears at 400-500ºC (Akai 1992). The thermal decomposition temperatures for carbonates are between ~470ºC and ~900ºC (Tonui et al. 2003). Therefore, T-T-T diagram for bulk Murchison in the presence of minerals such as serpentine is plausible for the temperature lower than 400-500ºC. Lower limit of T-T-T diagram (Fig. 6-7) is unknown. However, the thermal transformation of terrestrial kerogen in natural sedimentary rocks to generate aliphatic hydrocarbons is considered to occur from about 50ºC to 150ºC (Tissot et al. 1971; Albrecht et al. 1976). Therefore, the T-T-T diagram (Fig. 6-5 and Fig. 6-7) can be applicable to at least until 50ºC.

A crossover of curves with (bulk Murchison) and without minerals (Murchison IOM) occurs at around 350ºC (Fig. 6-7). This means that the aliphatic C−H became stable in the presence of minerals above this temperature, contrary to the trend at lower temperatures. This crossover is originated from that occurring for extrapolation to higher temperatures of rate constants of aliphatic C−H decrease with and without minerals in the Arrhenius diagram (Fig. 6-4b). However, I do not know if I can extrapolate the same mechanism to higher temperatures. Therefore, I had better limit the evaluation to the temperature below this crossover point (< ~350ºC) (Fig. 6-7). In the following discussion, the maximum temperature condition in the parent body is set lower than this temperature.

In order to confirm validity of estimated kinetic parameters, the step heating experiments of Murchison are simulated using equation (6-1) with estimated activation energies E_a and frequency factors A. During the step heating experiments (see Chapter 4.3.2), the samples are heated at 10 ºC/min from room temperature up to 600ºC, and the temperature is hold for 80 seconds, at every 20ºC to collect sample spectra, i.e., temperature increases 20ºC per 200 seconds. Therefore, for this calculation, temperature change is approximated by a linear increase at 6 ºC/min. Temperature increases with time, equation (6-1), can be expressed as

$$g(x) = A\int_0^t \exp\left(-\frac{E_a}{RT(t)}\right)dt \qquad (6\text{-}2)$$

where x is the degree of reaction progress, $g(x)$ is the conversion function, t is the time, R is the gas constant, and $T(t)$ is the temperature which changes with time. The $g(x)$ of Ginstling-Brounshtein's three dimensional diffusion model is express as

$$g(x) = 1 - \frac{2}{3}x - (1-x)^{2/3} \qquad (6\text{-}3)$$

Decreases of aliphatic C−H for IOM and bulk of Murchison are calculated using above equations with the activation energies and frequency factors obtained by fitting the kinetic heating experimental data with the diffusion model (IOM: E_a = 107 kJ/mol and $A = 5.2 \times 10^4$ s^{-1}, bulk: E_a = 72 kJ/mol and A = 48 s^{-1}). Fig. 6-8 shows calculated curves with errors (IOM: ± 3 kJ/mol for E_a and ± 0.73 for ln A, bulk: ± 6 kJ/mol for E_a and ± 1.4 for ln A). Step heating experimental results of aliphatic C−H peak height changes with temperature for Murchison IOM were well represented within errors by the simulation curves based on obtained kinetic parameters. Murchison bulk data somewhat deviate from the simulation curve but still within large error ranges. However, differences in simulation curves between IOM and bulk are not significant in Fig. 6-8. This is due to small differences between the two in aliphatic C−H decrease rates at higher temperatures until 350ºC observed in Fig. 6-7. The differences would become more significant at lower temperatures for longer durations.

Tochilinite, which is present in bulk Murchison, is reported to decompose at ~250ºC (Nakamura 2005). This tochilinite decomposition might therefore affect the thermal decomposition profile at this temperature. However, experimental decreases of aliphatic C−H (Fig. 6-8) do not show significant differences between below and above 250ºC, and tochilinite does not seem to affect aliphatic C−H decrease.

Aliphatic decrease profiles in a parent body are estimated using time–temperature history model of Young (2001). Fig. 6-9 shows the temperature history up to 1 m.y. based on the model calculations by Young (2001) for the small body (a radius of 9 km), assuming the initial condition including 0.2 volume fraction water ice, 0.1 volume fraction open pore space, a temperature of 180K, and ^{26}Al/^{27}Al value of 1×10^{-5}.

Decreases of aliphatic C−H at each radial distance r (km) from the parent body center are calculated using equations (6-2) and (6-3) with the activation energy and frequency factor of Murchison IOM (E_a = 107 kJ/mol and $A = 5.2 \times 10^4$ s^{-1}) (Fig. 6-10). The kinetic parameters were applied to the temperature range of about −100ºC to 200ºC occurring in the parent body (Fig. 6-9). Based on the calculation, aliphatic C−H is almost stable at r = 8 km (maximum temperature is approximately −30ºC) (Fig. 6-10). Aliphatic C−H decreases very rapidly and disappears less than 3×10^5 years, at $r \leq 6$ km (maximum temperature is approximately 80ºC to 200ºC) (Fig. 6-10).

At r = 7 km (2km depth from the parent body surface), aliphatic C−H decreases greatly around 4×10^5 to 5×10^5 years, where the temperature reach the maximum of ~40ºC (Fig. 6-9). The C−H decrease then stops after ~7×10^5 years (Fig. 6-10). It should be noted that under this condition, aliphatic C−H survives afterwards.

These simulations indicate that the obtained kinetic parameters can be used to constrain temperature-time history for the decrease of aliphatic C−H in chondrite parent bodies.

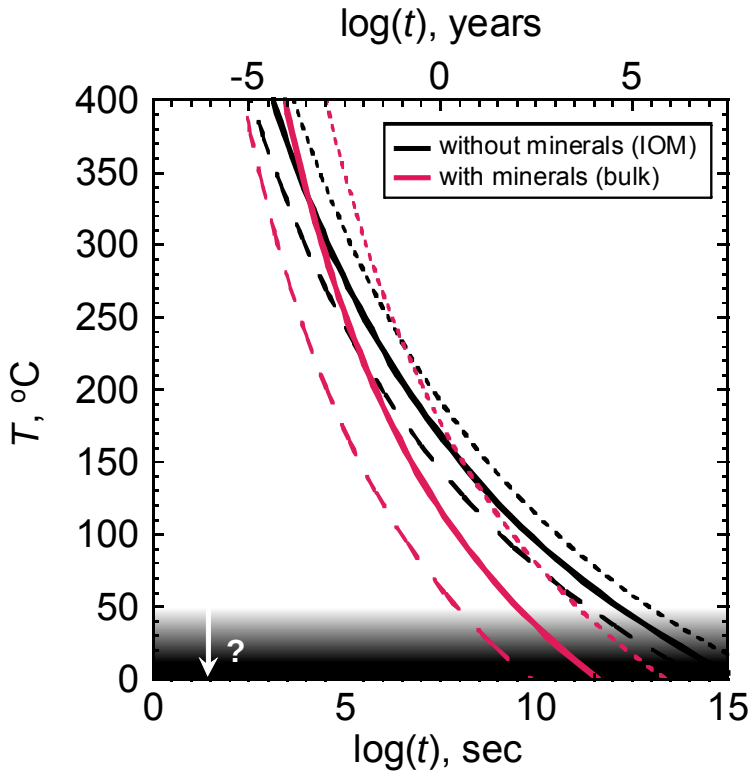

Fig. 6-7. Time-temperature-transformation (T-T-T) diagram for Murchison aliphatic C−H (Fig. 6-5) with errors. The solid curves show complete depletion of aliphatic C−H. Dotted curves and dashed curves are maximum error and minimum error, respectively.

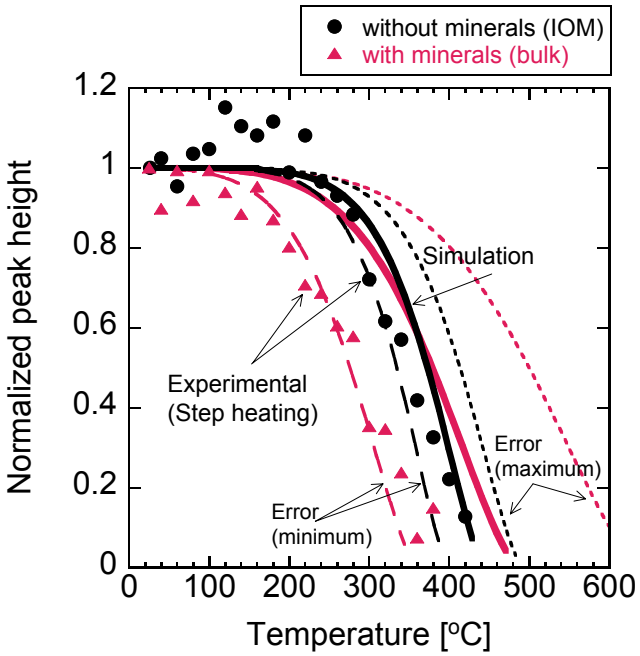

Fig. 6-8. Experimental results of step heating experiments (see Chapter 4.3.2) of Murchison aliphatic C−H, with (bulk) and without minerals (IOM), simulated by the kinetic model with obtained parameters.

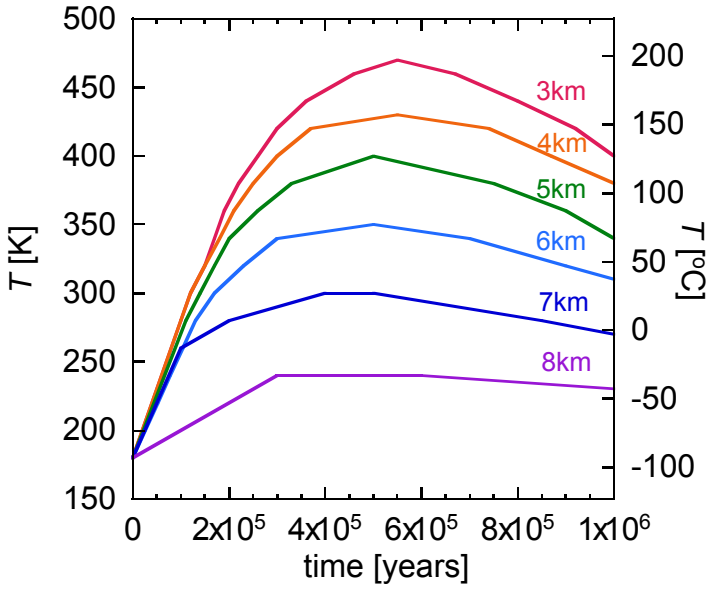

Fig. 6-9. Temperature history up to 1 m.y. based on the model calculations by Young (2001) for the small parent body (a radius of 9 km), assuming the initial condition including 0.2 volume fraction water ice, 0.1 volume fraction open pore space, a temperature of 180K, and $^{26}Al/^{27}Al$ value of 1×10^{-5}.

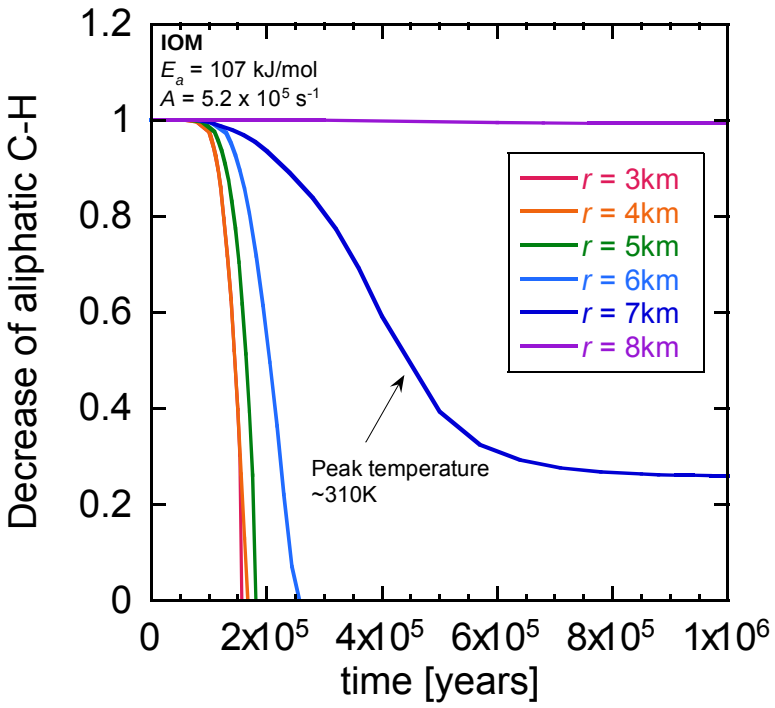

Fig. 6-10. Decreases of aliphatic C−H at each radial distance r (km) from the parent body center calculated based on the time-temperature model by Young (2001), with the activation energy (E_a = 107 kJ/mol) and frequency factor (A = 5.2 × 10^4 s^{-1}) of Murchison IOM.

References

Akai J. 1992. T-T-T diagram of serpentine and saponite, and estimation of metamorphic heating degree of Antarctic carbonaceous chondrites. *Proceedings of the NIPR Symposium on Antarctic Meteorites* 5: 120-135.

Albrecht P., Vandenbroucke M., and Mandengué M. 1976. Geochemical studies on the organic matter from the Douala Basin (Cameroon) − I. Evolution of the extractable organic matter and the formation of petroleum. *Geochimica et Cosmochimica Acta* 40: 791-799.

Cody G. D., Alexander C. M. O'D., Yabuta H., Kilcoyne A. L. D., Araki T., Ade H., Dera P., Fogel M., Militzer B., Mysen B. O. 2008. Organic thermometry for chondritic parent bodies. *Earth and Planetary Science Letters* 272: 446-455.

Nakamura T. 2005. Post-hydration thermal metamorphism of carbonaceous chondrites. *Journal of Mineralogical and Petrological Sciences* 100: 260-272.

Garvie L. A. J. and Buseck P. R. 2007. Prebiotic carbon in clays from Orgueil and Ivuna (CI), and Tagish Lake (C2 ungrouped) meteorites. *Meteoritics & Planetary Science* 42: 2111-2117.

Grimm R. E. and McSween H. Y., Jr. 1989. Water and the thermal evolution of carbonaceous

chondrite parent bodies. *Icarus* 82: 244-280.

Pearson V. K., Sephton M. A., Kearsley A. T., Bland P. A., Franchi I. A., and Gilmour I. 2002. Clay mineral-organic matter relationships in the early solar system. *Meteoritics & Planetary Science* 37: 1829-1833.

Sears D. W. G., Batchelor J. D., Lu J., and Keck B. D. 1991. Metamorphism of CO and CO-like chondrites and comparisons with type 3 ordinary chondrites. *Proceedings of the NIPR Symposium on Antarctic Meteorites* 4: 319-343.

Tissot B., CalifetdY., Deroo G., and Oudin J. L. 1971. Origin and evolution of hydrocarbons in early Toarcian Shales, Paris Basin, France. *American Association of Petroleum Geologists bulletin* 55: 2177-2193.

Tonui E. K., Zolensky M. E., Lipschutz M. E., Wang, M. -S., and Nakamura, T. 2003. Yamato-86029: Aqueously altered and thermally metamorphosed CI chondrite with unusual textures. *Meteoritics & Planetary Science* 38: 269-292.

Young E. D. 2001. The hydrology of carbonaceous chondrite parent bodies and the evolution of planet progenitors. *Philosophical Transactions of the Royal Society A* 359: 2095-2110.

Zolensky M. and McSween H.Y., Jr. 1988. Aqueous alteration. In *Meteorites and Early Solar System*, edited by Kerridge J. R. and Matthews M. S. Tucson, Arizona: The University of Arizona Press. pp. 114-143.

Zolensky M. Barrett R., and Browning L. 1993. Mineralogy and composition of matrix and chondrules rims in carbonaceous chondrites. *Geochimica et Cosmochimica Acta* 57: 3123-3148.

February 4, 2009